


Winter 11-15-2016

Development of In Vivo Systems for Detecting and Studying Ribosome Inhibition by Small Molecules

Shijie Huang

The University of New Mexico

Follow this and additional works at: https://digitalrepository.unm.edu/chem_etds

 Part of the [Biochemistry Commons](#), [Biological Engineering Commons](#), [Biotechnology Commons](#), and the [Chemistry Commons](#)

Recommended Citation

Huang, Shijie. "Development of In Vivo Systems for Detecting and Studying Ribosome Inhibition by Small Molecules." (2016). https://digitalrepository.unm.edu/chem_etds/60

This Dissertation is brought to you for free and open access by the Electronic Theses and Dissertations at UNM Digital Repository. It has been accepted for inclusion in Chemistry ETDs by an authorized administrator of UNM Digital Repository. For more information, please contact disc@unm.edu.

Shijie Huang

Candidate

Chemistry & Chemical Biology

Department

This dissertation is approved, and it is acceptable in quality and form for publication:

Approved by the Dissertation Committee:

Charles E. Melançon III, Chairperson

Debra Dunaway-Mariano

Jeremy S. Edwards

Fu-Sen Liang

**Development of *In Vivo* Systems for Detecting and Studying Ribosome
Inhibition by Small Molecules**

by

SHIJIE HUANG

B.S., Biological Science, South China Agricultural University, 2008

M.S., Microbiology, South China Agricultural University, 2011

DISSERTATION

Submitted in Partial Fulfillment of the
Requirements for the Degree of

Doctor of Philosophy

Chemistry

The University of New Mexico
Albuquerque, New Mexico

December, 2016

Acknowledgements

I would like express my deepest gratitude to my dissertation mentor Dr. Chad Melançon. It has been a great fortune for me to work under his guidance during the past five and a half years. As an academic advisor, Chad has taught me how to think creatively, how to work efficiently and how to encourage myself consistently. His knowledge of both chemistry and biology inspire me to approach scientific questions in different ways. Chad has also shown me how to be a good teacher, to care about students' futures, and to patiently help students understand complex science. His encouragement and guidance have been invaluable in helping me finish my PhD degree.

I would like to thank the committee members Dr. Debra Dunaway-Mariano, Dr. Jeremy Edwards and Dr. Fu-Sen Liang for their helpful suggestions and critical questions regarding my dissertation. They have helped me better understand the importance of the work I am doing.

I also want to thank the Melançon lab members for supporting my research project and making the lab a great place to work. I would like to thank Mr. Xuechen Zhu for helping me perform key experiments on developing the aminoglycoside antibiotics detection system. Without his assistance I would never be able to publish my first paper in ACS Chemical Biology. I am also very grateful to Ms. Han Nguyen for helping me prepare experimental figures and photos with her awesome Photoshop skills. Special thanks to Dr. Yasushi Ogasawara for his smart suggestions and critical comments, which encouraged me to think positively about my research. I want to thank all the other current and past group members, Jingxuan He, Wubin Gao, Ara Kooser, Joe Villanueva and Briana Van Treeck, for their helpful comments and cooperation during my PhD studies.

Last but not least, I would like to thank my lovely parents and girlfriend Wen-Hui Lee for their unconditional love. Their support and encouragement free me from disruption so that I can pursue my dream and dedicate myself to scientific research.

Development of *In Vivo* Systems for Detecting and Studying Ribosome Inhibition by Small Molecules

by

SHIJIE HUANG

B.S., Biological Science, South China Agricultural University, 2008

M.S., Microbiology, South China Agricultural University, 2011

PhD, Chemistry, University of New Mexico, 2016

ABSTRACT

The ribosome is the quintessential antibacterial drug target, with many structurally and mechanistically distinct classes of antibacterial agents acting by inhibiting ribosome function. Detecting and quantifying ribosome inhibition by small molecules and investigating their binding modes and mechanisms of action are critical to antibacterial drug discovery and development efforts. To develop a ribosome inhibition assay that is operationally simple, yet provides direct information on the drug target and the mechanism of action, we have developed engineered *E. coli* strains harboring an orthogonal ribosome controlled green fluorescent protein reporter that produce fluorescent signal when the O-ribosome is inhibited. As a proof of concept, we demonstrate that these strains act as sensitive and quantitative detectors of ribosome inhibition by a set of 12 structurally diverse 2-deoxystreptamine (2-DOS) aminoglycoside antibiotics, which target the A-site in helix 44 of the 16S rRNA. To prove the generality and promote the application of the system, we extended this system for detecting ribosome inhibition by a variety of structurally and mechanistically distinct drug classes targeting both small and

large subunits of the ribosome. We have engineered *E. coli* strains capable of detecting O-ribosome inhibition by other drugs targeting the 16S rRNA including the non-2-DOS aminoglycosides streptomycin and kasugamycin, and the aminocyclitol spectinomycin. Through integration of the Ribo-T tethered ribosome system with our system, we can also detect ribosome inhibition by the 23S rRNA inhibitors erythromycin, lincomycin and linezolid. These results suggest the generalizability of our strategy. We then applied the system to screen a set of spectinomycin analogs with unknown activity to demonstrate potential application. Three spectinomycin analogs were shown to possess higher or similar anti-ribosome activity compared to the parent compound.

We have also modified our system to enable rapid directed evolution of rRNA variants with specific properties from large rRNA libraries to study the impact of rRNA sequence variation on ribosome activity and drug resistance. By replacing the fluorescence reporter gene with the chloramphenicol acetyltransferase (CAT) gene, we are able to select for functional rRNA mutants and quantify their catalytic activities. A variety of drug-resistant and drug-dependent rRNA mutants, as well as hyper- and hypo-active mutants were found. We also performed directed evolution to select ribosome mutants capable of supporting cell growth, yet confer resistance to aminoglycoside antibiotics. Only two mutants (A1408G and G1491U) were identified from this experiment; and both mutants have broad spectrum aminoglycoside resistance. Our results demonstrate that the O-ribosome controlled reporter system is capable of efficiently identifying new rRNA mutants with unique properties. We suggest that our directed evolution approach has the potential to provide new insights into mechanisms of ribosome inhibition and evolution of antibiotic resistance.

Table of Contents

| | |
|---|-----|
| LIST OF TABLES | XI |
| LIST OF FIGURES | XII |
| LIST OF ABBREVIATIONS | XVI |
| | |
| CHAPTER 1. BACKGROUND AND SIGNIFICANCE | 1 |
| 1. The bacterial ribosome is the major target for antimicrobial agents | 1 |
| 2. Technology for detecting and studying ribosome inhibition | 9 |
| 3. Summary and Thesis Statement..... | 18 |
| 4. References..... | 20 |
| | |
| CHAPTER 2. DEVELOPMENT OF DETECTION AND QUANTIFICATION SYSTEMS FOR RIBOSOME INHIBITION BY AMINOGLYCOSIDE ANTIBIOTICS | 26 |
| 1. Introduction..... | 26 |
| 2. Experimental Procedures | 31 |
| General..... | 31 |
| Bacterial strains | 32 |
| Bacterial culture | 33 |
| General PCR conditions | 34 |
| Enforced replacement by sucrose counterselection | 34 |
| Cell density and fluorescence assays..... | 35 |
| Calculation of IC ₅₀ , LD ₅₀ values and correlation analysis..... | 35 |
| Construction of pRRSH2 | 36 |
| Construction of pRRSH2-A1408G and pRRSH2-U1406A | 38 |
| Functional verification of pRRSH2-A1408G and pRRSH2 in <i>E. coli</i> SQ380 | 40 |
| Sequential construction of the reporter plasmid..... | 41 |
| Construction and testing of pUC19-GFPuv..... | 41 |
| Construction of the pGBSH1 plasmid series | 44 |

| | |
|--|-----------|
| pGBSH1 series functional assays..... | 48 |
| Construction and testing of pGBSH3 | 49 |
| Construction and testing of pGBSH18..... | 51 |
| Construction and testing of pSH3-KF in <i>E. coli</i> DH5 α | 54 |
| Ribosome inhibition assay of kanamycin in <i>E. coli</i> SH391 | 58 |
| Construction and testing of pSH4-KF - pSH14-KF in <i>E. coli</i> SH386 | 58 |
| 3. Results and Discussion..... | 64 |
| Ribosome inhibition assays of aminoglycosides in <i>E. coli</i> SH399 | 64 |
| 4. Conclusion | 72 |
| 5. References..... | 74 |
| CHAPTER 3. EXTENDING THE DETECTION SYSTEM TO SENSE OTHER RIBOSOME SMALL SUBUNIT INHIBITORS AND LARGE SUBUNIT INHIBITORS | 81 |
| 1. Introduction..... | 81 |
| 2. Experimental procedures | 88 |
| General..... | 88 |
| Bacterial strains | 88 |
| Bacterial culture | 89 |
| PCR conditions..... | 89 |
| Enforced replacement by sucrose counterselection..... | 89 |
| Cell density and fluorescence assays..... | 89 |
| Construction of <i>E.coli</i> strain SH435..... | 89 |
| Construction of pRRSH2 plasmid series with various mutations..... | 90 |
| Construction of detector strains SH442, SH446 and SH456..... | 93 |
| Optimization of the streptomycin detector | 94 |
| Construction of pRiboT2-A2058G and pRiboT2-G2576U | 95 |
| Construction and function testing of pSH18 | 97 |
| Optimization of ribosome large subunit inhibitor detector strain..... | 102 |
| Direct measurement of ribosome inhibition by spectinomycin analogs..... | 105 |

| | |
|--|------------|
| 3. Results and discussion..... | 107 |
| Extending the detection system to other ribosome small subunit inhibitors | 107 |
| Extending the ribosome inhibition detector to ribosome large subunit inhibitors | 110 |
| Determination of ribosome inhibition by spectinomycin analogs | 112 |
| 4. Conclusion | 115 |
| 5. References..... | 116 |
| CHAPTER 4. STUDYING RIBOSOME INHIBITION BY DIRECT EVOLUTION OF RIBOSOMAL RNA VARIANTS | 120 |
| 1. Introduction..... | 120 |
| 2. Experimental procedures | 123 |
| General..... | 123 |
| Bacterial strains | 123 |
| Bacterial culture | 123 |
| PCR conditions..... | 124 |
| Enforced replacement by sucrose counterselection | 124 |
| Cell density and fluorescence assays..... | 124 |
| Construction of h44 9-site library on pRRSH2..... | 124 |
| Transferring the h44 library into SQ380+pSH6-KF..... | 126 |
| Aminoglycoside antibiotic selections on h44 9-site library | 127 |
| Construction and testing of pSH-OCAT..... | 127 |
| Construction of O-h44 9-site library on pSH-OCAT | 131 |
| Transferring the O-h44 library into SH471 | 131 |
| Ribosome activity selection and aminoglycoside antibiotics selection on O-h44 library | 132 |
| 3. Results and discussion..... | 133 |
| Aminoglycoside antibiotic resistant mutants from h44 9-site library | 133 |
| Ribosome activity selection on O-h44 9-site library | 135 |

| | |
|---|-----|
| Aminoglycoside antibiotics selection on O-h44 9-site library..... | 136 |
| 4. Conclusion | 140 |
| 5. References..... | 141 |

List of Tables

| | |
|---|-----|
| Table 2-1: Primers for constructing pRRSH2 plasmid | 37 |
| Table 2-2: Primers for constructing pRRSH2-A1408G and pRRSH2-U1406A | 39 |
| Table 2-3: Primers for constructing pUC19-GFPuv..... | 42 |
| Table 2-4: Primers for optimization of the <i>gfp-uv</i> 5'-untranslated (5'-UTR) region | 46 |
| Table 2-5: Summary of the sequences of 5'UTR..... | 47 |
| Table 2-6: Primers for constructing pGBSH3 | 50 |
| Table 2-7: Primers for constructing pGBSH18..... | 52 |
| Table 2-8: Primers for constructing pSH3-KF | 55 |
| Table 2-9: Primers for constructing pSH4-KF through pSH14-KF | 60 |
| Table 2-10: Sequences of the promoters used in constructing pSH4-KF through pSH14-KF | 62 |
| Table 2-11: Promoter combinations of pSH3-KF through pSH14-KF | 62 |
| Table 3-1: Primers for constructing pRRSH2-C1192U and pRRSH2-C1192U/A2058G..... | 91 |
| Table 3-2: Primers for constructing pRRSH2- A794G/C1192U/A2058G and pRRSH2-C912U/C1192U/A2058G..... | 93 |
| Table 3-3: Primers for constructing pRiboT2, pRiboT2-A2058G and pRiboT2-G2576U | 97 |
| Table 3-4: Primers for constructing pRRSH2b and pSH18BB..... | 99 |
| Table 3-5: Plasmid summary information | 103 |
| Table 4-1: Primers for constructing h44 9-site library | 125 |
| Table 4-2: Concentration of each aminoglycoside antibiotic used in chapter 4 | 127 |
| Table 4-3: Primers for constructing pSH-OCAT | 128 |
| Table 4-4: Chloramphenicol selection survival statistics | 132 |

List of Figures

| | |
|---|----|
| Figure 1-1. The spread of drug resistance to common antibiotics..... | 2 |
| Figure 1-2. Targets of antibiotics..... | 3 |
| Figure 1-3. Cheminformatic analysis of natural product chemotypes and their target sites..... | 4 |
| Figure 1-4. Antibiotics targeting ribosome small subunit..... | 6 |
| Figure 1-5. Antibiotics targeting ribosome large subunit..... | 7 |
| Figure 1-6. Overview of ribosome inhibitor target sites and modes of action..... | 8 |
| Figure 1-7. <i>In vitro</i> translation assay for detecting and quantifying ribosome inhibition..... | 11 |
| Figure 1-8. Crystal structure showing interactions between spectinomycin and ribosome..... | 12 |
| Figure 2-1. Structures of aminoglycosides used in this study and overlaid X-ray crystal structures of the decoding site (A-site) of the <i>E. coli</i> 16S rRNA with select aminoglycosides bound..... | 27 |
| Figure 2-2. Schematic showing the functionality of the orthogonal ribosome-controlled fluorescent reporter and cell pellet fluorescence and fluorescence quantification of <i>E. coli</i> DH5 α cells transformed with individual and combined functional elements of the orthogonal ribosome-controlled fluorescent reporter..... | 30 |
| Figure 2-3. PCR protocols used in this work..... | 33 |
| Figure 2-4. Plasmid map of pRRSH2..... | 38 |
| Figure 2-5. Plasmid map of pRRSH2-A1408G..... | 39 |
| Figure 2-6. OD600 readings of SH386 and SH430 grown in a range of kanamycin concentrations..... | 40 |
| Figure 2-7. Plasmid map of pUC19-GFPuv..... | 43 |
| Figure 2-8. Optimization of 5'UTR region of <i>gfp-uv</i> gene..... | 47 |
| Figure 2-9. Plasmid map of pGBSH1-BCD2..... | 48 |
| Figure 2-10. Cell pellet fluorescence and fluorescence quantification of pGBSH1 variants in which the <i>gfp-uv</i> 5'-UTR has been altered..... | 49 |
| Figure 2-11. Plasmid map of pGBSH3..... | 51 |
| Figure 2-12. Plasmid map of pGBSH18..... | 53 |
| Figure 2-13. The O-SD- <i>tetR</i> fragment..... | 54 |

| | |
|---|----|
| Figure 2-14. Cell pellet fluorescence and fluorescence quantification of <i>E. coli</i> DH5 α cells containing pSH3-KF grown in the presence of a range of anhydrotetracycline concentrations ... | 56 |
| Figure 2-15. Illustration of Plpp-O-16S-terminator fragment..... | 57 |
| Figure 2-16. Plasmid map of pSH3-KF..... | 57 |
| Figure 2-17. Plasmid map of pSH4-KF..... | 61 |
| Figure 2-18. Plasmid map of pSH6-KF..... | 61 |
| Figure 2-19. Cell pellet fluorescence of initial detector strain <i>E. coli</i> SH391 and 11 additional strains with tetR and O-16S promoter strengths combinatorially altered in response to increasing concentrations of kanamycin | 63 |
| Figure 2-20. Fluorescence quantification of <i>E. coli</i> SH386 cells containing pSH3-KF – pSH14-KF grown in the presence of a range of kanamycin concentrations..... | 63 |
| Figure 2-21. Cell pellet fluorescence of <i>E. coli</i> SH399 in response to increasing concentrations of aminoglycosides | 65 |
| Figure 2-22. Fluorescence quantification and OD600 quantification of <i>E. coli</i> SH399 cells grown in a range of concentrations of each of the twelve aminoglycosides examined, and OD600 quantification of <i>E. coli</i> SH434 cells grown in a range of concentrations of each of the twelve aminoglycosides examined | 68 |
| Figure 2-23. Analysis of the correlations between IC ₅₀ values previously determined through <i>in vitro</i> translation assays and IC ₅₀ values determined from <i>E. coli</i> SH399-derived fluorescence data | 68 |
| Figure 2-24. Cell pellet fluorescence of <i>E. coli</i> SH431 in response to increasing concentrations of geneticin and hygromycin B | 71 |
| Figure 2-25. Fluorescence quantification and OD600 quantification of <i>E. coli</i> cells grown in a range of concentrations of G418, hygromycin, kanamycin, and gentamicins | 71 |
| Figure 2-26. Analysis of the correlations between LD ₅₀ values determined from growth inhibition assays of <i>E. coli</i> SH434 and IC ₅₀ values determined from <i>E. coli</i> SH431-derived fluorescence data for the subset of 3 compounds..... | 72 |
| Figure 3-1. Chemical structures of spectinomycin, kasugamycin and streptomycin..... | 83 |
| Figure 3-2. Crystal structures of streptomycin and kasugamycin bound to the ribosome..... | 84 |
| Figure 3-3. Schematic showing the ribosomal large subunit inhibitor sensor | 85 |
| Figure 3-4. Chemical structures of erythromycin, lincomycin and linezolid..... | 86 |
| Figure 3-5 Crystal structure of erythromycin bound to the ribosome | 87 |
| Figure 3-6. Construction of <i>E. coli</i> $\Delta 7$ strain SH435..... | 90 |

| | |
|--|-----|
| Figure 3-7. Plasmid map of pRRSH2-C1192U/A2058G..... | 92 |
| Figure 3-8. Cell pellet fluorescence showing anhydrotetracycline titration of 12 streptomycin detector strains | 94 |
| Figure 3-9. Cell pellet fluorescence showing ribosome inhibition by a range of streptomycin concentrations with 12 streptomycin detector strains | 95 |
| Figure 3-10. Plasmid map of pRiboT2-A2058G..... | 97 |
| Figure 3-11. Plasmid map of pRRSH2b..... | 100 |
| Figure 3-12. Plasmid map of pSH18BB..... | 100 |
| Figure 3-13. Plasmid map of pSH18 | 101 |
| Figure 3-14. Cell pellet fluorescence showing anhydrotetracycline titration of 8 large subunit unit inhibition detector strains | 104 |
| Figure 3-15. Cell pellet fluorescence showing ribosome inhibition by a range of erythromycin concentrations with the 8 detector strains | 105 |
| Figure 3-16. Chemical structures of spectinomycin analogs..... | 106 |
| Figure 3-17. Cell pellet fluorescence of <i>E. coli</i> SH442, SH475 and SH456 in response to increasing concentrations of target molecules..... | 108 |
| Figure 3-18. Bar graph figures showing the ATC titration of 5 detector strains | 109 |
| Figure 3-19. Cell pellet fluorescence of <i>E. coli</i> SH460 and SH493 in response to increasing concentrations of target molecules..... | 111 |
| Figure 3-20. Cell pellet fluorescence of <i>E. coli</i> SH442 in response to increasing concentrations of spectinomycin analogs..... | 113 |
| Figure 3-21. Cell pellet fluorescence of <i>E. coli</i> SH442 in response to increasing concentrations of glycoside analogs | 114 |
| Figure 4-1. O-ribosome controlled CAT and its advantages..... | 122 |
| Figure 4-2. Fragment 5 for construction h44 9-site library | 126 |
| Figure 4-3. Plasmid map of pSH-OCAT..... | 129 |
| Figure 4-4. Growth curves of <i>E. coli</i> $\Delta 7$ strain with different rRNA mutations..... | 130 |
| Figure 4-5. Chloramphenicol resistance levels of different O-16S rRNA mutations Figure 4-6. The phenotypes of mutants from h44 9-site library group I and group II | 130 |
| Figure 4-6. The phenotypes of mutants from h44 9-site library group I and group II..... | 134 |

| | |
|--|-----|
| Figure 4-7. Sequence preferences of mutants obtained from ribosome activity selection | 136 |
| Figure 4-8. Sequence preference of mutants obtained from kanamycin, neomycin and gentamicin selections | 138 |
| Figure 4-9. Ribosome activity of 155 unique mutants with and without kanamycin, neomycin and gentamicin..... | 140 |

List of Abbreviations

| | |
|-------------|--|
| WHO | World Health Organization |
| PTC | Peptidyl-transferase center |
| IF | Initiation factor |
| EF | Elongation factor |
| NPET | Nascent polypeptide exit tunnel |
| PrAMPs | Proline-rich antimicrobial peptides |
| FRET | Fluorescence resonance energy transfer |
| MIC | Minimum inhibitory concentration |
| RiboT | Ribosome with tethered subunits |
| h44 | Helix 44 of 16S rRNA |
| H69 | Helix 69 of 23S RNA |
| SPR | Surface plasmon resonance |
| NMR | Nuclear magnetic resonance |
| smFRET | Single molecule fluorescence resonance energy transfer |
| RT-PCR | Reverse transcriptase PCR |
| O-ribosomes | Orthogonal ribosome |
| ASD | Anti-Shine-Dalgarno |
| SD | Shine-Dalgarno |
| GFP | Green fluorescent protein |
| G418 | Geneticin |
| PCR | Polymerase chain reaction |
| COE-PCR | Circularly overlapping extension PCR |
| 5'-UTR | 5'-untranslated region |
| O-SD | Orthogonal Shine-Dalgarno |
| O-ASD | Orthogonal anti-Shine-Dalgarno |
| ATC | Anhydrotetracycline |

| | |
|-------|--|
| 2-DOS | 2-deoxystreptamines |
| SAR | Structure-activity relationships |
| WT | Wild type |
| CAT | Chloramphenicol acetyltransferase gene |
| cfu | Colony forming unit |

CHAPTER 1. BACKGROUND AND SIGNIFICANCE

1. The bacterial ribosome is the major target for antimicrobial agents.

Antibiotics are one of the greatest medical innovations in human history. However, antibiotic resistance has arisen with the development of antibiotics. The continuous emergence of drug-resistant pathogens has greatly impacted human health.¹ It has become a major social issue, and even a popular cause of human extinction in disaster films. According to the World Health Organization (WHO), around six percent of all death in the world is caused by bacterial infection; and is the primary cause of death in low-income nations.² Unfortunately, due to economic concerns, many large pharmaceutical companies have discontinued their antibiotic development programs in recent years. Only 14 new antibiotics have been approved and sold in the past 15 years.³ However, due to the fact that drug resistance will continue to emerge due to the evolution of bacterial pathogens, research on development of antimicrobial agents and their mechanisms must continue. There are reports of newly isolated drug resistant pathogens every year all over the world. In 2011, the super-resistant *Gonorrhea* strain H041, which is resistant to all known antibiotics, was found in Japan.⁴ In 2015, the *Listeria* outbreak from Blue Bell ice cream products caused serious concern and panic on the social media.⁵ In 2016, the ‘nightmare bacteria’, a multi-drug resistant *E.coli*, was identified in the US; and was found to be resistant to the “antibiotic of last resort” colistin.⁶ These are just a few examples found mainly in developed countries. There are many unreported cases all over the world. Figure 1-1 shows the spread of drug resistance against commonly used antibiotics worldwide.⁷ As globalization continues, the risk of ‘super-bugs’ spreading worldwide will increase if we fail to address this issue.

THE SPREAD OF ANTIBIOTIC RESISTANCE

An increasing proportion of bacteria display resistance to common antibiotics.

— Fluoroquinolones — Cephalosporins (3rd gen) — Aminoglycosides
— Carbapenems — Polymyxins

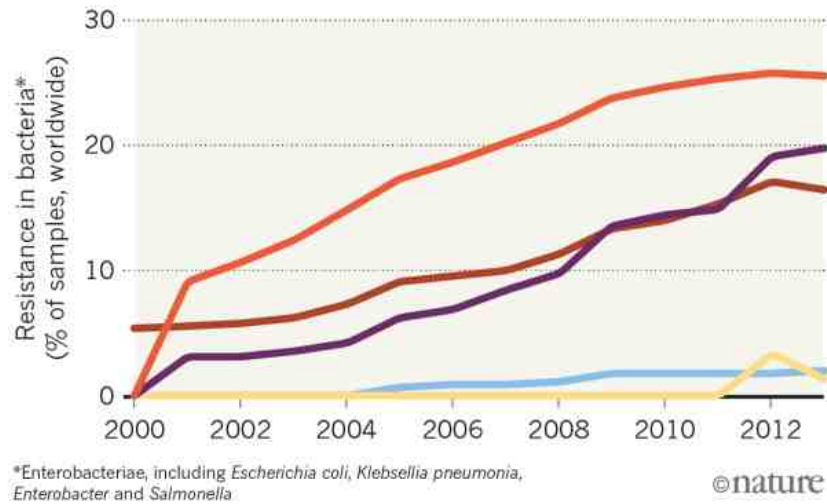


Figure 1-1. The spread of drug resistance to common antibiotics.⁷

To develop novel antimicrobial agents, it is important to study both the mechanisms of action of drugs and the mechanisms of resistance to these drugs. Antibiotics kill bacterial pathogens by targeting essential cellular components. Currently there are several well characterized antibiotic targets in bacteria (Figure 1-2). For instance, β -lactams and their derivatives target cell-wall synthesis, trimethoprim targets folic acid metabolism, quinolones target DNA gyrase and rifamycin targets RNA polymerase.⁸ Among all antibiotic targets, the ribosome is the most common. More than 50% of natural and synthetic antimicrobial agents inhibit bacterial pathogens by targeting the ribosome⁹ (Figure 1-3). The ribosome is a complex bimolecular machine found in all living cells. The ribosome is the protein synthesis machinery that catalyzes the formation of the polypeptide chain. It is an essential cellular component to support cell survival and growth. In most bacteria, the ribosome is the most abundant

intracellular structure. Although the structure and function of the ribosome are phylogenetically conserved across all bacterial species, there are significant structural differences between prokaryotic and eukaryotic ribosomes.¹⁰ The eukaryotic ribosome is larger than the prokaryotic ribosome. This is reflected by the sedimentation coefficient (80S vs. 70S) and the molecular mass (3.2×10^6 vs 2.0×10^6). The length of rRNA sequence is also different between eukaryotic ribosome and prokaryotic ribosome.¹¹ These differences make it possible to develop inhibitors that selectively target the bacterial ribosome. Therefore, the essentiality of the ribosome and the differences between prokaryotic and eukaryotic ribosomes make the ribosome an excellent target for antimicrobial agents.¹² The fact that the ribosome is the most frequent target of antibacterial agents is likely due to the abundance of the ribosome in the cell, its essentiality, and its ancient origin.

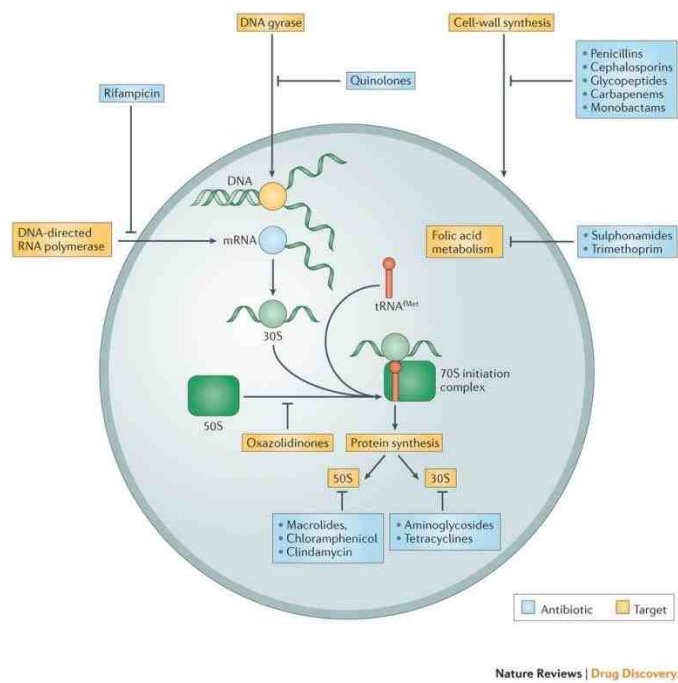


Figure 1-2. Targets of antibiotics⁸

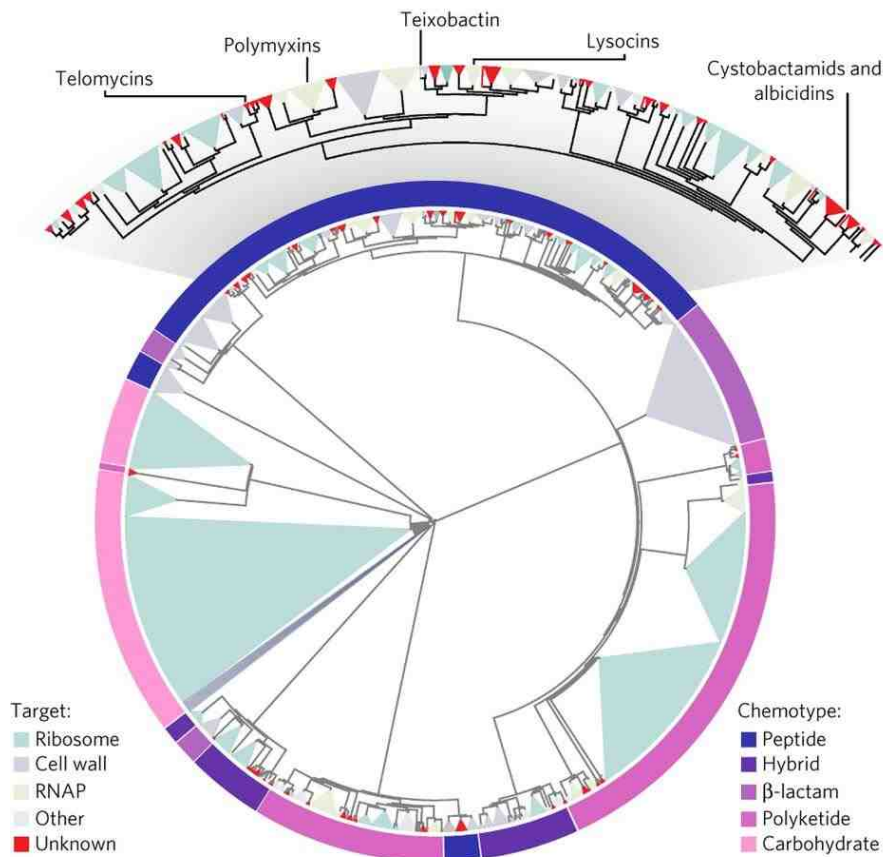


Figure 1-3. Cheminformatic analysis of natural product chemotypes and their target sites⁹

The structure and function of bacterial ribosome and protein synthesis have been well studied, aided greatly by X-ray crystallography. The bacterial ribosome consists of three ribosomal RNA (known as 23S, 16S and 5S rRNA) and 54 ribosomal proteins. The ribosomal RNA is a ribozyme which catalyzes peptide bond formation at the peptidyl-transferase center (PTC).¹³ Functional studies of ribosomal proteins are ongoing. In general, the proposed function of the ribosomal proteins is to coordinate ribosome subunit assembly.¹⁴ The protein synthesis process includes 4 major steps: translation initiation, elongation, termination and ribosome recycling. Translation initiation is the rate limiting step in the protein synthesis. It involves the formation of 30S initiation complex, 50S recruitment and 70S assembly.¹⁵ Translation elongation

involves the delivery of aminoacylated tRNA to the decoding site (A-site), peptide bond formation, tRNA translocation and nascent peptide elongation inside the exit tunnel. Elongation is terminated by binding of release factors. As a result, the polypeptide is released from the ribosome and the ribosome will be recycled for the next round of translation.¹⁶ Most components of the ribosome, and all steps of translation, are essential for protein production by the cell. Therefore protein synthesis is quite fragile; and any molecule that can interfere with translation can adversely affect cell survival.

There are many classes of antimicrobial agents that target the bacterial ribosome. A few of these are clinically used antibiotics, while others are used in the laboratory for ribosome functional studies. In general, they can be divided into 2 groups: those that inhibit the small ribosomal subunit and those that inhibit the large ribosomal subunit inhibitors. Nearly all small subunit inhibitors are small molecules. Their mechanisms of action have been studied in detail by using biochemical techniques^{17, 18, 19}, X-ray crystallography^{16, 20, 21} and single molecule techniques.^{22, 23} As a result of advances in X-ray crystallography of the ribosome, representatives of most major classes of ribosome inhibitors have been co-crystallized with the 70S ribosome.¹⁶ Different types of small subunit inhibitors target different sites on the ribosomal small subunit; but in general they are clustered along the path that the mRNA and tRNAs follow during translation (Figure 1-4). The mechanisms of action of different classes of molecules are distinct. For instance, aminoglycoside antibiotics bind to the h44 region (decoding site), which blocks translocation of mRNA-tRNA and induces miscoding during translation. Tetracycline class antibiotics bind to the h31 region (near the P-site) and block incoming tRNA from binding. Kasugamycin binds to the h24 (also near the P-site) and prevents the recognition of the start codon by the initiator tRNA.¹⁶

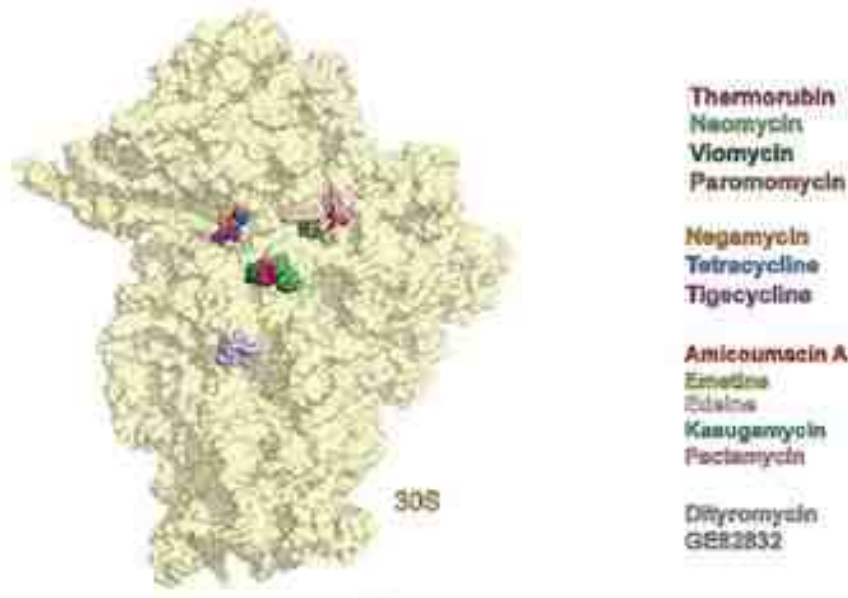


Figure 1-4. Antibiotics targeting the small ribosomal subunit²¹

Large ribosomal subunit inhibitors are comprised of both small molecules and peptides of intermediate molecular weight.²¹ Unlike small ribosomal subunit inhibitors, which bind to several distinct sites, most large subunit inhibitors bind in or near the peptidyl-transferase center (PTC) (Figure 1-5). This is probably due to the importance of the PTC as the catalytic center of ribosome responsible for catalyzing peptide bond formation. However, there are also two known classes of antibiotics that target other regions of the 23S rRNA. Orthosomycins bind to H89 and H91, and block the binding of initiation factor 2 (IF2) to the translation initiation complex.²⁴ Thiopeptides bind to H43 and H44, and block the binding of elongation factors (EF-G and EF-Tu).²⁵ Large subunit inhibitors that target the PTC can be divided into two groups based on their mechanisms of action. Group 1 is comprised of the antibiotics that bind to the PTC itself, such as chloramphenicol, lincosamides, oxazolidinones, puromycin, sparsomycin, blasticidin S, pleuro-mutilin and streptogramin A. Among these antibiotics, some bind to the A-site and compete with the incoming tRNAs (chloramphenicol, lincosamides, oxazolidinones, puromycin and

sparsomycin). Others bind to both A-site and P-site of the PTC (blasticidin S, pleuromutilin and streptogramin A)¹⁶, preventing correct positioning of the aminoacylated ends of tRNAs. Group 2 is comprised of the antibiotics that bind to the nascent polypeptide exit tunnel (NPET). They include the macrolides and streptogramin B. By binding to the NPET, they block elongation of the nascent peptide and cause premature peptidyl-tRNA release, which terminates translation.¹⁶ In addition to these two groups of large subunit inhibitors, it has been recently shown that the proline-rich antimicrobial peptides (PrAMPs) also target the ribosome by binding to the NPET. The PrAMPs were previously thought to target heat-shock protein DnaK. However, recent studies show that PrAMPs bind to DnaK with very low affinity. Ribosome/PrAMP co-crystal structures and biochemical evidence indicate that the ribosome is likely the true target site of PrAMPs.²⁶ This finding could lead to new peptide-based antimicrobial agents. Figure 1-6 is an overview of the known target sites and modes of action of translation inhibitors.

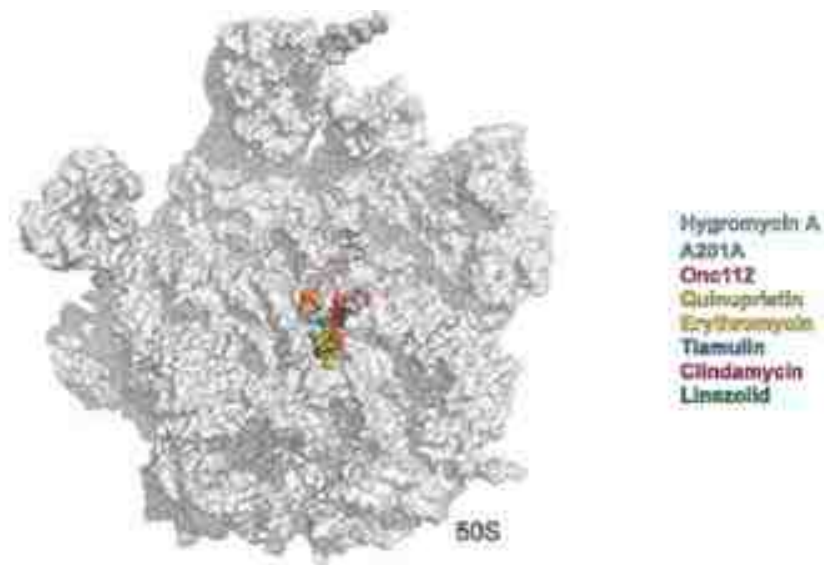
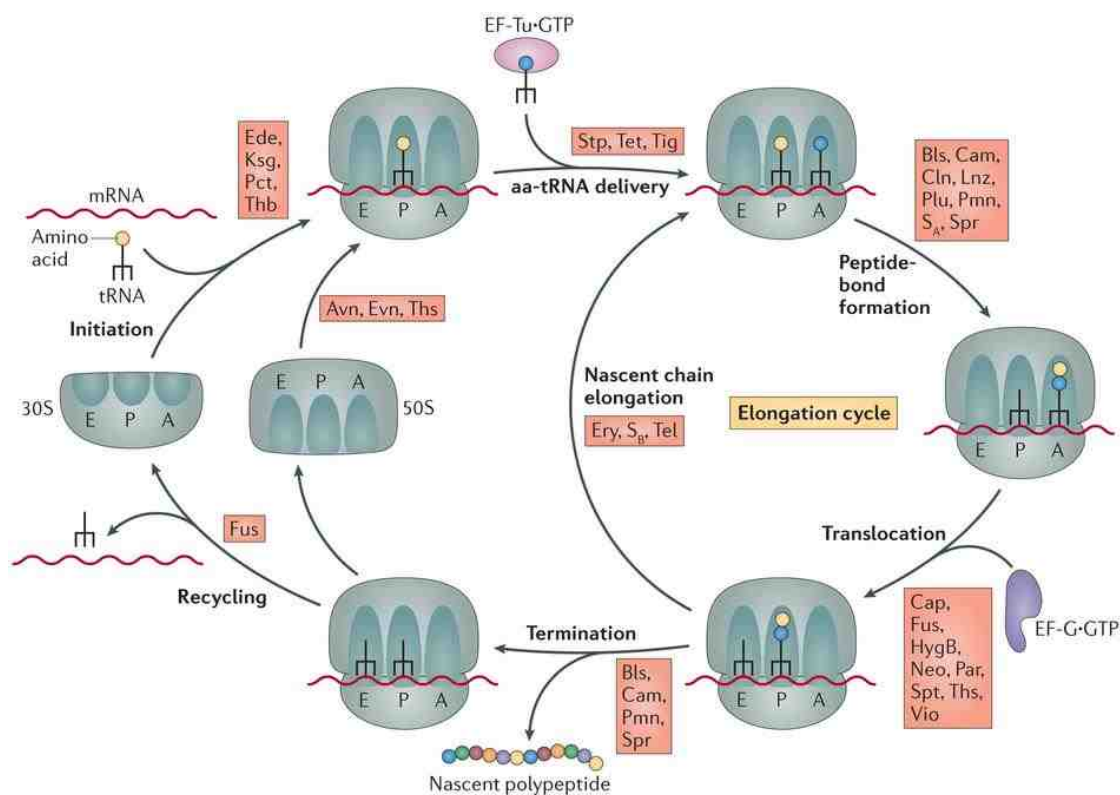


Figure 1-5. Antibiotics targeting the large ribosomal subunit²¹



Nature Reviews | Microbiology

Figure 1-6. Overview of the known target sites and modes of action of translation inhibitors.¹⁶ Ede represents edeine; Kas represents kasugamycin; Pct represents pactamycin; Tnb represents thermorubin; Avn represents avilamycin; Evn represents evernimicin; Ths represents thiostrepton; Stp represents streptomycin; Tet represents tetracyclines; Tig represents tigecycline; Bls represents blasticidin S; Cam represents chloramphenicol; Cln represents clindamycin; Lnz represents linezolid; Plu represents pleuromutilins; Pmn represents puromycin; S_A represents streptogramin A; Spr represents sparsomycin; HygB represents hygromycin; Neo represents neomycin; Par represents paromomycin; Fus represents fusidic acid; Spt represents spectinomycin; Ery represents erythromycin; Tel represents telithromycin.

Although ribosome is the most frequent target for antimicrobial agents, the number of target sites on ribosome is relatively small considering the large size of ribosome. A potential avenue for developing new antimicrobial agents is to identify new target sites on the bacterial ribosome. Yassin *et al* searched for the deleterious mutations on rRNA by functional screening of randomly mutated 16S and 23S rRNA libraries.²⁷ They proposed that sites where deleterious mutations were found are potential new antibiotic target sites due to their essentiality for

ribosome function. Cunningham *et al* also examined deleterious mutations on rRNA to identify potential new antibiotic target sites.²⁸ Instead of generating an rRNA library on the *E. coli* wild type 16S rRNA (as Yassin *et al* had done), they generated a randomly mutated rRNA library on an orthogonal 16S rRNA gene that controls the expression of a reporter gene. Since engineering the orthogonal ribosome doesn't interfere with the cell growth and deleterious mutations can also be studied, they proposed that this system could be used to comprehensively study ribosome sequence/function relationships. Both methods aim to identify functionally important sites in 16S rRNA. Although these methods have potential for identifying new druggable sites on the ribosome, they have not yet led to the discovery of new drugs or drug leads.

2. Technology for detecting and studying ribosome inhibition.

Methods to determine drug potency and study drug mechanisms of action are critical for discovery and development of new antimicrobial agents. Due to the importance of the ribosome as a drug target, several methods have been developed to determine the potency and study the mechanism of action of ribosome inhibitors. In general, these methods can be divided into *in vitro* methods and *in vivo* methods. Currently, *in vitro* methods are more amenable to performing high-throughput screening. However, *in vivo* methods can provide information that is more directly relevant to treating bacterial infections because they use live cells. Both *in vitro* and *in vivo* methods can provide useful information to assist in the development of new antimicrobial agents.

In vitro methods to detect and study ribosome inhibition are usually used to identify the target site and to validate the mechanism of action after identification of initial hit compounds from phenotypic screening. Several *in vitro* methods and systems for assaying ribosome inhibition have been developed. The most well-known method is the *in vitro* translation assay.

Due to its simplicity and accuracy, it is widely used in both academic labs and the pharmaceutical industry. *In vitro* translation assays are typically performed as coupled transcription-translation assays using a DNA template encoding a reporter protein and *E. coli* S-30 extracts. Luciferase is the most commonly used reporter for *in vitro* translation assays. Using the substrate luciferin, which is converted by luciferase to a chemiluminescent product, the relative amount of translation that occurred in a reaction over the time period of the assay can be determined without carrying out protein purification (Figure 1-7).²⁹ Fluorescent or radioactive proteins can be also used as reporters, but require protein purification prior to assay readout. In an *in vitro* translation assay, inhibition of translation can be detected and quantified by observing the decrease in production of reporter protein compared to a positive control. *In vitro* translation reactions can be miniaturized, and thus are amenable to high-throughput assay platforms. Lowell *et al* used *in vitro* translation assay to screen a collection of natural product extracts and identify several new ribosome inhibitors.³⁰ *In vitro* translation assays employing extracts from cells expressing mutant rRNA have been used to address the issue of drug selectivity toward prokaryotic ribosomes. The Böttger group has engineered the h44 region of 16S rRNA in *Mycobacterium smegmatis* to create hybrid ribosomes which contain a eukaryotic h44 region. Surprisingly, the resulting hybrid ribosomes can support cell survival and growth in the absence of a wild type copy of 16S rRNA.³¹ By isolating these hybrid ribosomes from the engineered *M. smegmatis* strain and using them in an *in vitro* translation assay with a luciferase reporter, aminoglycoside antibiotic analogs that are incapable of binding to the eukaryotic h44 site were identified. This system has proven to be an effective way of reducing the side effects of some aminoglycoside antibiotics toward human cells.

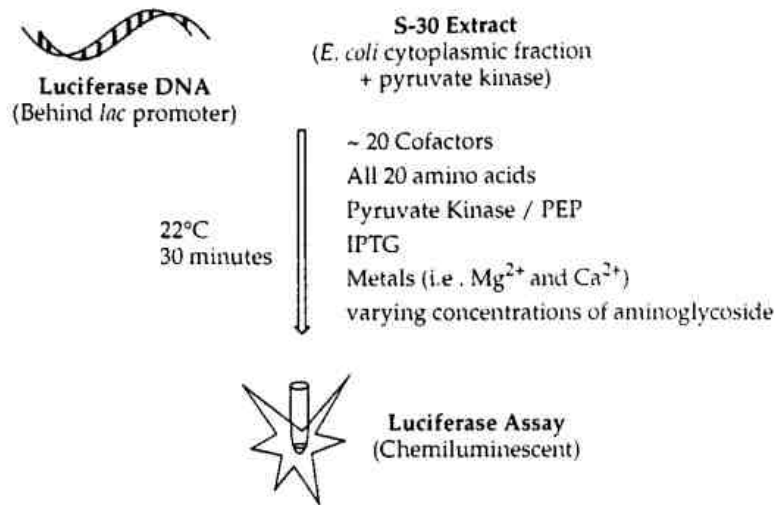


Figure 1-7 *In vitro* translation assay for detecting and quantifying ribosome inhibition²⁹

X-ray crystallography is another well-known and widely used *in vitro* technique to study ribosome inhibition through structural determination of ribosome-drug complexes. Because the ribosome is a large and complex biomolecule, it was extremely challenging to solve its structure. The first high resolution ribosome X-ray crystal structures were not solved until late 1990s. First, the Steitz group and the Yonath group solved structures of the large ribosomal subunits from *Haloarcula marismortui*³² and *Deinococcus radiourans*³³, respectively. Shortly after, the Ramakrishnan group solved the structure of the small ribosomal subunit from *Thermus thermophilus*.³⁴ These achievements led to receipt of the Nobel Prize in chemistry by these three groups in 2009. With continued advances in X-ray crystallography, additional ribosome structures, including those of the *E. coli* and *T. thermophilus* 70S ribosomes in complex with a number of ribosome inhibitors have been solved to date. As an example, Figure 1-9 shows the structure of spectinomycin bound to the *E. coli* 70S ribosome. The ability to solve ribosome-drug co-crystal structures has enabled structure-based drug design of ribosome inhibitors. This approach has been proved invaluable in the development of new antimicrobial agents. For

instance, Rib-X Pharmaceuticals used a structure-based approach to design a series of new oxazolidinone compounds with enhanced activity against drug-resistant pathogens.³⁵ The Lee group also used computer-aided design of new spectinomycin analogs based on the ribosome-spectinomycin co-crystal structure.³⁶ They rationally engineered the 3' ketone group in the C-ring of spectinomycin and generate a series of new compounds. Phenotypic assays demonstrated that some of these new compounds possess improved bioactivity against certain drug resistant pathogens. In summary, the availability of ribosome-drug co-crystal structures has accelerated the development of improved ribosome inhibitors.

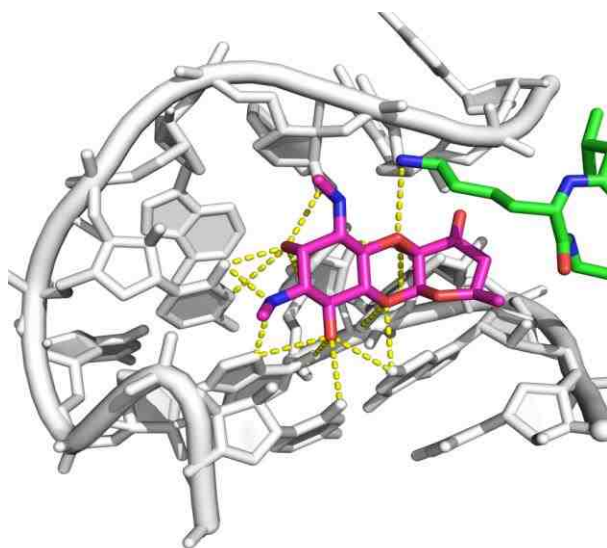


Figure 1-9 Crystal structure showing interactions between spectinomycin and the ribosome

Although X-ray crystallography is a powerful tool to study ribosome-drug interactions, it does not provide information on the effects of inhibitors on the kinetics and dynamics of the ribosome during translation. In recent years single molecule techniques have been used to study changes in ribosome dynamics resulting from inhibition by small molecules. The Puglisi lab used single-molecule fluorescence measurements combined with structural and biochemical

techniques to study the effects of apramycin, paromomycin and gentamicin on ribosome function.²² Although these three drugs bind to the same pocket of the ribosome, and all three were shown to cause miscoding during translation elongation, ribosome dynamics differed in the presence of each of the three drugs. Paromomycin and gentamicin displace the nucleotides A1492 and A1493 and block the intersubunit rotation. Apramycin has only little effect on A1492 and A1493 and causes limited miscoding. The Blanchard lab used single-molecule FRET (fluorescence resonance energy transfer) to study aminoglycoside-ribosome interactions.²³ They found that neomycin and paromomycin, which only differ in the identity of the ring-I 6'-substituent, drive ribosome subunit rotation in different directions. Single-molecule techniques allow us to observe, in unprecedented detail, the effects of antibiotics on the ribosome; and are exciting new tools for studying ribosome inhibition.

RNA footprinting is one of the oldest *in vitro* methods to identify binding sites of ribosome inhibitors. The Noller lab used RNA footprinting to identify the binding sites of several small ribosomal subunit inhibitors (streptomycin, tetracycline, spectinomycin, edeine, hygromycin and neomycin) in 1987.³⁷ A variation on this technology, toe-printing, has been used to identify sites on mRNA where ribosomes treated with drugs stall. Toe-printing uses the drug bound ribosome-mRNA complex derived from cell-free translation reactions as a template for reverse transcriptase PCR (RT-PCR). The RT-PCR reaction will terminate near the site where the ribosome has stalled. By running a DNA sequencing gel, the drug bound ribosome stalling site can be identified. This method is useful for studying the mechanisms of action of certain ribosome inhibitors, particularly those that act by blocking the polypeptide exit tunnel. The Mankin lab used toe-printing analysis to study erythromycin-dependent ribosome stalling. In this study, they determined that the sequence of amino acids of the nascent polypeptide, which

interact with bound drugs in the polypeptide exit tunnel, is the key factor that differentiates the mechanisms of action of erythromycin and telithromycin.³⁸ They also used toe-printing analysis to determine that different ribosome inhibitors display distinct ribosome stalling patterns.³⁹ These patterns can be used to differentiate ribosome inhibitors.

The Deuerling lab recently developed an assay system to identify conditions under which ribosome assembly is impaired. In this system, both the small and large subunit ribosomal subunits are fluorescently labeled.⁴⁰ By measuring the relative fluorescence intensity under various conditions, ribosome assembly can be studied, and the relative assembly rate can be calculated. Using this system, they demonstrated that the fluorescence intensity changes dramatically in the absence of ribosome assembly factors. They also found that the ribosome inhibitors erythromycin and chloramphenicol do not lead to obvious changes in fluorescence intensity, indicating that these two ribosome inhibitors do not affect ribosome assembly. This assay system offers a potential new way to identify inhibitors that specifically target ribosome assembly, and provides a new tool to study the mechanisms of action of known ribosome inhibitors on a deeper level.

As a final example of an *in vitro* method for studying ribosome inhibition, the Mankin lab developed a method whereby an environmentally sensitive fluorophore was installed at several sites of ribosomal protein S12. The fluorescence intensity of the fluorophore will change if an inhibitor binds at a nearby site. Using this method, they were able to determine the K_d values of several ribosome inhibitors. These K_d values correlated well with those obtained using previously published methods. In theory, this approach is general provided that an environmentally sensitive fluorophore can be installed at the desired site.

In contrast to *in vitro* methods, *in vivo* methods for studying ribosome inhibition are limited due to the fact that ribosome is an essential cellular component. There are several reports describing the development of biosensor strains to detect ribosome and translation inhibition. The Karp lab developed an engineered *E.coli* strain which uses a luciferase reporter gene controlled by a temperature sensitive promoter, bacteriophage λ leftward promoter.⁴² Ribosome inhibition was detected and quantified by measuring the luminescence signal upon promoter induction in the presence and absence of inhibitor. This method was able to detect the ribosome inhibition by a panel of known inhibitors. This assay is performed over a 30-45 minute time period due to negative effects on cell viability after exposure to the drug. Later, the authors also improved the signal intensity of the biosensor system by replacing the bacteriophage λ promoter with the tetracycline inducible promoter.⁴³ The assay can also be performed using lyophilized cells. However, low signal intensity and propensity for error limit application of the system.

Another biosensor system to detect ribosome inhibition was developed by Sergiev Lab.⁴⁴ They used an engineered tryptophan attenuator *trpL* placed upstream of a cerulean fluorescent reporter gene. Replacement of two tryptophan codons in *trpL* with alanine renders *trpL* translation independent of the concentration of tryptophan. In the absence of ribosome inhibitors, the *trpL* mRNA adopts a secondary structure that prevents translation of the reporter gene. In the presence of sub-lethal concentration of ribosome inhibitors, the drug-bound ribosome will stall at the *trpL* sequence with increasing frequency, which relieves repression of the reporter gene and results in a fluorescent signal. The biosensor can detect a variety of both small and large ribosomal subunit inhibitors with sub-lethal concentration; and has been used to identify the new ribosome inhibitor amicoumacin A.⁴⁵ The disadvantage of this system is that it is not quantitative, and therefore can only be used to detect ribosome inhibitors.

Use of a similar attenuator-based system to detect ribosome inhibition by macrolides and ketolides was recently reported.⁴⁶ The Mankin lab used the leader sequence of the *ermC* gene (*ermCL*) to control the expression of the *LacZ* reporter gene.⁴⁶ *ermCL* is a regulatory sequence naturally found upstream of the *ermC* rRNA methyltransferase resistance gene in the erythromycin biosynthetic gene cluster. In the absence of 14-membered ring macrolides or ketolides, *ermCL* forms a secondary structure that can prevent expression of downstream genes. In the presence of these compounds, the drug-bound ribosome will stall in the *ermCL* region, changing the secondary structure and allowing translation of downstream genes. This system can be used to detect 14-membered ring macrolides and ketolides, but not 16-membered ring macrolides or other ribosome inhibitors.

A number of biosensors capable of detecting specific natural products, including some ribosome inhibitors, not *via* their interaction with the ribosome, but through interaction with a transcriptional regulator, have been developed. For example, the Karp lab developed a tetracycline biosensor which uses a tetracycline responsive transcriptional repressor protein together with its promoter/operator sequence controlling a gene encoding a bioluminescent reporter.⁴⁷ In the presence of tetracycline class compounds, the repressor protein will dissociate from the promoter upon drug binding, allowing transcription of the promoter gene.

In addition to the *in vivo* systems described above, measuring the growth inhibitory effects of ribosome inhibitors on bacterial pathogens can also be considered an *in vivo* method to evaluate the ribosome inhibition if the compound being studied is already known to be a ribosome inhibitor. This method is usually referred to as the minimum inhibitory concentration (MIC) assay. By measuring concentration dependent growth inhibition of a wild type bacterial strain or one carrying a ribosomal resistance mutation, the potency of the compound against a

specific bacterial strain can be evaluated. Limitations of this method are that it requires the appropriate laboratory environment for working with pathogenic bacterial strains, and it does not provide any *a priori* information regarding the target of the compound.

In summary, both *in vitro* and *in vivo* technologies for detecting and studying ribosome inhibition are useful and valuable for drug development efforts. *In vitro* methods and systems are more favorable because they are fairly straightforward to develop, and produce results that are often more accurate than *in vivo* techniques. However, *in vitro* techniques are more difficult to carry out from a technical standpoint. For example, *in vitro* translation systems employ reagents that require specialized skill to prepare, and are expensive to purchase. Others, such as X-ray crystallography and single-molecule techniques, require specialized instruments and skills to perform the experiments and analyze the data. *In vivo* techniques, on the other hand, are generally more amenable to being carried out in a typical laboratory setting. The disadvantages of most *in vivo* techniques are that they are not quantitative, and do not provide direct information on the interactions between drugs and their targets. Other disadvantages of *in vivo* systems are that most *in vivo* can only detect the ribosome inhibitors at sub-lethal concentrations, and thus cannot accurately assess compound potency; and are narrow with respect to the compounds they can detect. While the currently available *in vitro* and *in vivo* techniques have greatly facilitated the identification and mechanistic study of ribosome inhibitors, there is a need for additional tools that allow simple, high throughput, inexpensive study of ribosome-drug interactions in living bacterial cells.

3. Summary and thesis statement.

Due to the fact that drug-resistant pathogens continually evolve resistance mechanisms upon exposure to new drugs, discovery and development of antimicrobial agents is critical to human health. Current efforts to advance antimicrobial drug discovery include natural product biosynthetic engineering, structure-based drug design, bioinformatics-guided discovery of novel natural products, and exploring novel therapeutic approaches that are less susceptible to drug resistance.⁴⁸ Technologies that can evaluate the activity and study the mechanism of action of compounds generated from these drug development efforts are important for efficiently identifying new drugs and drug leads. Since the bacterial ribosome is the most frequent target for antimicrobial agents, technologies that can detect and study ribosome inhibition by small molecules will greatly accelerate the drug development process.

The work described in this dissertation focuses on the development of novel *in vivo* systems for simply and accurately detecting, quantifying, and studying ribosome inhibition. These systems are based on novel orthogonal ribosome-controlled reporter systems. Chapter 2 describes the development of *in vivo* systems for detecting and quantifying ribosome inhibition by aminoglycoside antibiotics. This system was constructed using an orthogonal ribosome-controlled fluorescent reporter, and was used to examine the potency of a panel of 12 aminoglycoside antibiotics in parallel. The drug activity data obtained using these systems correlate well with previous results obtained using an *in vitro* translation assay.

As described in Chapter 3, these systems were then extended to detect and quantify ribosome inhibition by other small ribosomal subunit inhibitors with binding sites distinct from that of aminoglycosides, including spectinomycin, kasugamycin, and streptomycin. As a proof of

concept, a spectinomycin detection strain was used to screen a set of chemically synthesized spectinomycin analogs which were designed based on the spectinomycin-ribosome co-crystal structure. Three compounds were identified as having ribosome inhibitory activity comparable to or higher than the parent compound. To extend the system to detect inhibitors that bind to the large ribosomal subunit, we employed engineered tethered ribosomes (RiboT) in conjunction with our detection system. The resulting systems are capable of detecting the large ribosomal subunit inhibitors erythromycin, lincomycin, and linezolid. Although some detection systems required optimization during the development process, each final optimized system is ready to use for drug screening applications, and is amenable to high-throughput assay platforms. Potential future applications of these systems include detecting ribosome inhibitors from natural product extracts, engineering natural product biosynthetic enzymes and pathways *in vivo*, and screening compound libraries for ribosome inhibitors.

Identifying drug resistance mutations is an important step both in understanding the mechanism of action of a drug and in assessing the ease with which resistance to the drug can arise due to mutation. Use of orthogonal ribosome systems creates a population of ribosomes free from the constraints of essentiality, which facilitates studies of the effects of rRNA mutations on drug resistance and ribosome fitness. As described in Chapter 4, we used an orthogonal ribosome-controlled selectable marker together with a directed evolution approach to identify mutant rRNA sequences that confer aminoglycoside resistance or dependence; or that affect ribosome fitness, from a large A-site saturation mutagenesis library. We identified and characterized a pool of novel rRNA mutants obtained from selections without aminoglycoside and in the presence of each of the three aminoglycosides kanamycin, neomycin, and gentamicin.

We identified novel aminoglycoside resistant and aminoglycoside dependent mutants, and both hyper- and hypo-active mutants using this approach.

In summary, the work described in this dissertation provides a set of new and powerful tools for detecting, quantifying and studying ribosome inhibition. The engineered *E.coli* strains developed in this work are non-pathogenic and simple to culture. The fluorescence quantification method is general and easy to perform. Therefore, we anticipate that these tools will find broad utility both in the medicinal chemistry and ribosome molecular and synthetic biology communities.

4. References

1. Gould, I.M., A review of the role of antibiotic policies in the control of antibiotic resistance. *J Antimicrob Chemother.* 1999; 43(4):459-65.
2. Chang, J.H., Hung, W.Y., Bai, K.J., Yang, S.F., Chien, M.H. Utility of Plasma Osteopontin Levels in Management of Community-Acquired Pneumonia. *Int J Med Sci.* 2016; 13(9):673-9.
3. Newman, D.J., Cragg, G.M. Natural products as sources of new drugs over the last 25 years. *J Nat Prod.* 2007; 70(3):461-77.
4. Shimuta, K., Unemo, M., Nakayama, S., et al. Antimicrobial resistance and molecular typing of *Neisseria gonorrhoeae* isolates in Kyoto and Osaka, Japan, 2010 to 2012: intensified surveillance after identification of the first strain (H041) with high-level ceftriaxone resistance. *Antimicrob Agents Chemother.* 2013; 57(11):5225-32.

5. Rietberg, K., Lloyd, J., Melius, B., *et al.* Outbreak of *Listeria monocytogenes* infections linked to a pasteurized ice cream product served to hospitalized patients. *Epidemiol Infect.* 2016; 144(13):2728-31.
6. Stoesser, N., Sheppard, A.E., Peirano, G., *et al.* First Report of *bla*MP-14 on a Plasmid Harboring Multiple Drug Resistance Genes in *Escherichia coli* Sequence Type 131. *Antimicrob Agents Chemother.* 2016; 60(8):5068-71.
7. Reardon, S. Spread of antibiotic-resistance gene does not spell bacterial apocalypse — yet. *Nature.* 2015.
8. Kohanski, M.A., Dwyer, D.J., Collins, J.J. How antibiotics kill bacteria: from targets to networks. *Nat Rev Microbiol.* 2010; 8(6):423-35.
9. Johnston, C.W., Skinnider, M.A., Dejong, C.A., *et al.* Assembly and clustering of natural antibiotics guides target identification. *Nat Chem Biol.* 2016; 12(4):233-9.
10. Ben-shem, A., Garreau de loubresse, N., Melnikov, S., Jenner, L., Yusupova, G., Yusupov, M. The structure of the eukaryotic ribosome at 3.0 Å resolution. *Science.* 2011; 334(6062):1524-9.
11. Kozak, M. Initiation of translation in prokaryotes and eukaryotes. *Gene.* 1999; 234(2): 187–208
12. Walsh, C. Where will new antibiotics come from? *Nat Rev Microbiol.* 2003; 1(1):65-70.
13. Ramakrishnan, V. Ribosome Structure and the Mechanism of Translation. *Cell.* 2002; 108(4): 557–572
14. Korobeinikova, A.V., Garber, M.B., Gongadze, G.M. Ribosomal proteins: structure, function, and evolution. *Biochemistry Mosc.* 2012; 77(6):562-74.

15. Espah borujeni, A., Salis, H.M. Translation initiation is controlled by RNA folding kinetics via a ribosome drafting mechanism. *J Am Chem Soc.* 2016; 138(22):7016-23.
16. Wilson, D.N. Ribosome-targeting antibiotics and mechanisms of bacterial resistance. *Nat Rev Microbiol.* 2014; 12(1):35-48.
17. De stasio, E.A., Moazed, D., Noller, H.F., Dahlberg, A.E. Mutations in 16S ribosomal RNA disrupt antibiotic-RNA interactions. *EMBO J.* 1989; 8(4):1213-6.
18. Recht, M.I., Puglisi, J.D. Aminoglycoside resistance with homogeneous and heterogeneous populations of antibiotic-resistant ribosomes. *Antimicrob Agents Chemother.* 2001; 45(9):2414-9.
19. Hobbie, S.N., Pfister, P., Bruell, C., *et al.* Binding of neomycin-class aminoglycoside antibiotics to mutant ribosomes with alterations in the A site of 16S rRNA. *Antimicrob Agents Chemother.* 2006; 50(4):1489-96.
20. Poehlsgaard, J., Douthwaite, S. The bacterial ribosome as a target for antibiotics. *Nat Rev Microbiol.* 2005; 3(11):870-81.
21. Arenz, S., Wilson, D.N. Blast from the Past: Reassessing Forgotten Translation Inhibitors, Antibiotic Selectivity, and Resistance Mechanisms to Aid Drug Development. *Mol Cell.* 2016; 61(1):3-14.
22. Tsai, A., Uemura, S., Johansson, M., *et al.* The impact of aminoglycosides on the dynamics of translation elongation. *Cell Rep.* 2013; 3(2):497-508.
23. Wasserman, M.R., Pulk, A., Zhou, Z, *et al.* Chemically related 4,5-linked aminoglycoside antibiotics drive subunit rotation in opposite directions. *Nat Commun.* 2015; 6:7896.

24. Belova, L., Tenson, T., Xiong, L. Q., *et al.* A novel site of antibiotic action in the ribosome: interaction of evernimicin with the large ribosomal subunit. *Proc. Natl Acad. Sci. USA.* 2001; **98**, 3726–3731.
25. Wilson, D. N. The A-Z of bacterial translation inhibitors. *Crit. Rev. Biochem. Mol. Biol.* 2009; **44**, 393–433.
26. Gagnon, M.G., Roy, R.N., Lomakin, I.B., *et al.* Structures of proline-rich peptides bound to the ribosome reveal a common mechanism of protein synthesis inhibition. *Nucleic Acids Res.* 2016; 44(5):2439-50.
27. Yassin, A., Fredrick, K., Mankin, A.S. Deleterious mutations in small subunit ribosomal RNA identify functional sites and potential targets for antibiotics. *Proc Natl Acad Sci USA.* 2005; 102(46):16620-5.
28. Cunningham, P. Targets for the identification of antibiotics that are not susceptible to antibiotic resistance. 2015; U.S Patent. US 8987432 B2
29. Greenberg, W. A., Priestley, E. S., Sears, P. S., *et al.* Design and synthesis of new aminoglycoside antibiotics containing neamine as an optimal core structure: correlation of antibiotic activity with in vitro inhibition of translation. *J. Am. Chem. Soc.* 1999; 121, 6527–6541.
30. Lowell, A.N.; Santoro, N.; Swaney, S.M., *et al.* Microscale adaptation of *in vitro* transcription/translation for high-throughput screening of natural product extract libraries. *Chem. Biol. Drug Des.* 2015; 86, 1331–1338.
31. Hobbie, S.N., Kalapala, S.K., Akshay, S, *et al.* Engineering the rRNA decoding site of eukaryotic cytosolic ribosomes in bacteria. *Nucleic Acids Res.* 2007; 35(18):6086-93.

32. Ban, N., Nissen, P., Hansen, J., Moore, P.B., Steitz, T.A. The complete atomic structure of the large ribosomal subunit at 2.4 Å resolution. *Science*. 2000; 289(5481):905-20.
33. Harms, J., Schluenzen, F., Zarivach, R., *et al.* High resolution structure of the large ribosomal subunit from a *mesophilic eubacterium*. *Cell*. 2001; 107(5):679-88.
34. Wimberly, B.T., Brodersen, D.E., Clemons, W.M., *et al.* Structure of the 30S ribosomal subunit. *Nature*. 2000; 407(6802):327-39.
35. Lawrence, L., Danese, P., Sutcliffe, J. *In vitro* activity of designer oxazolidinones against Gram-positive hospital pathogens. In: Proceedings of the 45th Interscience Conference on Antimicrobial Agents and Chemotherapy, Abstract A-3434. Washington, DC; 2005.
36. Bruhn, D.F., Waidyarachchi, S.L., Madhura, D.B., *et al.* Aminomethyl spectinomycins as therapeutics for drug-resistant respiratory tract and sexually transmitted bacterial infections. *Sci Transl Med*. 2015; 7(288):288ra75.
37. Moazed, D., Noller, H.F. Interaction of antibiotics with functional sites in 16S ribosomal RNA. *Nature*. 1987; 327(6121):389-94.
38. Gupta, P., Liu, B., Klepacki, D., *et al.* Nascent peptide assists the ribosome in recognizing chemically distinct small molecules. *Nat Chem Biol*. 2016; 12(3):153-8.
39. Orelle, C., Carlson, S., Kaushal, B., *et al.* Tools for characterizing bacterial protein synthesis inhibitors. *Antimicrob Agents Chemother*. 2013; 57(12):5994-6004.
40. Nikolay, R., Schloemer, R., Schmidt, S., *et al.* Validation of a fluorescence-based screening concept to identify ribosome assembly defects in *Escherichia coli*. *Nucleic Acids Res*. 2014; 42(12):e100.
41. Llano-sotelo, B., Hickerson, R.P., Lancaster, L., *et al.* Fluorescently labeled ribosomes as a tool for analyzing antibiotic binding. *RNA*. 2009; 15(8):1597-604.

42. Lampinen, J., Virta, M., Karp, M. Use of controlled luciferase expression to monitor chemicals affecting protein synthesis. *Appl Environ Microbiol.* 1995; 61(8):2981-9.
43. Galluzzi, L., Karp, M. Amplified detection of transcriptional and translational inhibitors in bioluminescent *Escherichia coli* K-12. *J. Biomol. Screen.* 2003, 8, 340–346.
44. Osterman, I.A., Prokhorova, I.V., Sysoev, V.O., *et al.* Attenuation-based dual-fluorescent-protein reporter for screening translation inhibitors. *Antimicrob. Agents Chemother.* 2012, 56, 1774–1783.
45. Polikanov, Y.S, Osterman, I.A, Szal, T., *et al.* Amicoumacin A inhibits translation by stabilizing mRNA interaction with the ribosome. *Mol Cell.* 2014; 56(4):531-40.
46. Bailey, M., Chettiath, T., Mankin, A.S. Induction of *erm(c)* expression by non-inducing antibiotics. *Antimicrob. Agents Chemother.* 2008, 52, 866–874.
47. Kurittu, J., Karp, M., Korpela, M. Detection of tetracyclines with luminescent bacterial strains. *Lumin J. Biol. Chem. Lumin.* 2000, 15, 291–297.
48. Bikard, D., Euler, C.W., Jiang, W., *et al.* Exploiting CRISPR-Cas nucleases to produce sequence-specific antimicrobials. *Nat Biotechnol.* 2014; 32(11):1146-50.

CHAPTER 2. DEVELOPMENT OF DETECTION AND QUANTIFICATION SYSTEMS FOR RIBOSOME INHIBITION BY AMINOGLYCOSIDE ANTIBIOTICS

1. Introduction

The ribosome is a complex, highly conserved biomolecular machine essential for the biosynthesis of cellular proteins and peptides. The essentiality and ancient origin of the ribosome have made it one of the most frequent targets of antibacterial natural products.¹ Of the many known classes of ribosome inhibitors, the aminoglycosides (Figure 2-1) are perhaps the best-studied with regard to their mechanisms of action,²⁻⁴ drug resistance,²⁻⁴ and biosynthesis.⁵⁻⁷ Aminoglycosides are a clinically useful class of ribosome inhibitors with broad spectrum activity toward a variety of microbial pathogens. However, their widespread clinical use has been hampered by low-level toxicity to human mitochondrial ribosomes.²⁻⁴ Aminoglycosides can impair ribosome function by affecting the efficiency of intersubunit rotation,^{8 - 10} translocation,^{2,3,11,12} and ribosome recycling⁸ and by inducing translational miscoding^{2-4,13} through specific interactions with the decoding site (A-site) of the 16S rRNA in helix 44 (h44) of the small (30S) ribosomal subunit¹⁴⁻¹⁷ (Figure 2-1), and in the case of some aminoglycosides, with helix 69 (H69) of the large (50S) ribosomal subunit.^{8,10,12,15,18} Aminoglycosides also show promise as treatments for other diseases, including HIV², human genetic disorders, where their ability to induce miscoding has been used to suppress disease-associated premature termination codons,^{2,19} and fungal infection, where amphiphilic aminoglycoside analogs have been shown to perturb the function of the fungal plasma membrane.²⁰

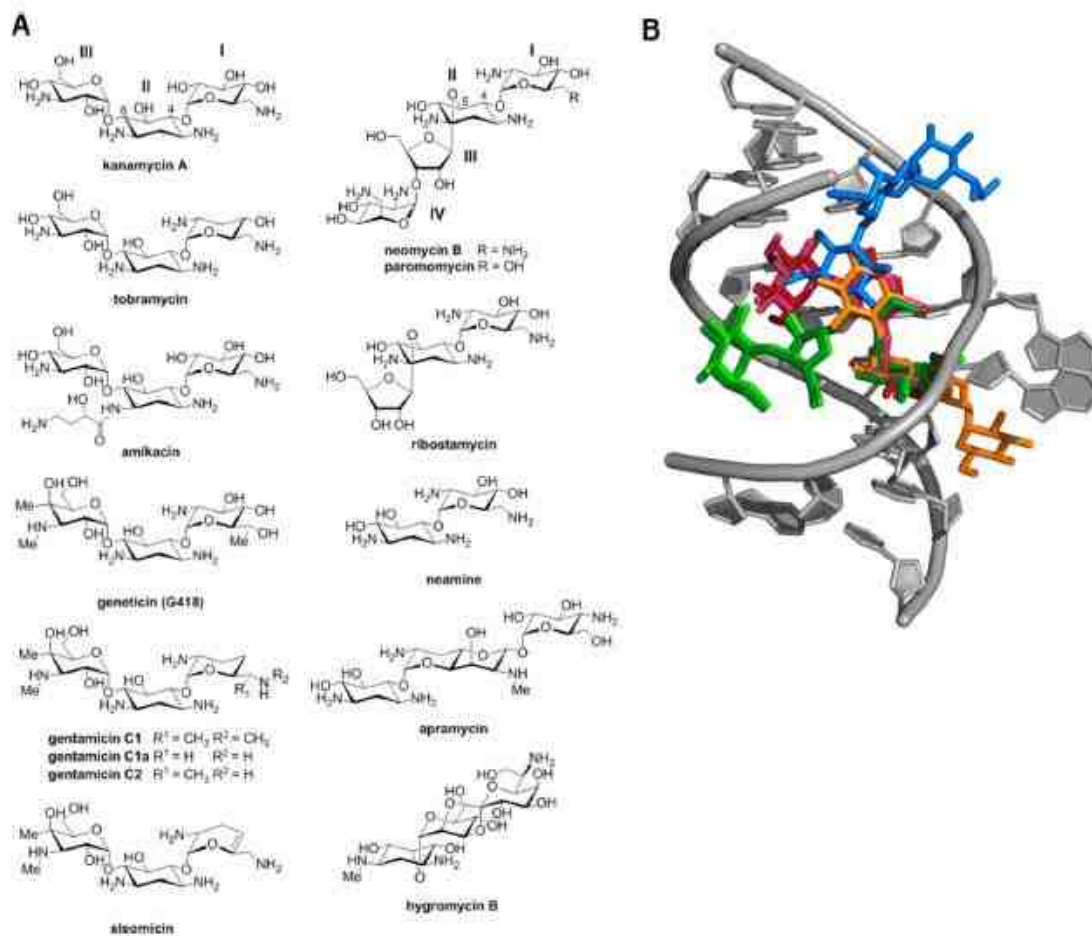


Figure 2-1 (A) Structures of aminoglycosides used in this study. (B) Overlaid X-ray crystal structures of the decoding site (A-site) of the *E. coli* 16S rRNA with select aminoglycosides bound. Residues 1403–1411 and 1489–1498 of 16S rRNA are shown in gray. Aminoglycosides are color-coded as follows, and the source PDB file for each is given in parentheses: kanamycin A, maroon (2ESI²³); gentamicin, purple (2QB9¹⁵); geneticin (G418), pink (1MWL²²); neomycin B, dark green (2QAL¹⁵); paromomycin, light green (2Z4K¹⁵); apramycin, orange (4AQY¹⁷); hygromycin, blue (3DF1¹⁶).

Much of our current understanding of aminoglycoside/rRNA interactions, potency as ribosome inhibitors, and mechanisms of action comes from *in vitro* studies. The target sites of several aminoglycosides were first identified using RNA footprinting¹⁴ and were later examined in detail by X-ray crystallography.^{15–17,21,22} Affinities of aminoglycosides for rRNA hairpins mimicking the A-site have been assessed using mass spectrometry,²³ surface plasmon resonance (SPR),²⁴ NMR,¹⁸ and competition assays.²⁵ However, it has been observed that binding affinities

of some aminoglycosides to A-site rRNA mimics do not correlate linearly with inhibition of translation *in vitro* or antibacterial potency *in vivo*,²⁶ indicating that the results of assays using A-site mimics are not fully equivalent to those obtained when employing intact ribosomes *in vitro* or *in vivo*. Ribosome inhibition is also commonly measured directly using *in vitro* translation systems. These studies have revealed that individual aminoglycosides differ significantly with respect to their potencies as ribosome inhibitors.²⁶⁻³⁰ Recently, such systems have been combined with powerful single molecule techniques such as smFRET to probe the effects of aminoglycosides on the kinetics and dynamics of the individual steps of translation, revealing that individual aminoglycosides differ markedly with respect to their effects on these steps.^{8-10,12} However, *in vitro* translation experiments designed to investigate drug binding mode or mechanism of action are technically challenging to carry out, and *in vitro* translation assays in general either require expensive reagents or specialized preparation methods and cannot provide information on *in vivo* properties such as compound membrane permeability or efflux.

In contrast to the breadth of techniques available for *in vitro* studies, *in vivo* analyses of the effects of aminoglycosides have been limited to measuring the growth inhibitory effects (most commonly reported as minimum inhibitory concentrations, MICs) of the compounds on wild-type bacterial strains and on those carrying ribosomal resistance mutations.³¹⁻³³ Although such assays are operationally simple and provide direct information on a compound's ability to inhibit bacterial growth, they do not provide any information a priori regarding the biomolecular target(s) of a drug (the ribosome in the case of aminoglycosides), the target binding site(s) (the A-site, and in some cases H69 for aminoglycosides), or the mechanism(s) by which a drug exerts its effects on the target.

Considering the limitations of existing *in vitro* and *in vivo* technologies, we envisioned an alternative *in vivo* strategy for investigating ribosome inhibition by small molecules that combines the ability of *in vitro* assays to quantitatively probe the effects of binding to a specific target site with the operational ease and *in vivo* relevance of live cell antibacterial assays. This strategy utilizes orthogonal ribosomes (O-ribosomes) - specialized mutant ribosomes that, by virtue of a mutated 16S rRNA anti-Shine-Dalgarno (ASD) sequence, are unable to translate native mRNA, yet retain the ability to translate mRNA carrying a complementary mutant Shine-Dalgarno (SD) sequence³⁴⁻³⁶ to circumvent the limitations imposed by ribosome essentiality. We hypothesized that O-ribosomes, if used to control expression of an engineered genetic circuit that results in a quantifiable “turn-on” phenotype upon ribosome inhibition, could be used to quantify ribosome inhibition by aminoglycosides or other ribosome inhibitors, providing a means of rapidly assessing the target specificity and ribosome inhibiting potency of these compounds in live bacterial cells. Such an O-ribosome-based assay would facilitate studies of mechanisms of drug action and of the relationship between target rRNA sequence and drug activity that can lead to discovery of ribosome inhibitors with improved therapeutic properties.

Our aminoglycoside responsive strains were designed to harbor an engineered plasmid-borne reporter system comprised of three elements (Figure 2-2): (1) a constitutively expressed aminoglycoside-sensitive orthogonal 16S rRNA (O-16S) gene bearing a mutated anti-Shine-Dalgarno (O-ASD) sequence,³⁵ (2) the *tetR* gene encoding a constitutively expressed tetracycline-responsive repressor protein TetR37 with orthogonal SD (O-SD) sequence complementary to the 16S rRNA OASD sequence,³⁵ and (3) the *gfp-uv* gene encoding green fluorescent protein variant GFPuv³⁸ under transcriptional control of the TetR-repressed promoter PLtetO-1.³⁹ In the absence of aminoglycoside (Figure 2-2), cells bearing these three elements

would produce O-ribosome-derived TetR that represses transcription of *gfp-uv*, resulting in no fluorescence. However, in the presence of aminoglycoside (Figure 2-2), the O-ribosome is inhibited, resulting in a reduced level of TetR, derepression of *gfp-uv* transcription, and production of GFP. The system is designed to be highly sensitive by substantially amplifying the aminoglycoside input signal through transcription and translation of *gfp-uv*, resulting in production of multiple GFP proteins per aminoglycoside molecule.

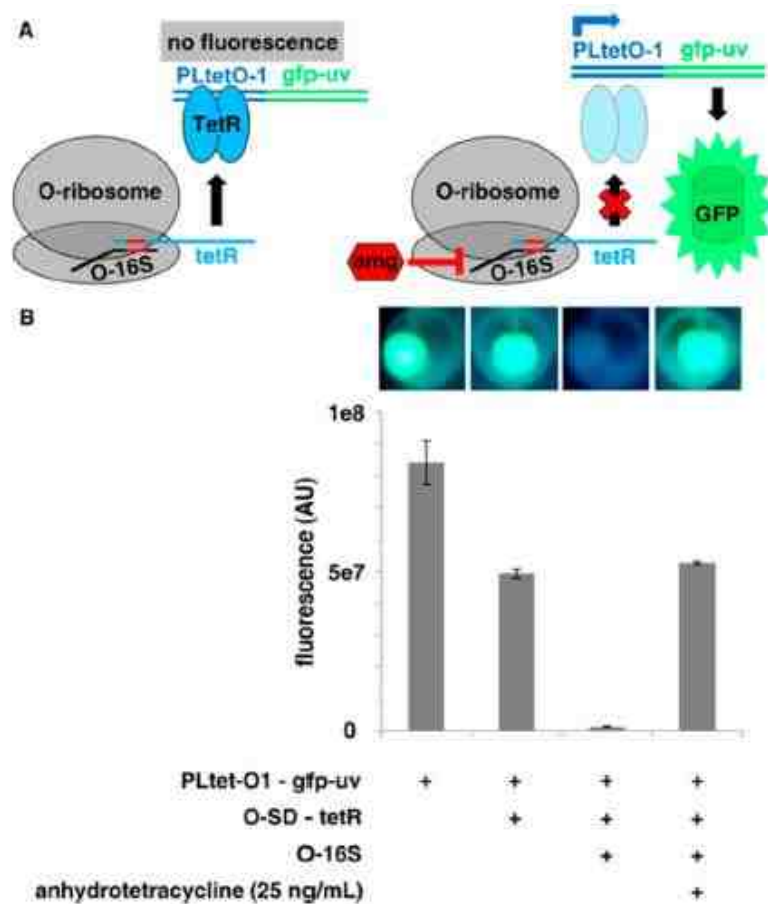


Figure 2-2. (A) Schematic showing the functionality of the orthogonal ribosome-controlled fluorescent reporter in the absence (left panel) and presence (right panel) of aminoglycoside. The O-16S rRNA is shown in black, O-SD/O-ASD pair is shown in red, tetR mRNA and TetR protein are shown in cyan, PLtetO-1 is shown in blue, the *gfp-uv* gene and GFP protein are shown in green, and aminoglycoside is shown as a red hexagon. (B) Cell pellet fluorescence and fluorescence quantification of *E. coli* DH5 α cells transformed with individual and combined functional elements of the orthogonal ribosome-controlled fluorescent reporter.

To protect the *E. coli* host itself from inhibition by aminoglycosides, the strain's native rRNA was made aminoglycoside resistant using a previously developed host, *E. coli* SQ380, in which all seven chromosomal copies of the rRNA operon were deleted and replaced by a single rRNA operon on plasmid prnC-sacB bearing the counter-selectable marker sacB gene. The A1408G 16S rRNA mutation, which confers resistance to many aminoglycosides,³¹ was introduced into rRNA operon expressing plasmid pRRSH2. The resulting plasmid, pRRSH2-A1408G, was used to replace prnC-sacB in SQ380. The aminoglycosides resistant strain was then used as the host to harbor the O-ribosome-controlled tetR-gfpuv genetic circuit.

Here, we have created engineered *E. coli* strains harboring the O-ribosome-controlled green fluorescent protein (GFP) reporter that are non-fluorescent in the absence of a drug but express GFP upon O-ribosome inhibition. We show that these strains are able to detect ribosome inhibition by a collection of 12 structurally diverse aminoglycosides in a highly sensitive, dose-dependent manner with essentially no background. The fluorescence dose response patterns we observed for engineered *E. coli* detection strains treated with these aminoglycosides correlate with the results of *in vitro* translation inhibition assays, validating the accuracy of our assay in assessing the potencies of aminoglycosides as ribosome inhibitors. Our results provide a full comparative assessment of the ribosome inhibiting potencies of the 12 aminoglycosides assayed. Thus, the O-ribosome reporter system developed here provides a powerful new tool for easily and rapidly assessing the relative potencies of aminoglycosides as ribosome inhibitors in live bacterial cells.

2. Experimental procedures

General. All general molecular biological and biochemical reagents, including Luria Bertani (LB) media (Miller), were purchased from VWR (Atlanta, GA) and were used without

further purification. Water used for media was obtained from a Barnstead/Thermolyne HN Ultrapure water purification system. Gentamicin sulfate, paromomycin sulfate, geneticin (G418) sulfate, neomycin sulfate, hygromycin B, amikacin disulfate, sisomicin sulfate, tobramycin sulfate, ribostamycin sulfate, and neamine hydrochloride were purchased from Santa Cruz Biotechnology (Dallas, TX). Kanamycin sulfate was purchased from Genlantis (San Diego, CA). Apramycin sulfate was purchased from Research Products International (Mount Prospect, IL). Restriction enzymes, Phusion DNA polymerase, T4 DNA ligase and calf intestinal alkaline phosphatase were purchased from New England Biolabs (Ipswich, MA). DNA purification and concentration was performed using the DNA Clean & Concentrator Kit; and agarose gel DNA extraction was performed using the Gel DNA Recovery Kit, both from Zymo Research (Irvine, CA). Plasmid extractions were performed using the QIAprep Spin Miniprep Kit from Qiagen (Valencia, CA). Oligonucleotides were obtained from Integrated DNA Technologies (Coralville, IA). DNA sequencing was performed by Genewiz (South Plainfield, NJ). PCR reactions were carried out using a Bio-Rad S1000 thermal cycler. Cell density and fluorescence measurements were taken using a Molecular Devices SpectraMax M2 Multi-Mode Microplate Reader. Plasmid and DNA sequence design and management was conducted using Vector NTI 10 (Life Technologies). Chemically competent *E. coli cells* were prepared using the rubidium chloride method.⁴⁰ Standard molecular biological methods, protocols, reagents, and materials⁴⁰ were used for PCR, restriction enzyme digestion, ligation, transformation, selection of transformants, agarose gel electrophoresis, gel extraction, and plasmid isolation unless otherwise specified.

Bacterial strains. *E. coli* DH5 α and *E. coli* TOP10 were used for routine DNA cloning and manipulation. *E. coli* SQ380 (*E. coli* MG1655/ Δ rrnGADEHBC/prnC-sacB⁴¹/ptRNA67⁴¹, S. Quan and C. Squires, unpublished), in which all seven genomic rRNA operons have been deleted

and replaced with a single plasmid-borne rRNA operon expressed from the sucrose counter-selectable plasmid prrnC-sacB, was used as the starting point for construction of strains capable of detecting ribosome inhibition by aminoglycoside antibiotics.

Bacterial culture. Routine liquid culture of *E. coli* DH5 α and *E. coli* TOP10 for cloning purposes was carried out in 2-5 mL of Luria-Bertani broth in sterile 15 mL conical tubes at 37 °C, 250 rpm overnight (12-16 h). Selection of *E. coli* DH5 α and *E. coli* TOP10 transformants was carried out on Luria-Bertani agar plates containing the appropriate antibiotic(s) at 37 °C overnight (12-16 h). All cell growth and fluorescence assays were performed in sterile Cellstar 96-well deep well culture plates sealed with breathable sealing film, with one mL of LB media per well and with appropriate concentrations of the necessary antibiotics (ampicillin - 100 μ g/mL, chloramphenicol - 35 μ g/mL, kanamycin - 50 μ g/mL, spectinomycin - 100 μ g/mL), anhydrotetracycline (1-100 ng/mL) and aminoglycoside (1-1024 μ M).

| <u>Protocol 1</u> | | <u>Protocol 2</u> | <u>Protocol 3</u> | | <u>Protocol 4</u> | |
|-------------------|----------|---|--------------------------------------|--|-----------------------------|---------|
| 98 °C | 30 s | Same as Protocol 1, but with no template, and with 0.1 μ M inside primer, 0.5 μ M of each of the two outside primers. | 98 °C | 30 s | Used 10 nM of each fragment | |
| 98 °C | 10 s | | 98 °C | 10 s | | |
| Tm-prim - 5 | 30 s | | Tm-OE - 5 | 30 s | | |
| 72 °C | 30 s/kb | | 72 °C | 30 s/kb | 98 °C | 30 s |
| Repeat 2 times | | | Repeat 1-9 times | | 98 °C | 10 s |
| 98 °C | 10 s | | (primerless) | | 48-50 °C | 30 s |
| Tm-ext - 5 | 30 s | | Add 0.5 μ M of 2 outside primers | | 72 °C | 15 s/kb |
| 72 °C | 30 s/kb | | | | (of final plasmid size) | |
| Repeat 26 times | | | 98 °C | 10 s | Repeat 29-34 times | |
| 72 °C | 10 m | | Tm-ext - 5 | 30 s | 72 °C | 10 m |
| 4 °C | ∞ | 72 °C | 30 s/kb | 4 °C | ∞ | |
| | | Repeat 29 times | | Fragment junctions were designed to have Tm of 55 +/- 5 °C | | |
| | | 72 °C | 10 m | | | |
| | | 4 °C | ∞ | | | |

Tm-prim = Tm of the portion of the primer that primes to the template
Tm-ext = Tm of the entire primer
Tm-OE = Tm of the junction between fragments

Figure 2-3. PCR protocols used in this work

General PCR conditions. Concentrations of template, primers, polymerase, dNTPs, and buffer recommended by NEB for Phusion DNA polymerase were used unless otherwise specified. We employed four types of PCR protocols to construct all fragments and all final constructs not obtained by ligation: Protocol 1) PCR amplification of a single fragment with two primers, Protocol 2) templateless (primer only) assembly with three primers, Protocol 3) two fragment overlap extension PCR, and Protocol 4) COE-PCR (see Section 2.2.1 for an explanation of this method). General PCR programs for each protocol are given in Figure 2-3

Enforced replacement by sucrose counterselection. To replace plasmid *prnC-sacB* (KanR, SucS) which is essential in *E. coli* SQ380 because it carries the only cellular copy of the ribosomal RNA (rRNA) operon, with pRRSH2 (AmpR), pRRSH2-A1408G, or pRRSH2-U1406A, we employed sucrose counterselection against the *sacB* (sucrose sensitivity gene)-containing plasmid *prnC-sacB*. *E. coli* SQ380 competent cells were grown in LB with kanamycin and spectinomycin (essential tRNA-bearing plasmid *ptRNA67* has a spectinomycin resistance marker) and transformed with pRRSH2, pRRSH2-A1408G, or pRRSH2-U1406A. Transformants were selected on LB agar with ampicillin and spectinomycin. One colony was picked and grown in LB liquid with ampicillin and spectinomycin overnight, and plated on LB agar with ampicillin, spectinomycin, and 5% (w/v) sucrose. Surviving colonies are resistant to both ampicillin and sucrose, and have therefore gained pRRSH2 and lost *prnC-sacB*. Elimination of *prnC-sacB* was verified by plasmid isolation and digestion of the resulting plasmid mixture with PvuI, which has 3 recognition sites in *prnC-sacB* but only a single site in pRRSH2 and *ptRNA67*, and therefore gives a distinctive digestion pattern if *prnC-sacB* is present. This, rather than replica plate screening of surviving colonies for kanamycin sensitivity, was done because pRRSH2-A1408G and pRRSH2-U1406A confer kanamycin resistance. The

resulting strains - SH430 containing pRRSH2, SH386 containing pRRSH2-A1408G, and SH424 containing pRRSH2-U1406A – were used for transformation with plasmids carrying the O-ribosome-based aminoglycoside detection systems (pSH3-KF through pSH14-KF).

Cell density and fluorescence assays. All cell density and fluorescence measurements were taken in triplicate. 96-well culture plates (1 mL LB per well) with appropriate concentrations of necessary antibiotics and aminoglycoside were inoculated 1:100 from a saturated overnight liquid culture and allowed to grow for 18-24 h at 37 °C, 200 rpm shaking. For cell density assays, 40 µL of sample was taken from each well, diluted 5-fold, and OD600 was measured by microplate reader. The OD600 of the original culture was calculated by multiplying the reading by the dilution factor (5). For cell pellet fluorescence imaging, cells were pelleted by centrifugation (4,000 g, 15 m, 4 °C) and the supernatant was decanted completely. The underside of the plate was illuminated at 365 nm using an ultraviolet handheld lamp and photographed with an 8 megapixel digital camera. For fluorescence quantification, cell pellets were resuspended in 1 mL of $\frac{1}{4}\times$ Ringer's solution (30.75 mM NaCl, 1.2 mM, KCl, 1.5 mM CaCl₂, pH 7.3-7.4), 200 µL of cells from each well were transferred to black 96-well plates, and GFP fluorescence was measured (excitation = 395 nm, bandwidth = 9 nm; emission = 509 nm, bandwidth = 15 nm). Fluorescence intensities were calculated as fluorescence/OD600 of the sample minus fluorescence/OD600 of a sample of a non-GFP-expressing *E. coli* strain parental to the strain being analyzed in order to correct for both cell density and *E. coli* auto-fluorescence.

Calculation of IC50, LD50 values and correlation analysis. Aminoglycoside IC50 values were calculated by fitting fluorescence data obtained by incubating detection strains SH399 or SH431 with aminoglycosides at concentrations from zero to the concentration that gives maximal fluorescence signal to a sigmoidal equation by non-linear regression. The IC50 value is

the concentration of aminoglycoside that gives half maximal fluorescence. Aminoglycoside LD50 values were calculated by fitting OD600 data obtained by incubating the parent aminoglycoside sensitive strain SH434 with aminoglycosides at concentrations from zero to 32 μM (or 1024 μM for neamine and hygromycin B) to a sigmoidal equation by non-linear regression. The LD50 value is the concentration of aminoglycoside that gives 50% growth inhibition (an OD600 value that is 50% of the maximal OD600 value). Correlation between IC50 values calculated from fluorescence data and either previously reported IC50 values obtained from *in vitro* translation assays²⁸ or LD50 values calculated from OD600 data were assessed by linear regression analysis. The IC50 and LD50 values determined, and the results of linear regression are summarized in Figure 2-23.

Construction of pRRSH2. Plasmid pKK3535⁴² (11.9 kb), which contains the constitutively expressed *rrnB* ribosomal rRNA operon, pMB1 origin of replication, and ampicillin resistance marker, as well as 4.2 kb of non-essential DNA sequence, was used as the starting point for construction of a simplified, refactored *rrnB*-expressing plasmid pRRSH2 (7.7 kb) (Figure 2-4), which also bears the ampicillin resistance marker, but contains the p15A origin of replication. To construct pRRSH2, we employed concatamerizing overlap extension PCR (COE-PCR, C. Melançon, unpublished), a *de novo* plasmid assembly method developed in our group that is similar to the CPEC method.⁴³ In COE-PCR, a circular plasmid is obtained by one pot PCR assembly of linear fragments with short (15-25 bp) overlapping ends followed by transformation of competent *E. coli* with the PCR assembly mixture. The 5.8 kb *rrnB* operon was amplified as three fragments from pKK3535 using primer pairs pRRSH-rRNA1-up/pRRSH-rRNA1-dn, pRRSH-rRNA2-up/pRRSH-rRNA2-dn, and pRRSH-rRNA3-up/pRRSH-rRNA3-dn. The fragment containing the promoter and coding region of the ampicillin resistance marker was

amplified from pKK3535 using primers pRRSH-AmpR-up and pRRSH-AmpR-dn. The fragment containing the p15A origin of replication was amplified from pRepCM3⁴⁴ using primers pRRSH-p15A-up and pRRSH-p15A-dn. The resulting five DNA fragments were assembled by COE-PCR and the reaction mixture was concentrated using the Zymo Clean and Concentrator Kit, and introduced into competent *E.coli* DH5a cells. The final pRRSH2 construct was verified by restriction mapping and sequencing. Primer information is given in table 2-1 below. The priming region of each primer is underlined.

| primer name | sequence (5' – 3') | amplicon size (bp) | template |
|----------------|---|--------------------|----------|
| pRRSH-rRNA1-up | <u>TTTGGTTGAATGTTGCCGCGGTC</u> | 2116 | pKK3535 |
| pRRSH-rRNA1-dn | <u>CGGTGTCCTGGGCCTCTAGAC</u> | | |
| pRRSH-rRNA2-up | <u>TCTAGAGGCCCCAGGACACCGCCCTTTCACGGCGGTAACAG</u> | 2022 | pKK3535 |
| pRRSH-rRNA2-dn | <u>CTGGTATCTTCGACTGATTTTCAGCTCCATCCGCGAGGGACC</u> | | |
| pRRSH-rRNA3-up | <u>GCTGAAATCAGTCGAAGATACCAGCTGGC</u> | 1677 | pKK3535 |
| pRRSH-rRNA3-dn | <u>AGCTGCTTTCCTGATGCAAAAACG</u> | | |
| pRRSH-AmpR-up | <u>CGTTTTTGCATCAGGAAAGCAGCTGATATCAGACGTCAGGTGGCACTTTTC</u> | 1077 | pKK3535 |
| pRRSH-AmpR-dn | <u>CATATGATCAATCTAAAGTATATATGAGTAAACTTGGTCTGACAG</u> | | |
| pRRSH-p15A-up | <u>CCAAGTTTACTCATATATACTTTAGATTGATCATATGCTTCGGATCCCTCGAGAGATC</u> | 934 | pRepCM3 |
| pRRSH-p15A-dn | <u>CCGCGCAACATTCAACCAAAATTACATGTGCGTCAGACCC</u> | | |

Table 2-1 Primers for constructing pRRSH2 plasmid

p15A origin of replication fragment sequence. Primer binding sites are underlined, and the p15A origin region is shown in blue.

ATTACATGTGCGTCAGACCCCTTAATAAGATGATCTTCTTGAGATCGTTTTGGTCTGCGCGTAATCTTCTGCTCTGAAAACGAAA
AAACCGCCTTGCAAGGTTCTCTGAGCTACCAACTCTTGAACCGAGGTAAGTGGCTTGGAGGAGCGCAG
TCACCAAACTTGCTTTTCAGTTTAGCCTTAACCGGCGCATGACTTCAAGACTAACTCTTAAATCAATTACCAGTGGCTGCT
GCCAGTGGTGTCTTTGCATGTCTTCCGGTTGGACTCAAGACGATAGTTACCGGATAAGGCGCAGCGTTCGGACTGAACGG
GGGGTTCGTGCATACAGTCCAGCTTGGAGCGAACTGCCTACCCGGAAGTGTGAGGCGTGAATTAGACAAACGCGGCC
ATAACAGCGGAATGACACCGGTAACCGAAAGGCAGGAACAGGAGAGCGCACGAGGGAGCCGCCAGGGGGAAACGCCTGG
TATCTTTATAGTCTGTCTGGTTTCGCCACCACTGATTTGAGCGTCAGATTCGTGATGCTTGTGAGGGGGCGGAGCCTATGG
AAAAACGGCTTTCGCCGCGCCCTCTCACTCCCTGTTAAGTATCTTCTGCGATCTTCCAGGAAATCTCCGCCCGTTCGTAAGC
CATTTCCGCTCGCCGAGTCGAACGACCGAGCGTAGCGAGTCAGTGTGAGCGAGGAAGCGGAATATATCTGTATCACATATTCT
GCTGACGACCGGTGCAGCCTTTTTCTCTGCCACATGAAGCACTTCACTGACACCCTCATCAGTGCCAACATAGTAAGCCAG
TATACTCCGCTAGCCATGGAGATCTCTCGAGGGATCCGAAG

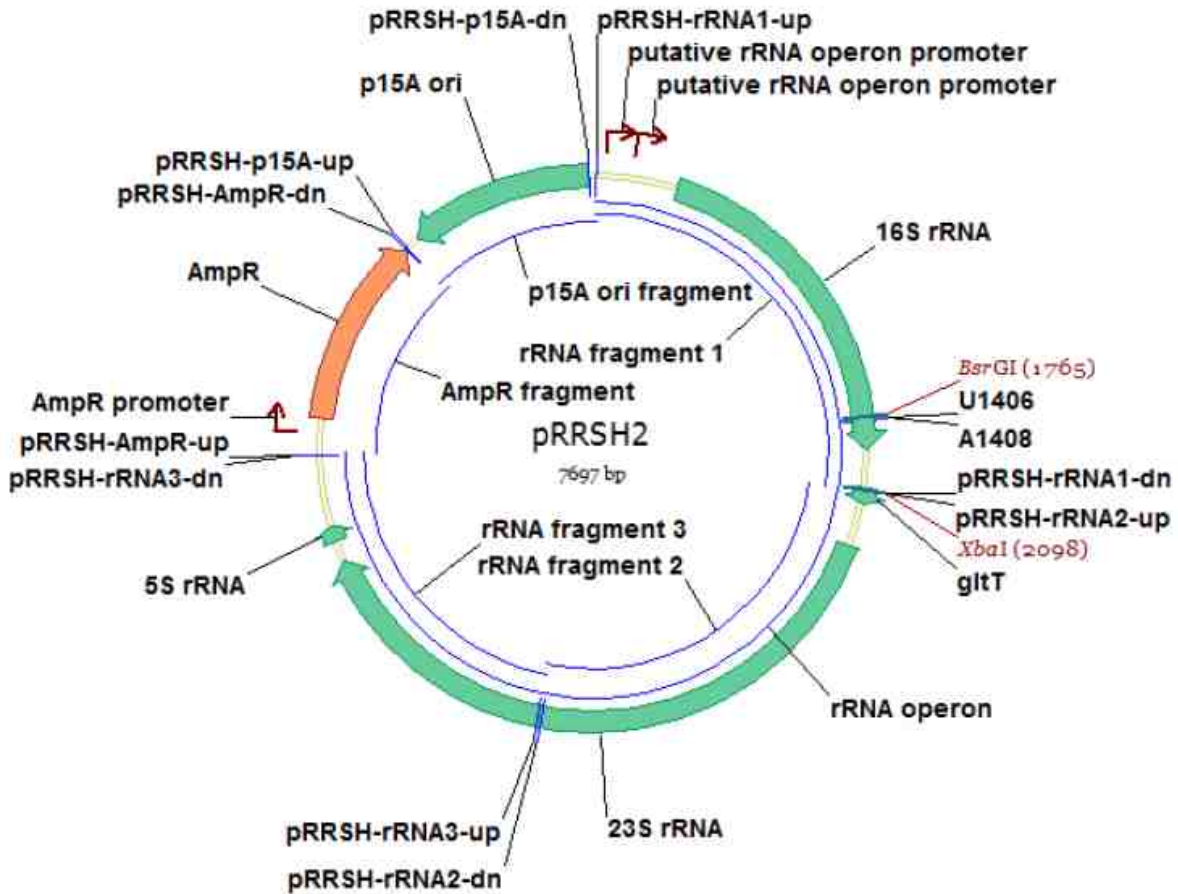


Figure 2-4 Plasmid map of pRRSH2

Construction of pRRSH2-A1408G and pRRSH2-U1406A. Both plasmids were constructed from pRRSH2. A 684 bp region of pRRSH2 containing the 16S rRNA A1408 and U1406 sites was amplified in two fragments with the mutation site at the junction of the fragments. In each case, the two fragments were joined by overlap extension PCR, the resulting PCR product digested with BsrGI and XbaI, and cloned into pRRSH2 digested with the same enzymes. For pRRSH2-A1408G (Figure 2-5), fragment 1 was amplified using primers pRRSH2-A1408G-1 and pRRSH2-A1408G-2, and fragment 2 was amplified using primers pRRSH2-A1408G-3 and pRRSH2-A1408G-4. For pRRSH2-U1406A, fragment 1 was amplified using primers pRRSH2-A1408G-1 and pRRSH2-U1406A-2, and fragment 2 was amplified using

primers pRRSH2-U1406A-3 and pRRSH2-A1408G-4. Introduction of the mutation into each plasmid was verified by sequencing the cloned region of the plasmid containing it. The vector map of pRRSH2-A1408G is given as an example. Primer information is given in the table 2-2 below. The A1408G and U1406A mutation sites are show in bold red in the primers that contain them. The priming region of each primer is underlined.

| primer name | sequence (5' – 3') | amplicon size (bp) | template |
|-----------------|---|--------------------|----------|
| pRRSH2-A1408G-1 | <u>TCTCAAACATC</u> ACCCGAAGATGAG | 457 | pRRSH2 |
| pRRSH2-A1408G-2 | <u>CCCGTCCACCCATGGGAGTG</u> | | |
| pRRSH2-A1408G-3 | <u>CCATGGTGC</u> GACGGGCGGTGTG | 242 | pRRSH2 |
| pRRSH2-A1408G-4 | <u>GAGGAAGGTGGGGATGACGTC</u> | | |
| pRRSH2-U1406A-2 | <u>CCCGACACCCATGGGAGTG</u> (used with pRRSH2-A1408G-1) | 457 | pRRSH2 |
| pRRSH2-U1406A-3 | <u>ACTCCCATGGTGTGT</u> CGGGCGGTG (used with pRRSH2-A1408G-4) | 246 | |

Table 2-2 Primers for constructing pRRSH2-A1408G and pRRSH2-U1406A

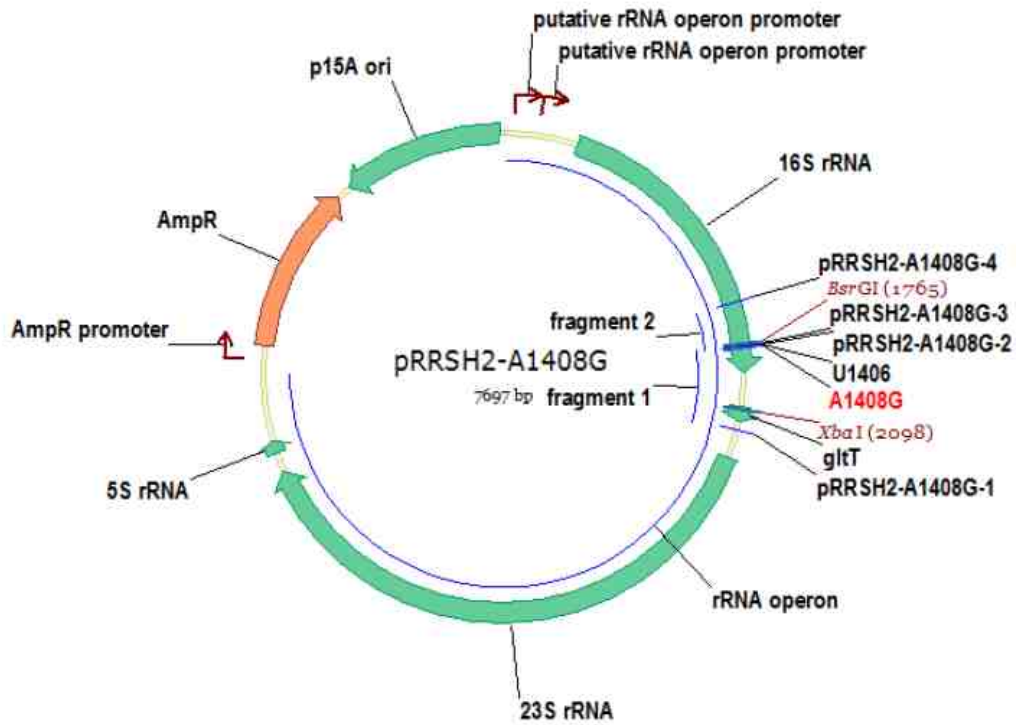


Figure 2-5. Plasmid map of pRRSH2-A1408G

Functional verification of pRRSH2-A1408G and pRRSH2 in E. coli SQ380. The ability of pRRSH2-A1408G to confer aminoglycoside resistance was confirmed through a cell viability assay. *E. coli* SQ380 was transformed with pRRSH2-A1408G; and prnC-sacB was removed by sucrose counter-selection, resulting in *E. coli* SH386. As a control, *E. coli* SQ380 was also transformed with pRRSH2; and prnC-sacB was removed by sucrose counter-selection, resulting in *E. coli* SH430. The growth inhibition of these two strains by various kanamycin concentrations was determined by inoculation of each strain (1:100 dilution of a saturated culture) into ten 1 mL wells of a 96-well culture plate containing LB broth with specific concentrations of kanamycin added (Figure 2-6), growth for 24 h at 37°C, 200 rpm shaking, and measurement of the OD600. The results (Figure 2-6) clearly demonstrate that *E. coli* SH430, which has no 16S rRNA aminoglycoside resistance mutation, experiences significant growth inhibition at 10 µM kanamycin, and cannot survive at concentrations above 10 µM kanamycin; whereas *E. coli* SH386, which has the A1408G mutation, shows no growth inhibition at any kanamycin concentration tested, indicating that the mutation confers robust resistance to kanamycin at concentrations as high as 500 µM.

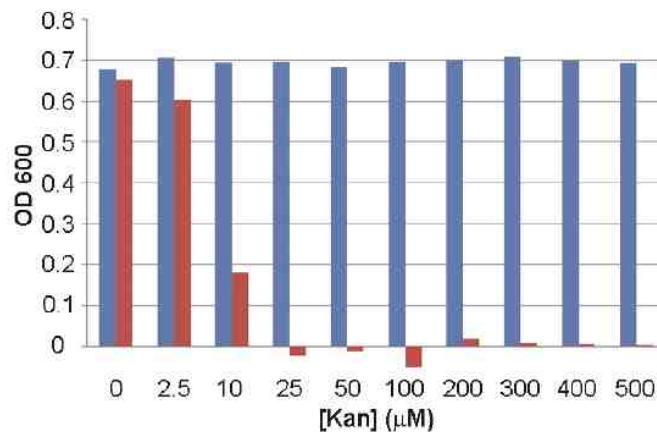


Figure 2-6. OD600 readings of SH386 (A1408G, blue bars) and SH430 (wild-type, red bars) grown in a range of kanamycin concentrations.

Sequential construction of the reporter plasmid The final reporter plasmid, pSH6-KF, was constructed in six steps:

1) Construction of pUC19-GFPuv, which contains the *gfp-uv* gene under control of the PLtetO-1 promoter.

2) Optimization of the *gfp-uv* 5'-untranslated (5'-UTR) region through construction of a five plasmid series pGBSH1-BCD2, pGBSH1-U2, pGBSH1-26.2, pGBSH1-pET, and pGBSH1-pBEST.

3) Replacement of the ampicillin resistance marker with a chloramphenicol resistance marker in pGBSH1-BCD2, the plasmid with the highest *gfp-uv* expression level from Step 2, to give pGBSH3.

4) Insertion of the cassette containing *tetR* with orthogonal Shine-Dalgarno (O-SD) sequence under control of medium strength promoter BBa_J23016 into pGBSH3 to give pGBSH18.

5) Insertion of the cassette containing the orthogonal 16S rRNA (O-16S) under control of the constitutive *lpp* promoter to give reporter plasmid pSH3-KF.

6) Optimization of the *tetR* and O-16S promoter strengths for use in *E. coli* SH386 through construction of an eleven plasmid series pSH4-KF through pSH14-KF.

Construction and testing of pUC19-GFPuv. This plasmid, which contains the *gfp-uv* gene under control of the PLtetO-1 promoter/operator⁴⁵, pMB1 origin of replication, and ampicillin resistance marker was constructed from four fragments by COE-PCR. The PLtetO-1 promoter/operator was amplified from pSR26_2 (J. Tabor, unpublished) using primers

pLtetO1N-up and pLtetO1-dn. The *gfp-uv* gene was amplified from plasmid pET101-GFP⁴⁶ using primers pGFP-up and pCL-F2-dn. The pMB1 origin of replication was amplified from pUC19 using primers pCL-F3-pMB1-up and pCL-F3-pMB1-dn. The ampicillin resistance marker was amplified from pUC19 using primers pCL-F4-up and pCL-F4-dn. The resulting four fragments were assembled by COE-PCR. The reaction mixture was concentrated using the Zymo Clean and Concentrator Kit, and introduced into competent *E.coli* DH5a cells. The final construct was verified by restriction mapping and sequencing. Primer information is given in the table 2-3 below. The priming region of each primer is underlined.

| primer name | sequence (5' - 3') | amplicon size (bp) | template |
|----------------|--|--------------------|------------|
| pLtetO1N-up | <u>ACAACTAGTGCGACCCCTGCGTATCAGGAGGCCCTTTGTC</u> | 159 | pSR26_2 |
| pLtetO1-dn | <u>CATGGTGAAGGGCTCCTGAATTCCTTCATTAATGGTCAGTGCCTCCTGCTGATG</u> | | |
| pGFP-up | <u>GAAGGAATTCAGGAGCCCTTCACCATG</u> | 1022 | pET101-GFP |
| pCL-F2-dn | <u>CCGGGCCTCTTGCGGGATATC</u> | | |
| pCL-F3-pMB1-up | <u>ATATCCCGCAAGAGGCCCGGGCGGTAATAAGCTTACGGTTATCCACAGAATCAGG</u> | 758 | pUC19 |
| pCL-F3-pMB1-dn | <u>AGACCCCGTCTAGATAGAAAAGATCAAAGGATCTTCTTGAG</u> | | |
| pCL-F4-up | <u>CTTTGATCTTTTCTATCTAGACGGGGTCTGACGCTCAGTG</u> | 1137 | pUC19 |
| pCL-F4-dn | <u>GCAGGGTCGCACCTAGTTTGTATTTTCTAAATACATTCARATATGTATCCGCTC</u> | | |

Table 2-3 Primers for constructing pUC19-GFPuv

gfp-uv fragment sequence. Primer binding sites are underlined, the *gfp-uv* coding region is shown in blue with start and stop codons underlined, and the T7 terminator sequence is shown in green.

GAAGGAATTCAGGAGCCCTTCACCATGAGTAAAGGAGAAGAAGACTTTTCACTGGAGTTGTCCCAATTCTGTTGAATTAGATGGTGATGTTAATGGGCACAAATTTTCTGTCACTGGAGAGGGTGAAGGTGATGCAACATACGGAAAACCTACCCTTAAATTTATTTGCACTACTGGAAAACCTACCTGTTCCATGGCCAACACTTGTCACTACTTTCTTTATGGTGTTCAATGCTTTTCCCGTTATCCGGATCACATGAAACGGCATGACTTTTTCAAGAGTGCCATGCCCGAAGGTTATGTACAGGAACGCACTATATCTTCAAAGATGACGGGAACTACAAGACGCGTGCTGAAGTCAAGTTTGAAGGTGATACCCTTGTTAATCGTATCGAGTTAAAAGGTATTGATTTTAAAGAAGATGGAAACATTCTCGGACACAACTCGAATACAACATAAATCACACAATGTATACATCACGGCAGACAAAACAAAAGAATGGAATCAAAGCTAACTTCAAATTCGCCACAACATTGAAGATGGATCCGTTCACTAGCAGACCATTATCAACAAAATACTCCAATTGGCGATGGCCCTGTCCTTTTACCAGACAACCATTACCTGTGACACAATCTGCCCTTTCGAAAGATCCCAACGAAAAGCGTGACCACATGGTCTTCTTGAGTTTGTAACTGCTGCTGGGATTACACATGGCATGGATGAGCTCTACAACTCGAGCACCACCACCACCACCTGAAGGGCGAGCTCAATTCGAAGCTTGAAGGTAAGCCTATCCCTAACCTCTCCTCGGTCTCGATTCTACGCGTACCGTCCATCATCACCATCACCATTGAGTTTGTATCCGGCTGCTAACAAAGCCCGAAAGGAAGCTGAGTTGGCTGCTGCCACCG

CTGAGCAATAACTAGCATAACCCCTTGGGGCCTCTAAACGGGTCTTGAGGGGTTTTTGCTGAAAGGAGGAACTATATCCGGA
TATCCCGCAAGAGGCCCGG

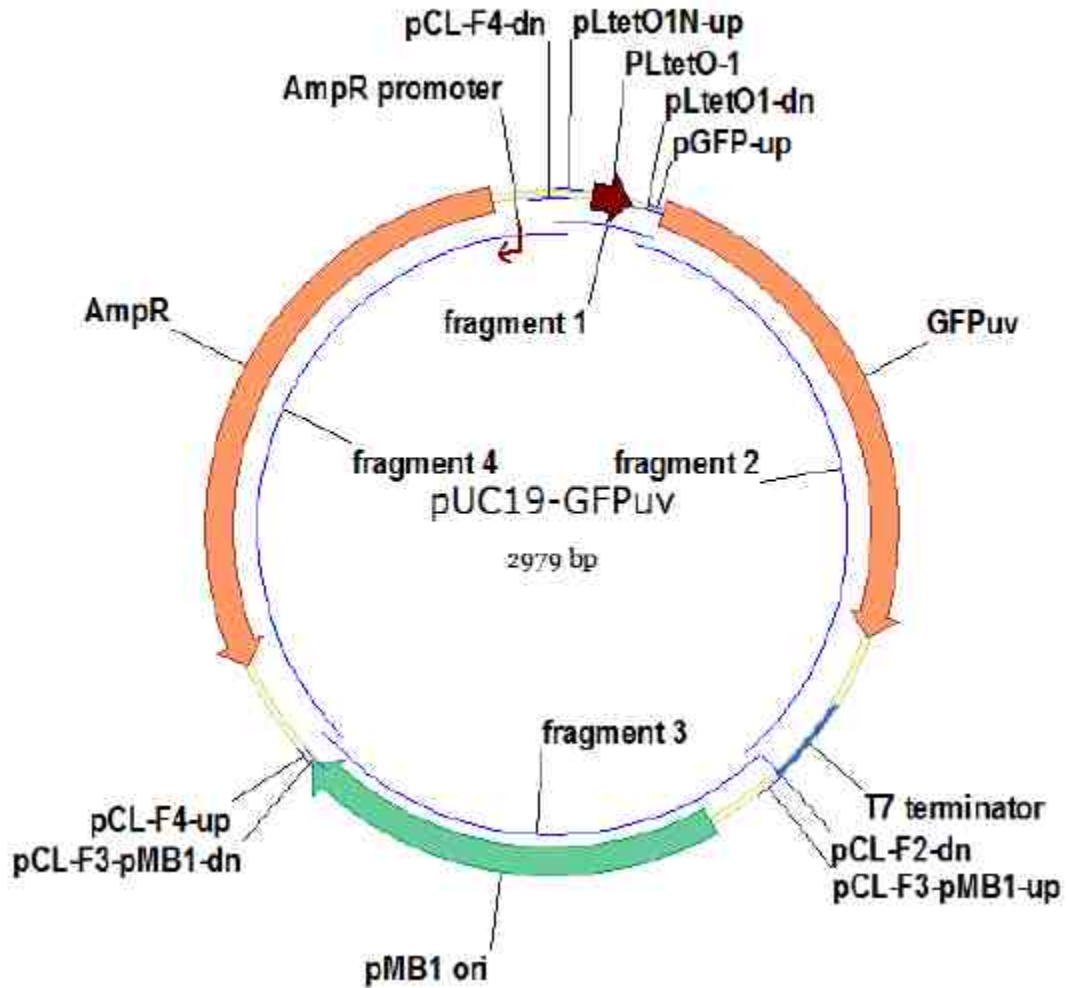


Figure 2-7 Plasmid map of pUC19-GFPuv

E. coli DH5 α transformed with pUC19-GFPuv displayed no fluorescence as determined by plate reader fluorescence assay (see cell density and fluorescence assays section, above, for experimental details). Reasoning that the lack of GFPuv expression was due to a non-optimal chimeric 5'-untranslated region (5'-UTR) derived from fusion of 5'-UTRs from pSR26_2 and pET101-GFP, we next constructed a series of five pUC19-GFPuv derivatives where the 5'-UTR was varied.

Construction of the pGBSH1 plasmid series. The pGBSH1 plasmid series was constructed by replacement of the *gfp-uv* 5'-UTR on pUC19-GFPuv with 5 different 5'-UTRs. We chose three 5'-UTRs that were reported to be strong [BCD2⁴⁷, U2⁴⁸, pBEST (unpublished, from Addgene #45784)] and two representing the intact 5'-UTRs associated with the GFPuv gene in pET101-GFP (pET) and the PLtetO-1 promoter in pSR26_2 (26.2). Additionally, a T0 spacer sequence was added between the ampicillin resistance gene and the PLtetO-1 portion to attempt to minimize any polar effects on GFP expression. The T0 spacer was appended to the 5' end of the PLtetO-1 fragment. Construction of these plasmids was accomplished by five COE-PCR reactions, each employing four fragments, three of which (pMB1 origin, ampicillin resistance marker, T0 spacer-PLtetO-1) were identical in all five reactions, and one (the 5'-UTR-*gfp-uv* fragment) of which was variable. The fragments containing the pMB1 origin and ampicillin resistance marker were identical to those used in construction of pUC19-GFPuv.

The T0 spacer-PLtetO-1 fragment was constructed by three sequential PCR reactions in which the product of the previous reaction was used as the template for the next reaction. The T0 spacer was amplified from plasmid pSR26_2 using primers pCL-F1-up and pCL-tetO1-dn-1. The resulting PCR product was used as the template for a second round of PCR using primers pCL-F1-up and pCL-tetO1-dn-2. The resulting PCR product was used as the template for a third round of PCR using primers pCL-F1-up and pCL-tetO1-dn-3 to generate the final fragment.

The five 5'-UTR-*gfp-uv* fragments were constructed as follows: The pET 5'-UTR-*gfp-uv* fragment was constructed in a single PCR reaction by amplification from plasmid pET101-GFP using primers pCL-GFPuv-up-tetO1 and pCL-F2-dn. The U2 5'-UTR-*gfp-uv*, 26.2 5'-UTR-*gfp-uv*, and pBEST 5'-UTR-*gfp-uv* fragments were each constructed by two sequential PCR reactions in which the product of the first reaction (the *gfp-uv*-containing fragment, which was

amplified from plasmid pET101-GFP), was used as the template for the second reaction. The U2 5'-UTR-*gfp-uv* fragment was constructed by amplification using primers pCL-u2-up-1 and pCL-F2-dn; and the resulting PCR product used as the template for a second round of PCR using primers pCL-u2-up-2-tetO1 and pCL-F2-dn. The 26.2 5'-UTR-*gfp-uv* fragment was constructed by amplification using primers pCL-pSR26-up-1 and pCL-F2-dn; and the resulting PCR product used as the template for a second round of PCR using primers pCL-pSR26-up-2-tetO1 and pCL-F2-dn. The pBEST 5'-UTR-*gfp-uv* fragment was constructed by amplification using primers pCL-45784-up-1 and pCL-F2-dn; and the resulting PCR product used as the template for a second round of PCR using primers pCL-45784-up-2-tetO1 and pCL-F2-dn. The BCD2 5'-UTR was constructed as a stand-alone fragment by templateless assembly using three primers (pCL-BCD2-1-tetO1, pCL-BCD2-2, and pCL-BCD2-3). A *gfp-uv*-containing fragment was amplified from pET101-GFP using primers pCL-F2-up-BCD2 and pCL-F2-dn; and the BCD2 5'-UTR and *gfp-uv*-containing fragments were joined by overlap extension PCR and amplified using outside primers pCL-BCD2-1-tetO1 and pCL-F2-dn to generate the final BCD2 5'-UTR-*gfp-uv* fragment. Each of the five 5'-UTR-*gfp-uv* fragment variants was then assembled with the T0 spacer-PLtetO-1, pMB1 origin, and ampicillin resistance marker fragments in a COE-PCR reaction. Each reaction mixture was concentrated using the Zymo Clean and Concentrator Kit and introduced into competent *E.coli* DH5α cells. Each final construct was verified by restriction mapping and sequencing. Primer information is given in the table 2-4 below. The priming region of each primer is underlined. The vector map of pGBSH1-BCD2 is given as an example. The figure 2-8 shows the constructs of the 5'-UTRs examined. The table 2-5 summarizing the 5'-UTRs examined is given below.

| primer name | sequence (5' - 3') | amplicon size (bp) | template |
|----------------------|--|--------------------|-----------------|
| pCL-F1-up | <u>ACAAACTAGTGGGACCCCTGCTGCTTGGATTCTCACCAATAAAAAAC</u> | 167 | pSR26_2 |
| pCL-tetO1-dn-1 | <u>TGTCAATCTCTATCACTGATAGGGATTTGATATCGAGCTCGCTTGGACTCCTGTTGATAG</u> | | |
| pCL-tetO1-dn-2 | <u>GCTCAGTATCTCTATCACTGATAGGGATGTCAATCTCTATCACTGATAGGGATTTG</u> | 194 | PCR pdt. |
| pCL-tetO1-dn-3 | <u>GGTCAGTGGCTCCTGCTGATGTGCTCAGTATCTCTATCACTGATAGGG</u> | 216 | PCR pdt. |
| pCL-GFPuv-up-tetO1 | <u>ATCAGCAGGACGCACTGACCCCTCTAGAAATAATTTTGTTTAACTTTAAGAAGGAATTC</u> | 1071 | pET101-GFP |
| pCL-F2-dn | <u>CCGGGCTCTTGGCGGATATC</u> (same is used to construct pUC19-GFPuv) | | |
| pCL-u2-up-1 | <u>AAAGAGGAGAAAGGTACCATGAGTAAAGGAGAAGAAGTTCCTCTGG</u> (used with pCL-F2-dn) | 1016 | pET101-GFP |
| pCL-u2-up-2-tetO1 | <u>ATCAGCAGGACGCACTGACCGAATTCATTTAAAGAGGAGAAGGTACCATGAG</u> (used with pCL-F2-dn) | 1045 | PCR pdt. |
| pCL-pSR26-up-1 | <u>AGCAAAGCCCAATTTTAAACAATGAGTAAAGGAGAAGAAGTTCCTCTGG</u> (used with pCL-F2-dn) | 1020 | pET101-GFP |
| pCL-pSR26-up-2-tetO1 | <u>ATCAGCAGGACGCACTGACCGCATAAAGGACTTAGCAAAGCCCAATTTTAAAC</u> (used with pCL-F2-dn) | 1053 | PCR pdt. |
| pCL-45784-up-1 | <u>ATTTTGTTTAACTTTAAGAAGGATCCATGAGTAAAGGAGAAGAAGTTCCTCTGG</u> (used with pCL-F2-dn) | 1024 | pET101-GFP |
| pCL-45784-up-2-tetO1 | <u>ATCAGCAGGACGCACTGACCGTAGCAATAATTTTGTTTAACTTTAAGAAGGATCCATG</u> (used with pCL-F2-dn) | 1054 | PCR pdt. |
| pCL-BCD2-1-tetO1 | <u>ATCAGCAGGACGCACTGACCGGGCCCAAGTTCACCTTAAAAAGGAGATCAAC</u> | 125 | primer assembly |
| pCL-BCD2-2 | <u>GATTAAGATGTTTCAGTACGAAAATTGCTTTTCATTGTTGATCTCCTTTTAAAG</u> | | |
| pCL-BCD2-3 | <u>AGTTCTTCTCCTTTACTCATTAGAAAACCTCCTTAGCATGATTAAGATGTTTCAGTAC</u> | | |
| pCL-F2-up-BCD2 | <u>ATGAGTAAAGGAGAAGAAGTTCCTCTGGAG</u> (used with pCL-F2-dn) | 988 | pET101-GFP |

Table 2-4 Primers for optimization of the *gfp-uv* 5'-untranslated (5'-UTR) region

T0 spacer fragment sequence. Primer binding sites are underlined, and the T0 spacer region is shown in blue.

TGCTTGGATTCTACCAATAAAAAACGCCGGCGGCAACCGAGCGTTCTGAACAAATCCAGATGGAGTTCTGAGGTCATTACTGGATCTATCAACAGGAGTCCAAGCGAGCTCGATATCAAAT

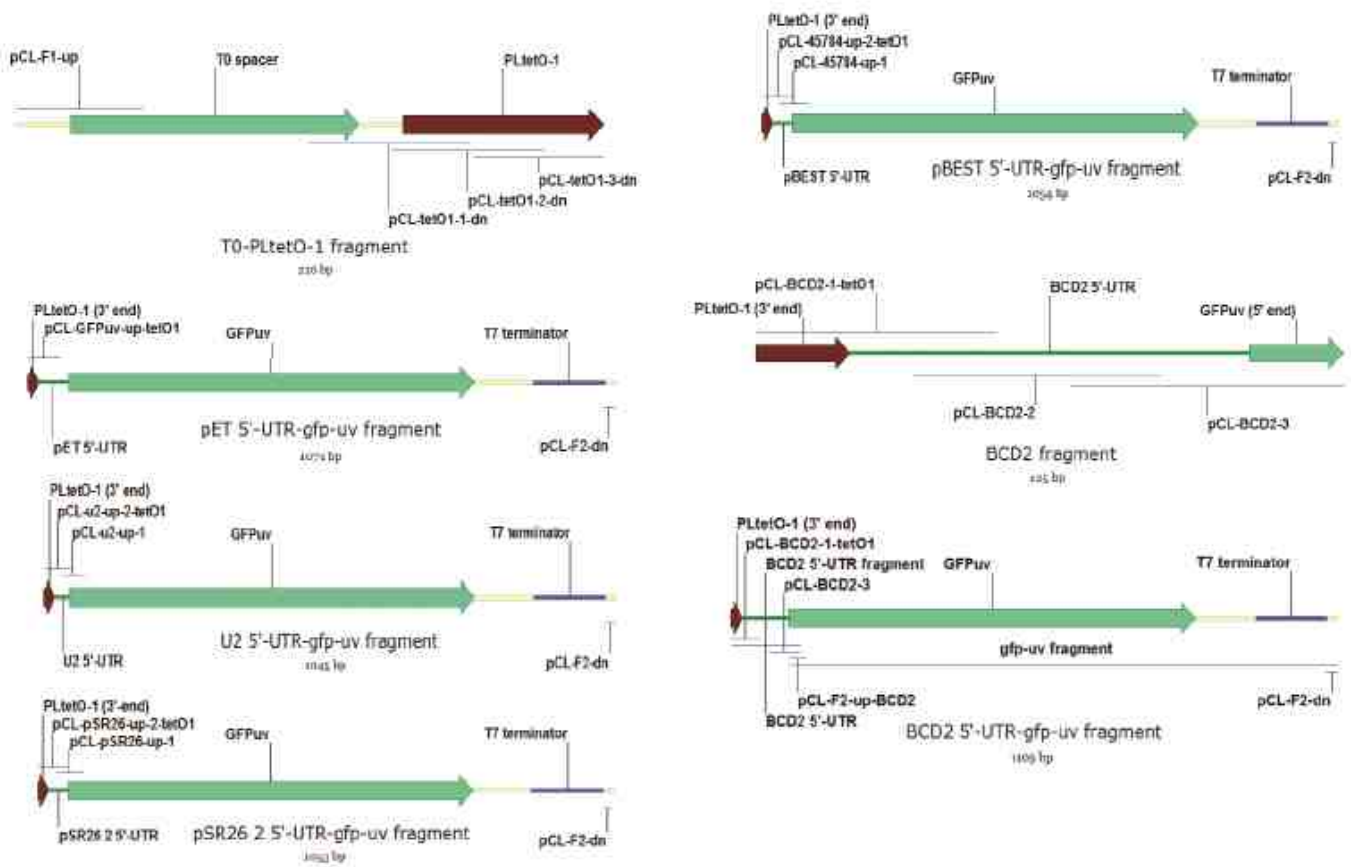


Figure 2-8 Optimization of 5'UTR region of gfpuv gene

| 5'-UTR | sequence | length (bp) |
|--------|--|-------------|
| pET | CCTCTAGAAATAATTTTGTTTAACTTTAAGAAGGAATTCAGGAGCCCTTCACC | 53 |
| U2 | GAATTCATTAAAGAGGAGAAAGGTACC | 27 |
| 26_2 | GCATAAAGGACTTAGCAAAGCCCAATTTTAAACAA | 35 |
| pBEST | GCTAGCAATAATTTTGTTTAACTTTAAGAAGGATCC | 36 |
| BCD2 | GGGCCCAAGTTCACTTAAAAAGGAGATCAACAATGAAAGCAATTTTCGTACTGAAACATCTTAATCATGCTAAGGAGGTTTCTA | 85 |

Table 2-5 Summary of the sequences of 5'UTR

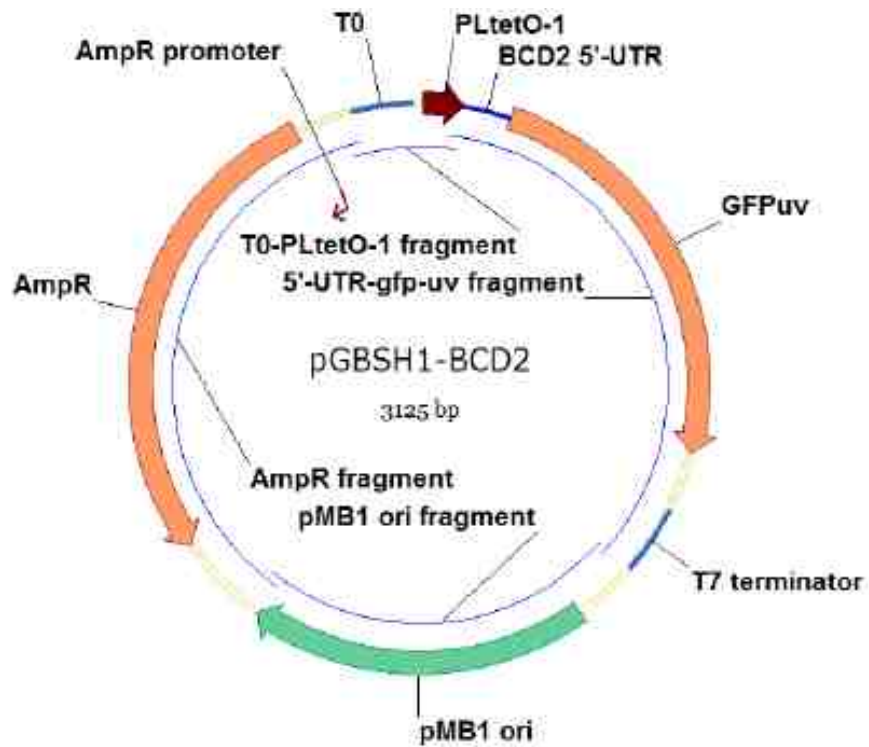


Figure 2-9 Plasmid map of pGBSH1-BCD2

pGBSH1 series functional assay. *E. coli* DH5 α transformed with pGBSH1-BCD2, pGBSH1-U2, pGBSH1-26.2, pGBSH1-pET, and pGBSH1-pBEST displayed a range of fluorescences (Figure 2-10) as determined by plate reader fluorescence assays (see cell density and fluorescence assays section, above, for experimental details), with pGBSH1-BCD2 resulting in the highest fluorescence. Thus, pGBSH1-BCD2 was selected for further development.

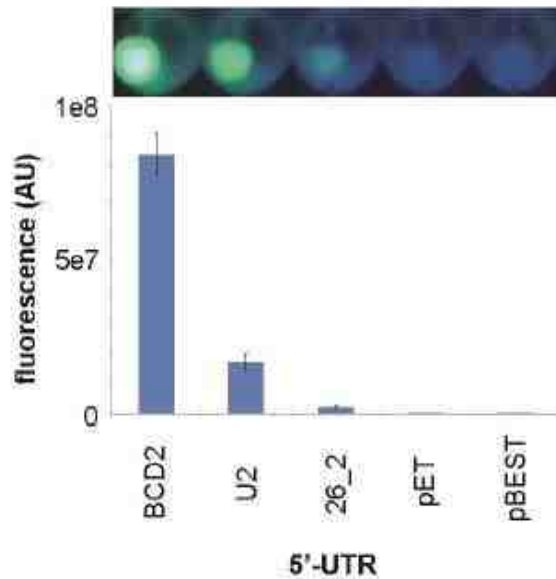


Figure 2-10 Cell pellet fluorescence and fluorescence quantification of pGBSH1 variants in which the *gfp-uv* 5'-UTR has been altered.

Construction and testing of pGBSH3. After identification of plasmid pGBSH1-BCD2 as the variant resulting in the highest fluorescence, the ampicillin resistance marker in pGBSH1-BCD2 was replaced with a chloramphenicol resistance marker so that the resulting plasmid, pGBSH3, could be co-transformed with pRRSH2-A1408G. A four fragment COE-PCR reaction was employed to construct pGBSH3. Three of the fragments (BCD2 5'-UTR-*gfp-uv*, pMB1 origin, and T0-PLtetO-1) were identical to those used to construct pGBSH1-BCD2. The fragment containing the chloramphenicol resistance marker was amplified from plasmid pBKCM7b (Charles E. Melancon III, unpublished) using primers cat-pBKCM7b-up and cat-pBKCM7b-dn. After COE-PCR, concentration using a Zymo Clean and Concentrator Kit, and transformation, the final construct was verified by restriction mapping and sequencing. Primer information is given in the table 2-6 below. The priming region of each primer is underlined. Retention of robust fluorescence by *E. coli* DH5 α cells transformed with pGBSH3 was verified

by plate reader fluorescence assays (see cell density and fluorescence assays section, above, for experimental details).

| primer name | sequence (5' – 3') | amplicon size (bp) | template |
|----------------|--|--------------------|----------|
| cat-pBKCM7b-up | <u>CTTTTCTATCTAGACGGGGTCTTTTGATAGAAAATCATAAAAGGATTGC</u> | 1069 | pBKCM7b |
| cat-pBKCM7b-dn | <u>GCAGGGTCGCACTAGTTTGTGGATCCAACTGCATTTCAGAATAAATAAATC</u> | | |

Table 2-6 Primers for constructing pGBSH3

Chloramphenicol resistance marker fragment sequence is shown below. Primer binding sites are underlined, the promoter sequence is shown in green, and the chloramphenicol acetyltransferase coding region is shown in blue with start and stop codons underlined.

GGATCCAACTGCATTTCAGAATAAATAAATCCTGGTGTCCCTGTTGATACCGGGAAGCCCTGGGCCAACTTTTGGCGAAAATGAGACGTTGATCGGCACGTAAGAGGGTTCCAACCTTTCACCATAATGAAATAAGATCACTACCGGGCGTATTTTTGAGTTGTCGAGATTTTCAGGAGCTAAGGAAGCTAAAATGAGAGAAAAAATCACTGGATATACCACCGTTGATATATCCCAATGGCATCGTAAAGAACATTTTGGAGCATTTCAGTCAGTTGCTCAATGTACCTATAACCAGACCGTTGAGCTGGATATTACGGCCTTTTTAAAGACCGTAAGAAAAATAAGCACAAAGTTTTATCCGGCCTTTATTACATTCTTGCCCGCTGATGAATGCTCATCCGGAATTACGTATGGCAATGAAAGACGGTGAGCTGGTGATATGGGATAGTGTCCACCCTGTTACACCGTTTTCCATGAGCAAACCTGAAACGTTTTCATCGCTCTGGAGTGAATACCACGACGATTTCCGGCAGTTTCTACACATATATTCGCAAGATGTGGCGTGTTACGGTGAAAACCTGGCCATTTCCCTAAAGGGTTTATTGAGAATATGTTTTTCGTCTCAGCCAATCCCTGGGTGAGTTTCACCAGTTTTGATTTAAACGTGGCCAATATGGCAAACCTTCTCGCCCCGTTTTCCACCATGGGCAAATATTATACGCAAGGCGACAAGGTGCTGATGCCGCTGGCGATTCAGGTTTCATCATGCCGTTTGTGATGGCTTCCATGTCGGCAGAATGCTTAATGAATTACAACAGTACTGCGATGAGTGGCAGGGCGGGCGTAAGGCGCGCCATTTAAATGAAGTTCCTATTCCGAAGTTCCTATTCTAGGGATTAATAAGGCAACTTTATGCCCATGCAACAGAAACTATAAAAAATACAGAGAATGAAAAGAAACAGATAGATTTTTAGTTCCTTAGGCCCGTAGTCTGCAAATCCTTTTATGATTTTCTATCAAA

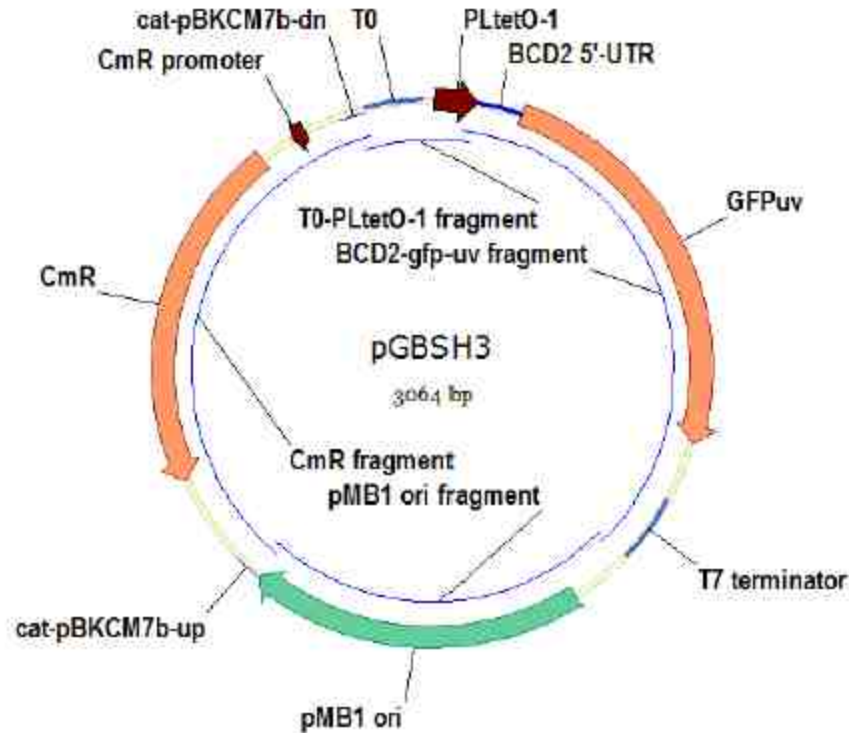


Figure 2-11 Plasmid map of pGBSH3

Construction and testing of pGBSH18. A cassette containing the *tetR* gene with orthogonal Shine-Dalgarno (O-SD) sequence (ATCCC)^{49, 50} under control of medium strength promoter BBa_J23106 (J. Christopher Anderson, unpublished) and containing the T1 terminator was inserted into pGBSH3 to generate pGBSH18. A five fragment COE-PCR reaction was employed to construct pGBSH18 (Figure 2-12). Three of the fragments (the BCD2 5'-UTR-*gfp-uv*, chloramphenicol resistance marker, and T0-PLtetO-1) were identical to those used to construct pGBSH1-BCD2 and pGBSH3. The pMB1 origin was amplified from pGBSH3 using primers F3-up-tetRassem and pCL-F3-pMB1-dn.

The fragment containing O-SD-*tetR* (Figure 2-13) was constructed by three sequential PCR reactions in which the product of the previous reaction was used as the template for the next reaction. The *tetR* gene with T1 terminator was amplified from pSR26_2 using primers ptetR-1-

KF-up and tetRassem1-dn-XmnI. The resulting PCR product was used as the template for a second round of PCR using primers ptetR-2-KF-up and tetRassem1-dn-XmnI. The resulting PCR product was used as the template for a third round of PCR using primers tetRassem1-up-XmnI and tetRassem1-dn-XmnI to generate the final fragment. After COE-PCR, concentration using a Zymo Clean and Concentrator Kit, and transformation, the final construct was verified by restriction mapping and sequencing. Primer information is given in the table below. The priming region of each primer is underlined. The O-SD sequence and ATG start codon are shown in bold red in the primers that contain them. Retention of robust fluorescence by *E. coli* cells DH5 α transformed with pGBSH18 was verified as by plate reader fluorescence assays (see cell density and fluorescence assays section, above, for experimental details). During the sequencing process, we discovered two spontaneous mutations in the pMB1 origin (see below for locations). It is unclear whether these mutations have any effect on plasmid copy number, but it is clear from fluorescence assays that they do not interfere with replication in *E. coli* DH5 α or *gfp-uv* expression.

| primer name | sequence (5' – 3') | amplicon size (bp) | template |
|--------------------|---|--------------------|----------|
| F3-up-tetRassem | <u>GCGGTAATAAGCTTACGGTTATCCAC</u> | 738 | pGBSH3 |
| pCL-F3-pMB1-dn | <u>AGACCCCGTCTAGATAGAAAAGATCAAAGGATCTTCTTGAG</u> (same as used to construct pUC19-GFPuv) | | |
| ptetR-1-KF-up | <u>ACAATCGATACATCCCCGCAAATGATGTCTCGTTAGATAAAAAGTAAAG</u> | 823 | pSR26_2 |
| tetRassem1-dn-XmnI | <u>TGTGGATAACCGTAAGCTTATTACCGCTTTGAGTGAGCTGATACCGC</u> | 863 | PCR pdt. |
| ptetR-2-KF-up | <u>CTAGCTCAGTCCTAGGTATAGTGCTAGCCGAGCCAGAGAAACAATCGATACATCCCC</u> | 863 | PCR pdt. |
| tetRassem1-up-XmnI | <u>ATATCCCGCAAGAGGGCCCGGTTTACGGCTAGCTCAGTCTAG</u> | 890 | PCR pdt. |

Table 2-7 Primers for constructing pGBSH18

Sequence of the tetR-T1 terminator fragment is shown below. Primer binding sites are underlined, the *tetR* coding sequence is shown in blue, and the T1 terminator region is shown in green.

ATGATGTCTCGTTTAGATAAAAAGTAAAGTGATTAACACGCGCATTAGAGCTGCTTAATGAGGTCGGAATCGAAGGTTTAAACAAC
 CCGTAAACTCGCCAGAAGCTAGGTGTAGAGCAGCCTACATTGTATTGGCATGTAAAAATAAGCGGGCTTTGCTCGACGCCT
 TAGCCATTGAGATGTTAGATAGGCACCATACTCACTTTTGCCTTTAGAAGGGGAAAGCTGGCAAGATTTTTACGTAATAACG
 CTAAGTTTTATAGATGTGCTTTACTAAGTCATCGCGATGGAGCAAAAGTACATTTAGGTACACGGCCTACAGAAAAACAGTAT
 GAAACTCTGAAAATCAATTAGCCTTTTTATGCCAACAAGGTTTTCTACTAGAGAATGCATTATATGCACTCAGCGCAGTGGGG
 CATTTTACTTTAGGTTGCGTATTGGAAGATCAAGAGCATCAAGTCGCTAAAGAAGAAAGGGAAACACTACTACTGATAGTAT
 GCCGCCATTATTACGACAAGCTATCGAATTATTTGATCACCAAGGTGCAGAGCCAGCCTTCTTATTCGGCCTTGAATTGATCATA
 TGCGGATTAGAAAAACAACCTTAAATGTGAAAGTGGGTCTTAAGGCATCAAATAAACGAAAGGCTCAGTCGAAAGACTGGGC
CTTTCGTTTTATCTGTTGTTTGTGCGGTGAACGCTCTCTGAGTAGGACAAATCCGCCGCCCTAGACCTAGGCGTTTCGGCTGCGG
CGAGCGGTATCAGCTCACTCAAAG

Sequence of the pMB1 origin in pGBSH18 with spontaneous mutations marked in bold underlined red. G at position 107 was mutated to C, and G at position 457 was mutated to A.

CGCGTTGCTGGCGTTTTTCCATAGGCTCCGCCCCCTGACGAGCATCACAAAAATCGACGCTCAAGTCAGAGGTGGC
 GAAACCCGACAGGACTATAAAGATAACCAGCCGTTTTCCCCCTGGAAGCTCCCTCGTGCGCTCTCCTGTTCCGACCCTG
 CCGCTTACCGGATACCTGTCCGCCTTTCTCCCTTCGGAAGCGTGGCGCTTTCTCATAGCTCACGCTGTAGGTATCT
 CAGTTCGGTGTAGGTTCGTTCCGCTCCAAGCTGGGCTGTGTGCACGAACCCCCCGTTTCAGCCCGACCGCTGCGCCTTAT
 CCGGTAACCTATCGTCTTGAGTCCAACCCGGTAAGACACGACTTATCGCCACTGGCAGCAGCCACTGGTAACAGGATT
 AGCAGAGCGAGGTATGTAGGCGGTGCTACAGAGTTCTTGAAGTGGTGGCCTAACTACGGCTACACTAGAAGAACAGT
 ATTTGGTATCTGCGCTCTGCTGAAGCCAGTTACCTTCGAAAAAGAGTTGGTAGCTCTTGATCCGGCAAACAAACCA
 CCGCTGGTAGCGGTGGTTTTTTTTGTTTGCAAGCAGCAGATTACGCGCAGAAAAAAGGATCTCAAGAAGATCCTTT

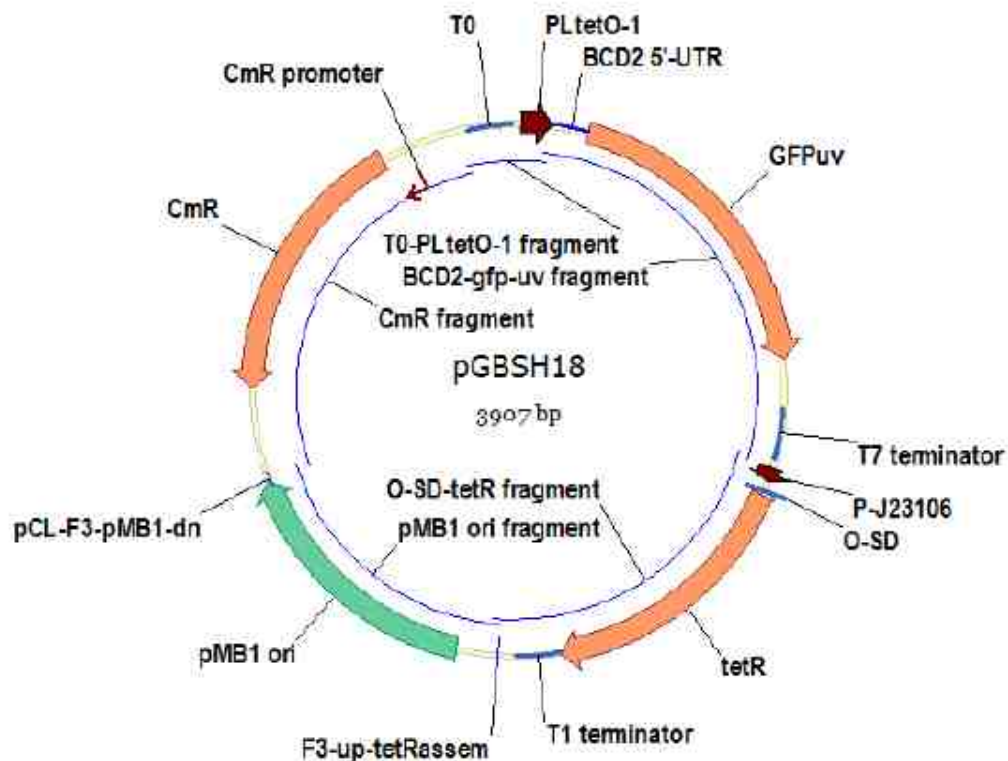


Figure 2-12 Plasmid map of pGBSH18

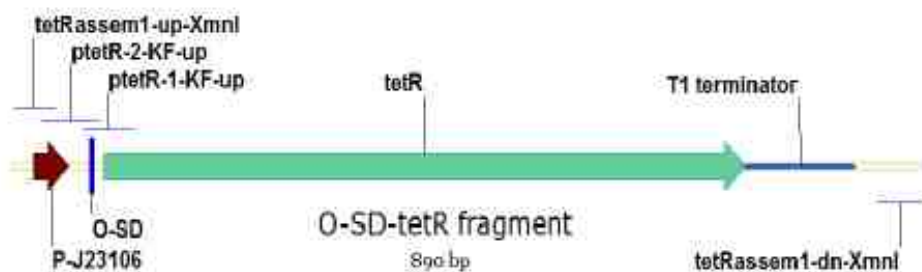


Figure 2-13 The O-SD-tetR fragment

Construction and testing of pSH3-KF in E. coli DH5a. A cassette containing the orthogonal 16S rRNA (O-16S) with orthogonal anti-Shine-Dalgarno (O-ASD) sequence (TGGGG)^{49, 50} was inserted into pGBSH18 to generate pSH3-KF, which contains all the components of the orthogonal ribosome-based fluorescent reporter. A five fragment COE-PCR reaction was employed to construct pSH3-KF.

Two of the fragments (the O-SD-*tetR* and pMB1 origin) were identical to those used to construct pGBSH18. The chloramphenicol resistance marker fragment was amplified from pGBSH18 using primers cat-pBKCM7b-up and pCAT-OKF-dn. A fragment containing T0-PLtetO-1 and BCD2 5'-UTR-*gfp*-uv was also amplified from pGBSH18 using primers pGFP-OKF-up and pCL-F2-dn.

The fragment containing the orthogonal 16S rRNA (O-16S) under control of the reportedly strong *lpp* promoter (Plpp)⁵¹ was constructed by amplifying the Plpp-16S rRNA cassette from plasmid pTrcSS1d-rrsBb (Shinichiro Shoji, unpublished) using upstream primer pO16S-up and mutagenic downstream primer pO16S-KF-dn which was used to install the orthogonal anti-Shine-Dalgarno (O-ASD) sequence. The strong terminator BBa_B0015⁵² was amplified from plasmid pSR26_2 using primers pB15-up and pB15-dn and appended to the 3'

end of the P1pp-O-16S fragment by overlap extension PCR to attempt to minimize any polar effects on other genes in the construct. After COE-PCR, concentration using a Zymo Clean and Concentrator Kit, and transformation, the final construct was verified by restriction mapping and sequencing. Primer information is given in the table 2-8 below. The priming region of each primer is underlined. The *lpp* promoter and O-ASD sequences are shown in bold red in the primers that contain them.

As expected, a nearly complete lack of fluorescence by *E. coli* DH5 α cells transformed with pSH3-KF was observed as determined by plate reader fluorescence assays (see cell density and fluorescence assays section, above, for experimental details). However, as expected, fluorescence of *E. coli* DH5 α cells transformed with pSH3-KF could be recovered in a dose-dependent manner by addition of various concentrations of anhydrotetracycline (ATC), which binds to TetR and causes its dissociation from PLtetO-1 thereby relieving repression of transcription (Figure 2-14).

| primer name | sequence (5' – 3') | amplicon size (bp) | template |
|----------------|--|--------------------|--------------------|
| pGFP-OKF-up | <u>GAATTCGGTGGCCCTGCATGCACAACTAGTGCCGACCCCTGCTGC</u> | 1319 | pGBSH18 |
| pCL-F2-dn | <u>CCGGGCCCTCTGCGGGATATC</u> (same is used to construct pUC19-GFPuv) | | |
| cat-pBKCM7b-up | <u>CTTTTCTATCTAGACGGGGTCTTTTGATAGAAAATCATAAAAAGGATTTC</u> (same as used to construct pGBSH3) | 1091 | pGBSH18 |
| pCAT-OKF-dn | <u>GTACCCGTGGATCCTCTAGAGGATCCAACCTGCATTTCAGAATAAATAAATC</u> | | |
| pO16S-up | <u>GCATGCAGGGCCACGAA</u> <u>TTCTCAACATAAAAACTTTGTGTAATACT</u> <u>TGTAACGCTAGATC</u> <u>CGGTAGCGATCGAAAGCGAAGCGGCAC</u> | 1824 | pTrcSS1d- rrsBb |
| pO16S-KF-dn | <u>CTGCAGTATCAGACAATCTGTGTGAGCACTACAAAGTACGCTTCTTTAAGGT</u> <u>CCCCATGA</u> <u>TCCAACCG</u> | | |
| pB15-up | <u>CAGATTGTCTGATACTGCAGGCATGATAATAATCTAGACCAGG</u> | 188 | pSR26_2 |
| pB15-dn | <u>TCTAGAGGATCCACGGGTACC</u> | | |

Table 2-8 Primers for constructing pSH3-KF

Sequence of the *lpp* promoter - O16S fragment is shown below. Primer binding sites are underlined, the *lpp* promoter is shown in green, the O-16S rRNA coding region is shown in blue, and the O-ASD sequence is shown in red.

ATTCTCAACATAAAAAAAGCTTTGTGTAATACTTGTAAACGCTAGATCCGGTAGCGATCGAAAGCGAAGCGGCACTGCTC
TTTAACAATTTATCAGACAATCTGTGTGGGCACTCGAAGATACGGATTCTTAACGTCGCAAGACGAAAAATGAATAC
CAAGTCTCAAGAGTGAACACGTAATTCATTACGAAGTTTAATTTCTTTGAGCGTCAAACCTTTTAAATTGAAGAGTTTG
ATCATGGCTCAGATTGAACGCTGGCGGCAGGCCTAACACATGCAAGTCGAACGGTAACAGGAAGAAGCTTGCTTCTT
TGCTGACGAGTGGCGGACGGGTGAGTAATGTCTGGGAAACTGCCTGATGGAGGGGGATAACTACTGGAAACGGTAGC
TAATACCGCATAACGTCGCAAGACCAAAGAGGGGGACCTTCGGGCCTCTTGCCATCGGATGTGCCAGATGGGATTA
GCTAGTAGGTGGGGTAACGGCTCACCTAGGCGACGATCCCTAGCTGGTCTGAGAGGATGACCAGCCACACTGGAAC
GAGACACGGTCCAGACTCCTACGGGAGGCAGCAGTGGGGAATATTGCACAATGGGCGCAAGCCTGATGCAGCCATGC
CGCGTGTATGAAGAAGGCCTTCGGGTTGTAAAGTACTTTTCAGCGGGGAGGAAGGGAGTAAAGTTAATACCTTTGCTC
ATTGACGTTACCCGCAGAAGAAGCACCAGGCTAATCCGTGCCAGCAGCCGCGGTAATACGGAGGGTGAACGCGTTAA
TCGGAATTACTGGGCGTAAAGCGCACGCAGGCGGTTTGTAAAGTCAAGTGTGAAATCCCCGGGCTCAACCTGGGAAC
TGCATCTGATACTGGCAAGCTTGAGTCTCGTAGAGGGGGTGAATTCAGGTGTAGCGGTGAAATGCGTAGAGATC
TGGAGGAATACCGGTGGCGAAGGCGGCCCTGGACGAAGACTGACGCTCAGGTGCGAAAGCGTGGGGAGCAAACAG
GATTAGATACCCTGGTAGTCCACGCCGTAAACGATGTGCACTTGGAGGTTGTGCCCTTGAGGCGTGGCTTCCGGAGC
TAACGCGTTAAGTCGACCGCCTGGGGAGTACGGCCGCAAGGTTAAAACCTCAAATGAATTGACGGGGGCCGCACAAG
CGGTGGAGCATGTGGTTTAATTCGATGCAACGCGAAGAACCTTACCTGGTCTTGACATCCACGGAAGTTTTTCAGAGA
TGAGAATGTGCCTTCGGGAACCGTGAGACAGGTGCTGCATGGCTGTGTCAGCTCGTGTGTTGTGAAATGTTGGGTTAA
GTCCCGCAACGAGCGCAACCCTTATCCTTTGTTGCCAGCGGTCCGGCCGGGAACCTCAAAGGAGACTGCCAGTGATAA
ACTGGAGGAAGGTGGGGATGACGTCAAGTCATCATGGCCCTTACGACCAGGGCTACACACGTGCTACAATGGCGCAT
ACAAAGAGAAGCGACCTCGCGAGAGCAAGCGGACCTCATAAAGTGCCTGCTAGTCCGGATTGGAGTCTGCAACTCGA
CTCCATGAAGTCGGAATCGCTAGTAATCGTGGATCAGAATGCCACGGTGAATACGTTCCCGGGCCTTGACACACCG
CCCGTCACACCATGGGAGTGGGTTGCAAAGAAGTAGGTAGCTTAACCTTCGGGAGGGCGCTTACCACCTTTGTGATT
CATGACTGGGGTGAAGTCGTAACAAGGTAACCGTAGGGGAACCTGCGGTTGGATCATGGGGTACCTTAAAGAAGCGT
ACTTTGTAGTGCTCACACAGATTGTCTGATA

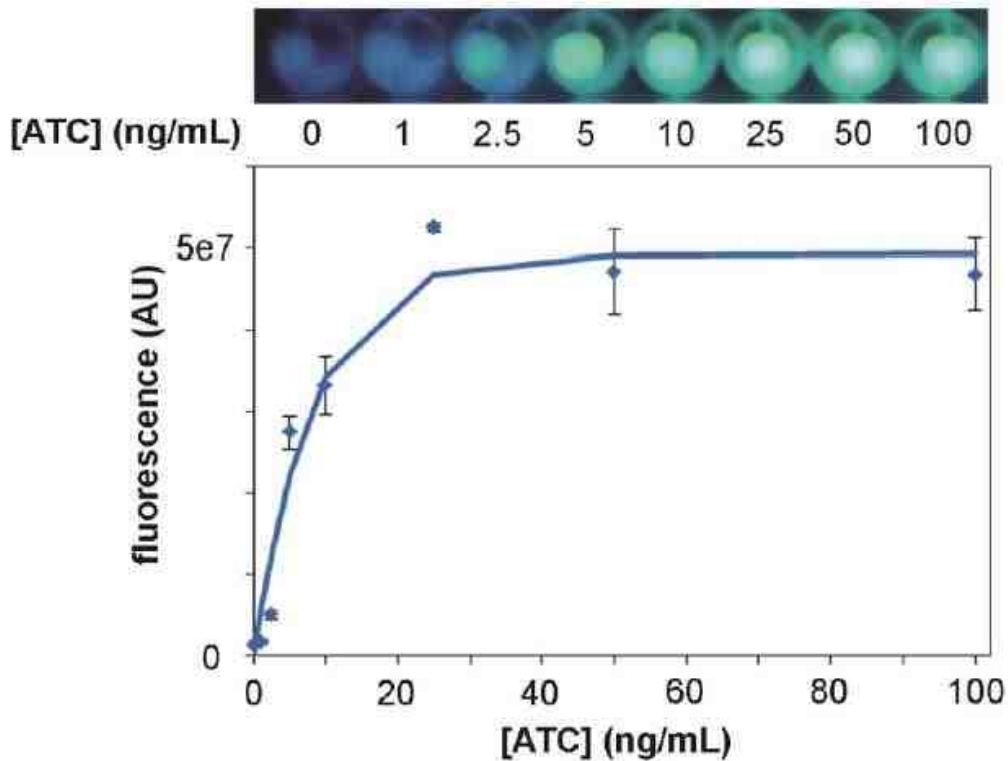


Figure 2-14 Cell pellet fluorescence and fluorescence quantification of *E. coli* DH5 α cells containing pSH3-KF grown in the presence of a range of anhydrotetracycline concentrations.

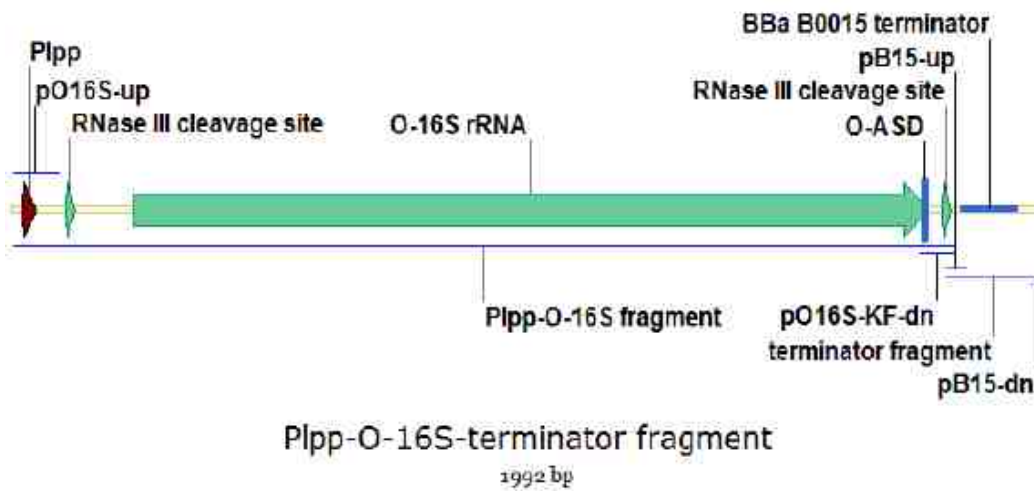


Figure 2-15 Illustration of Plpp-O-16S-terminator fragment

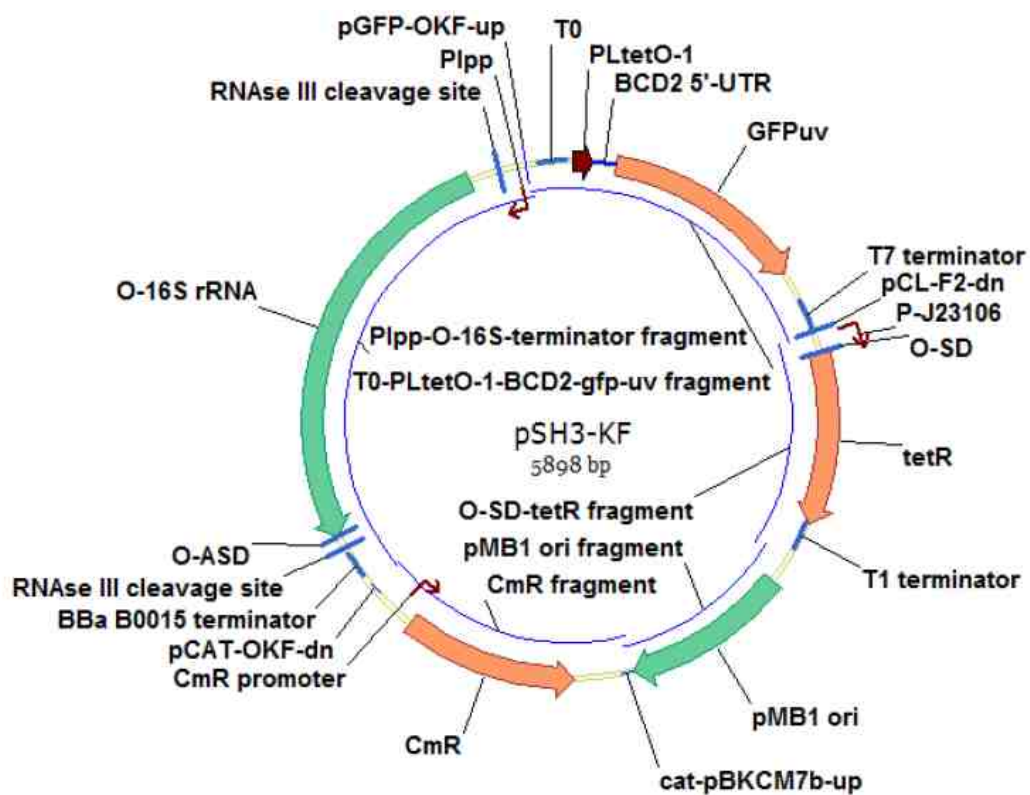


Figure 2-16 Plasmid map of pSH3-KF

Ribosome inhibition assay of kanamycin in E. coli SH391. We tested the ability of *E. coli* SH386 cells transformed with pSH3-KF (referred to as *E. coli* SH391) to detect ribosome inhibition by kanamycin. *E. coli* SH391 cells were grown in the presence of various concentrations of kanamycin ranging from 0-500 μ M and analyzed by fluorescence assay. *E. coli* SH391 displayed strong fluorescence in the absence of kanamycin and only a modest (~50%) increase in fluorescence when kanamycin was added. This result led us to construct and test plasmids pSH4-KF – pSH14-KF in *E. coli* SH386.

Construction and testing of pSH4-KF - pSH14-KF in E. coli SH386. To attempt to overcome the low sensitivity to kanamycin and high background fluorescence imparted by pSH3-KF in *E. coli* SH386, we constructed a series of eleven pSH3-KF variants in which the strengths of the two promoters controlling expression of *tetR* and O-16S rRNA were combinatorially altered using synthetic constitutive promoters with characterized strengths (J. Christopher Anderson, unpublished,). In addition to the original medium strength synthetic promoter BBa_J23106 controlling *tetR* expression, strong promoter BBa_J23100 and weak promoter BBa_J23115 were selected for use with *tetR*. In addition to the original *lpp* promoter controlling O-16S rRNA expression, strong promoter BBa_J23100, medium strength promoter BBa_J23108, and weak strength promoter BBa_J23114 were selected for use with O-16S rRNA. The DNA sequence of these promoter were shown in table 2-10.

We first constructed two plasmids, pSH4-KF (Figure 2-17) and pSH5-KF, in which the BBa_J23106 promoter controlling expression of *tetR* was replaced with strong promoter BBa_J23100 and a weak promoter BBa_J23115, respectively. Promoter replacement was accomplished by overlap extension PCR of two fragments amplified from pSH3-KF whose junction encompassed each promoter to be inserted, digestion of both the resulting PCR product

and pSH3-KF with unique restriction sites MfeI and NdeI, and ligation of the PCR product into the vector. For construction of pSH4-KF, primer pSH4-KF-1 and mutagenic primer pSH4-KF-2 were used to amplify fragment 1; and mutagenic primer pSH4-KF-3 and primer pSH4-KF-4 were used to amplify fragment 2. For construction of pSH5-KF, primer pSH4-KF-1 and mutagenic primer pSH5-KF-2 were used to amplify fragment 1; and mutagenic primer pSH5-KF-3 and primer pSH4-KF-4 were used to amplify fragment 2. Plasmids pSH4-KF and pSH5-KF were verified by sequencing the cloned region. Primer information is given in the table 2-9 below. The priming region of each primer is underlined.

To construct the remaining nine plasmid variants bearing strong (pSH6-KF, pSH9-KF, pSH12-KF), medium (pSH7-KF, pSH10-KF, pSH13-KF), and weak (pSH8-KF, pSH11-KF, pSH14-KF) strength promoters controlling expression of O-16S, we used a similar overlap extension PCR strategy. Two fragments amplified from pSH3-KF whose junction encompassed each promoter to be inserted were joined by overlap extension PCR. The PCR product bearing strong promoter BBa_J23100 was constructed using primer pSH6-KF-1 and mutagenic primer pSH6-KF-2 to amplify fragment 1; and mutagenic primer pSH6-KF-3 and primer pSH6-KF-4 to amplify fragment 2. The PCR product bearing medium promoter BBa_J23108 was constructed using primer pSH6-KF-1 and mutagenic primer pSH7-KF-2 to amplify fragment 1; and mutagenic primer pSH7-KF-3 and primer pSH6-KF-4 to amplify fragment 2. The PCR product bearing weak promoter BBa_J23114 was constructed using primer pSH6-KF-1 and mutagenic primer pSH8-KF-2 to amplify fragment 1; and mutagenic primer pSH8-KF-3 and primer pSH6-KF-4 to amplify fragment 2. Each of the resulting three PCR products was digested with unique restriction enzymes PstI and SpeI and ligated into each pSH3-KF, pSH4-KF, and pSH5-KF digested with the same enzymes to generate the nine final constructs pSH6-KF (Figure 2-18)

through pSH14-KF. All nine plasmids were verified by sequencing the cloned region. Primer information is given in the table below. The priming region of each primer is underlined. Regions of the mutagenic primers containing promoter regions are shown in bold red. Diagrams of pSH4-KF and pSH6-KF are shown as examples. Summaries of the names, sequences, and strengths (as measured by J. Christopher Anderson, unpublished) of the promoters used and of the *tetR* and O-16S promoters found in each plasmid are summarized in two tables (table 2-10 and table 2-11) below. *E. coli* SH386 cells transformed with pSH4-KF – pSH14-KF displayed a range of kanamycin concentration-dependent fluorescent phenotypes as determined by plate reader fluorescence assays (see cell density and fluorescence assays section, above, for experimental details). *E. coli* SH386 cells transformed with pSH6-KF (referred to as *E. coli* SH391) displayed the most favorable properties: essentially no background fluorescence in the absence of kanamycin, and a robust dose-dependent increase in fluorescence in response to kanamycin (Figure 2-19). Thus, *E. coli* SH391 was selected for subsequent experiments. Interestingly, the results are consistent with the *lpp* promoter being the weakest of the six promoters tested. The full fluorescence quantification data are shown in Figure 2-20.

| primer name | sequence (5' – 3') | amplicon size (bp) | template |
|-------------|---|--------------------|----------|
| pSH4-KF-1 | <u>ACGGGA</u> ACTACAGACGCGTGCTG | 725 | pSH3-KF |
| pSH4-KF-2 | GCTAGCACTGTACCTAGGACTGAGCTAGCCGTC AAACCGGGCCCTCTTGCGGG | | |
| pSH4-KF-3 | CAGTCCTAGGTACAGTGCTAGC CCAGCCAGAG | 769 | pSH3-KF |
| pSH4-KF-4 | <u>CCTACTCAGGAGAGCGTTACCCG</u> | | |
| pSH5-KF-2 | GCTAGCATTGTACCTAGGACTGAGCTAGCTATA AAACCGGGCCCTCTTGCGGG (used with pSH4-KF-1) | 725 | pSH3-KF |
| pSH5-KF-3 | CAGTCCTAGGTACAATGCTAGC CCAGCCAGAG (used with pSH4-KF-4) | 769 | pSH3-KF |
| pSH6-KF-1 | <u>GTGACTCTAGTAGAGAGCGTTCACCGAC</u> | 1926 | pSH3-KF |
| pSH6-KF-2 | TTGACGGCTAGCTCAGTCCTAGGTACAGTGCTAGC TACTTGTAACGCTAGATCCGG | | |
| pSH6-KF-3 | AGGACTGAGCTAGCCGTC AAATCGTGCCCTGCATGCAC | 375 | pSH3-KF |
| pSH6-KF-4 | <u>GGGACRACTCCAGTGAAAAGTTCCTCTCC</u> | | |
| pSH7-KF-2 | CTGACAGCTAGCTCAGTCCTAGGTATAATGCTAGC TACTTGTAACGCTAGATCCGG (used with pSH6-KF-1) | 1926 | pSH3-KF |
| pSH7-KF-3 | AGGACTGAGCTAGCCATA AAATCGTGCCCTGCATGCAC (used with pSH6-KF-4) | 375 | pSH3-KF |
| pSH8-KF-2 | TTTATGGCTAGCTCAGTCCTAGGTACRATGCTAGC TACTTGTAACGCTAGATCCGG (used with pSH6-KF-1) | 1926 | pSH3-KF |
| pSH8-KF-3 | AGGACTGAGCTAGCCATA AAATCGTGCCCTGCATGCAC (used with pSH6-KF-4) | 375 | pSH3-KF |

Table 2-9 Primers for constructing pSH4-KF through pSH14-KF

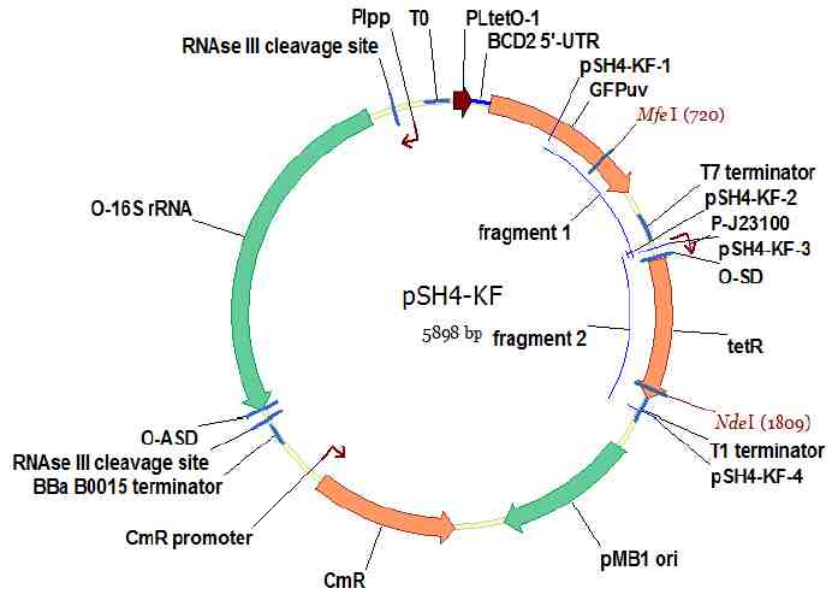


Figure 2-17 Plasmid map of pSH4-KF

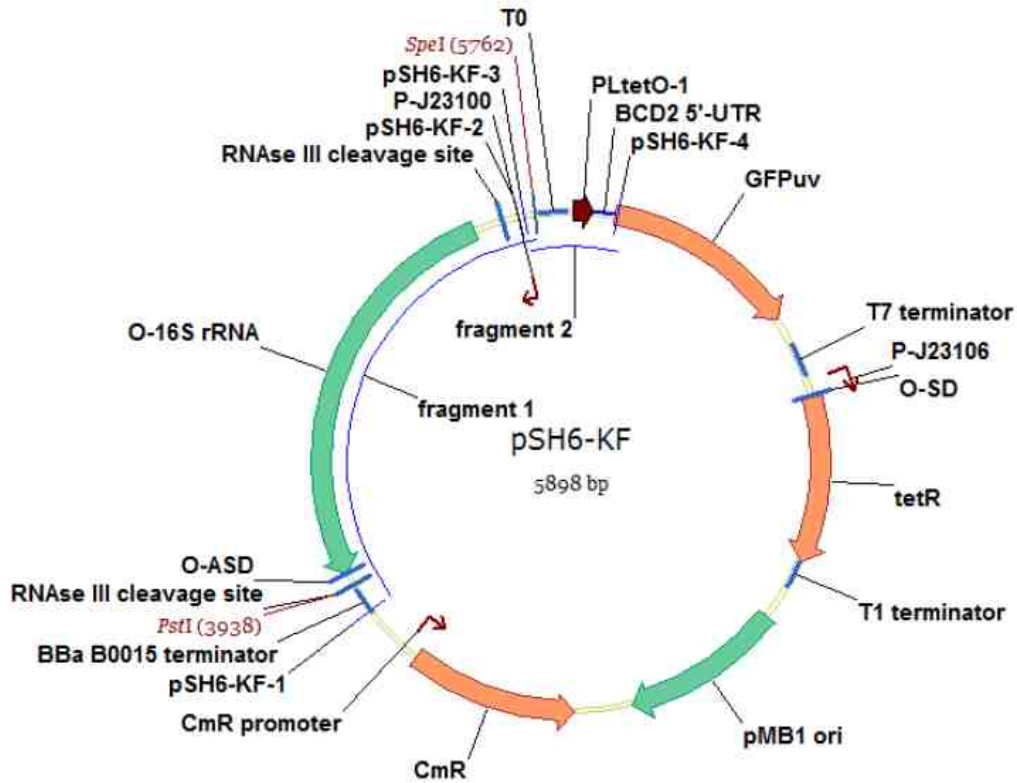


Figure 2-18 Plasmid map of pSH6-KF

| Name | Sequence | Strength |
|------------|---|---------------|
| BBa_J23100 | TTGACG GCTAGCTCAGTCCTAGG TACAGT GCTAGC | Strong (1.0) |
| BBa_J23106 | TTTACG GCTAGCTCAGTCCTAGG TATAGT GCTAGC | Medium (0.47) |
| BBa_J23115 | TTTATAG GCTAGCTCAGCCCTTGG TACAAT GCTAGC | Weak (0.15) |
| BBa_J23108 | CTGACAG GCTAGCTCAGTCCTAGG TATAAT GCTAGC | Medium (0.51) |
| BBa_J23114 | TTTATG GCTAGCTCAGTCCTAGG TACAAT GCTAGC | Weak (0.10) |
| lpp | TTCTCA ACATAAAAAACTTTGTGT AATACT | |

Table 2-10 Sequence of the promoters used in constructing pSH4-KF through pSH14-KF

| plasmid | tetR | | O-16S | |
|----------|------------|---------------|------------|---------------|
| | promoter | strength | promoter | strength |
| pSH3-KF | BBa_J23106 | Medium (0.47) | lpp | ND |
| pSH4-KF | BBa_J23100 | Strong (1.0) | lpp | ND |
| pSH5-KF | BBa_J23115 | Weak (0.15) | lpp | ND |
| pSH6-KF | BBa_J23106 | Medium (0.47) | BBa_J23100 | Strong (1.0) |
| pSH7-KF | BBa_J23106 | Medium (0.47) | BBa_J23108 | Medium (0.51) |
| pSH8-KF | BBa_J23106 | Medium (0.47) | BBa_J23114 | Weak (0.10) |
| pSH9-KF | BBa_J23100 | Strong (1.0) | BBa_J23100 | Strong (1.0) |
| pSH10-KF | BBa_J23100 | Strong (1.0) | BBa_J23108 | Medium (0.51) |
| pSH11-KF | BBa_J23100 | Strong (1.0) | BBa_J23114 | Weak (0.10) |
| pSH12-KF | BBa_J23115 | Weak (0.15) | BBa_J23100 | Strong (1.0) |
| pSH13-KF | BBa_J23115 | Weak (0.15) | BBa_J23108 | Medium (0.51) |
| pSH14-KF | BBa_J23115 | Weak (0.15) | BBa_J23114 | Weak (0.10) |

Table 2-11 Promoter combinations of pSH3-KF through pSH14-KF

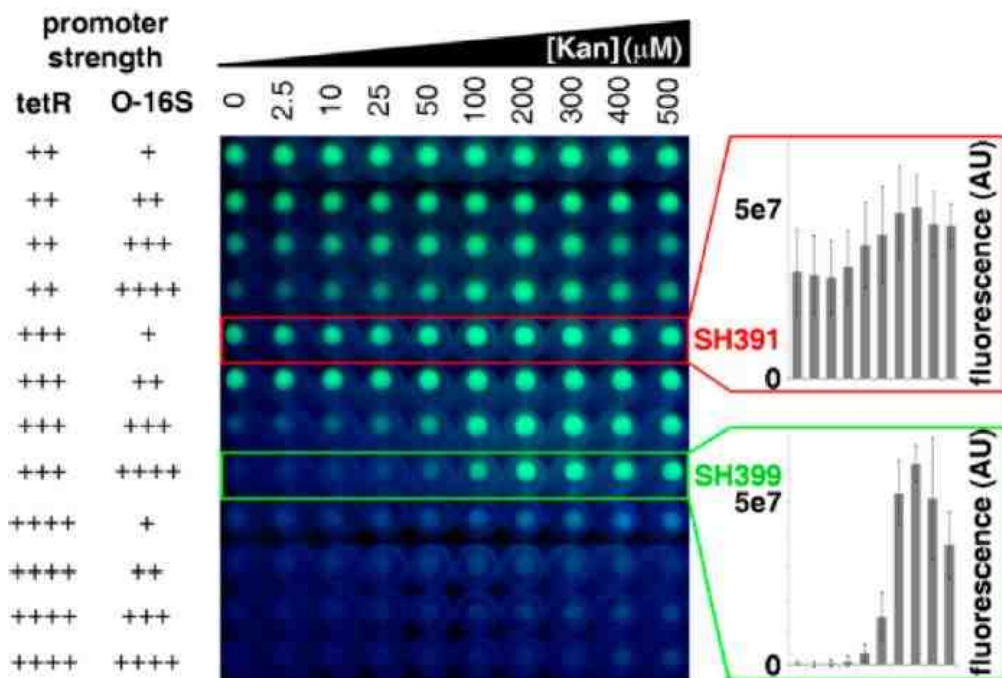


Figure 2-19 Cell pellet fluorescence of initial detector strain *E. coli* SH391 (boxed in red), 11 additional strains with tetR and O-16S promoter strengths combinatorially altered (promoter strengths are show on the left: +, very weak; ++, weak; +++, medium; +++++, strong), and *E. coli* SH399, the strain with the best detection performance (boxed in green), in response to increasing concentrations of kanamycin. Fluorescence quantification of *E. coli* SH391 and *E. coli* SH399 at each of the 10 kanamycin concentrations tested is shown in the bar graphs to the right.

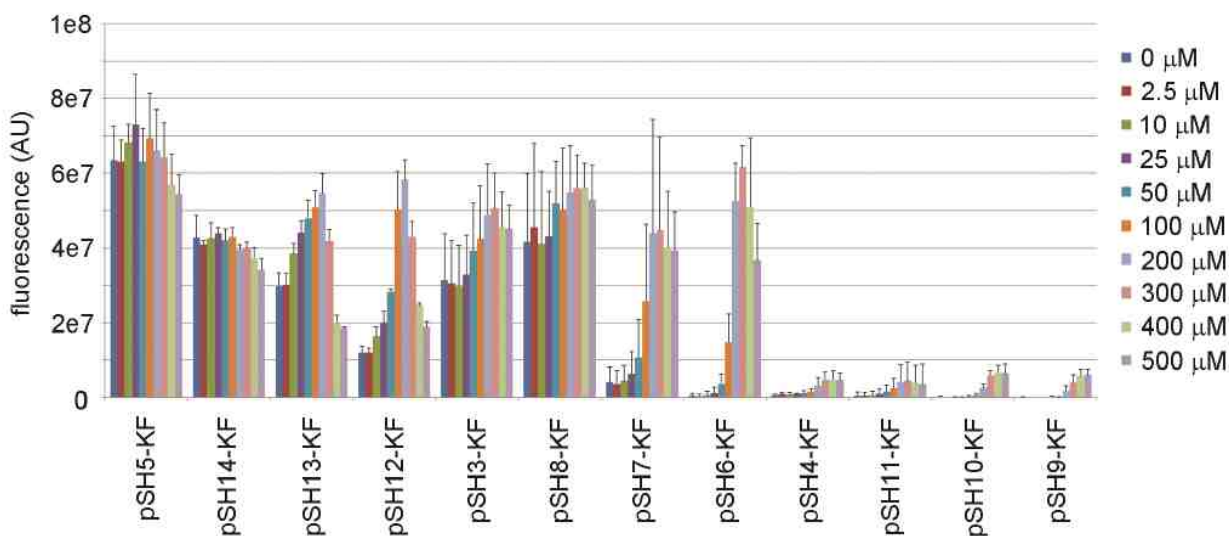


Figure 2-20 Fluorescence quantification of *E. coli* SH386 cells containing pSH3-KF – pSH14-KF grown in the presence of a range of kanamycin concentrations.

3. Results and discussion

Ribosome inhibition assays of aminoglycosides in E. coli SH399. *E. coli* SH399, which harbors detection plasmid pSH6-KF, was used to conduct ribosome inhibition assays using a range of concentrations of twelve structurally diverse aminoglycosides – including 4,6-disubstituted 2-deoxystreptamines (2-DOS) gentamicins, G418, sisomicin, tobramycin, and amikacin; 4,5-disubstituted 2-DOS paromomycin, neomycin B, and ribostamycin; and atypical 2-DOS apramycin, hygromycin B, and neamine (Figure 2-1). In addition to kanamycin A, SH399 grown to stationary phase (18 h) in the presence of a range of concentrations of each aminoglycoside was able to detect O-ribosome inhibition by nine of these compounds (Figure 2-21). The two compounds that failed to give a signal, G418 and hygromycin B, also caused significant growth inhibition of SH399 (Figure 2-22), indicating that the A1408G 16S rRNA mutation does not confer sufficient resistance to these compounds to allow survival of the detector strain. This observation is consistent with previously reported levels of resistance conferred by the A1408G mutation to a subset of the compounds examined,³¹ and for those compounds that were detectable, the A1408G mutation confers resistance well above the detection threshold (Figure 2-22).

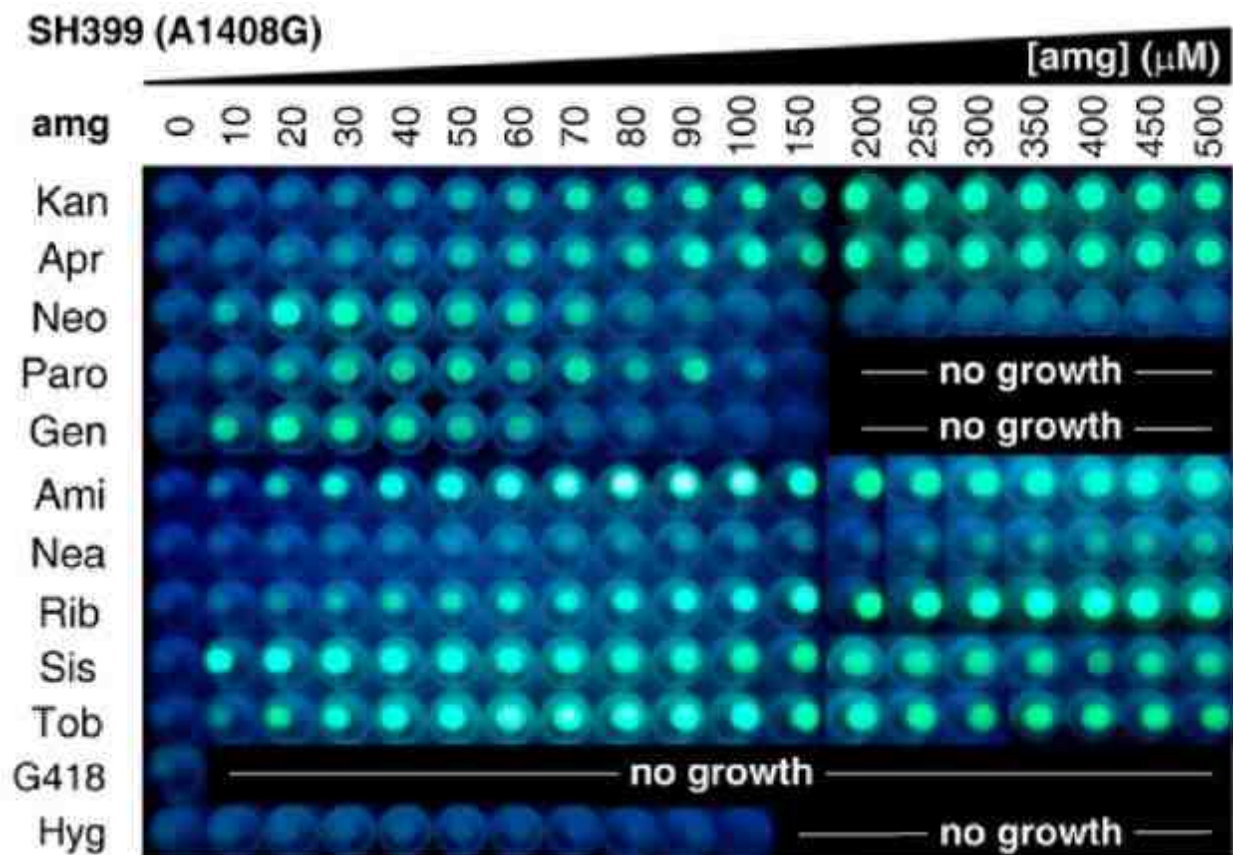


Figure 2-21 Cell pellet fluorescence of *E. coli* SH399 in response to increasing concentrations of aminoglycosides. Kan, kanamycin A; Apr, apramycin; Neo, neomycin B; Paro, paromomycin; Gen, gentamicins; Ami, amikacin; Nea, neamine; Rib, ribostamycin; Sis, sisomicin; Tob, tobramycin.

The fluorescence dose-response patterns observed for SH399 treated with these 10 aminoglycosides were different for each compound (Figure 2-21, Figure 2-22) and appeared upon qualitative inspection to correlate with previously reported compound potencies determined by both in vitro translation assays²⁶⁻³⁰ and *E. coli* growth inhibition assays,^{26, 28, 30} suggesting that the O-ribosome reporter system may be useful for comparing aminoglycoside potencies. To examine this possibility, we first compared IC50 values calculated from fluorescence data obtained from aminoglycoside-treated SH399 with previously determined IC50 values of a subset of six aminoglycosides (kanamycin A, neomycin B, paromomycin, gentamicins,

ribostamycin, and tobramycin) measured through inhibition of translation in vitro.²⁸ We found a strong correlation ($R^2 = 0.97$, Figure 2-23) between the two data sets, suggesting that IC50 values determined using the O-ribosome reporter assay are comparably accurate to those determined using in vitro translation assays. Next, to test whether the fluorescence dose-response patterns also correlate with inhibition of *E. coli* growth, we compared dose-dependent growth inhibition (represented as LD50 values) of the parent aminoglycoside sensitive *E. coli* strain SH434 with IC50 values calculated from fluorescence data obtained from aminoglycoside-treated SH399. While data obtained by the two methods correlated for a subset of the compounds (apramycin, gentamicins, amikacin, ribostamycin, sisomicin, and tobramycin; $R^2 = 0.97$, Figure 2-23), there was a lack of correlation between the two data sets for kanamycin A, neomycin B, and paromomycin, and therefore between the two data sets as a whole ($R^2 = 0.40$, Figure 2-23). While the reason for the incomplete correlation between inhibition of *E. coli* growth and fluorescence-derived IC50 values is unclear, we suggest that these inconsistencies are the result of differences between the pleiotropic effects of differentially inhibiting the ribosome, whose activity is required for synthesis of the entire *E. coli* proteome, on cell viability, and the effects of differentially inhibiting the O-ribosome, which are restricted to the TetR-GFP output system. Taken together, these results are consistent with the ability of the O-ribosome reporter system to compare the potencies of aminoglycosides as ribosome inhibitors. Of the 10 compounds examined, sisomicin was found to have the strongest ribosome inhibition activity, followed in order of decreasing activity by gentamicins, neomycin B, paromomycin, tobramycin, amikacin, ribostamycin, apramycin, kanamycin A, and neamine (Figure 2-22, 2-23). These results provide a complete comparative assessment of the ribosome inhibiting potencies of these 10 compounds that is consistent with previous reports of aminoglycoside potencies and structure-activity

relationships obtained through in vitro translation inhibition assays using subsets of these compounds.²⁶⁻³⁰

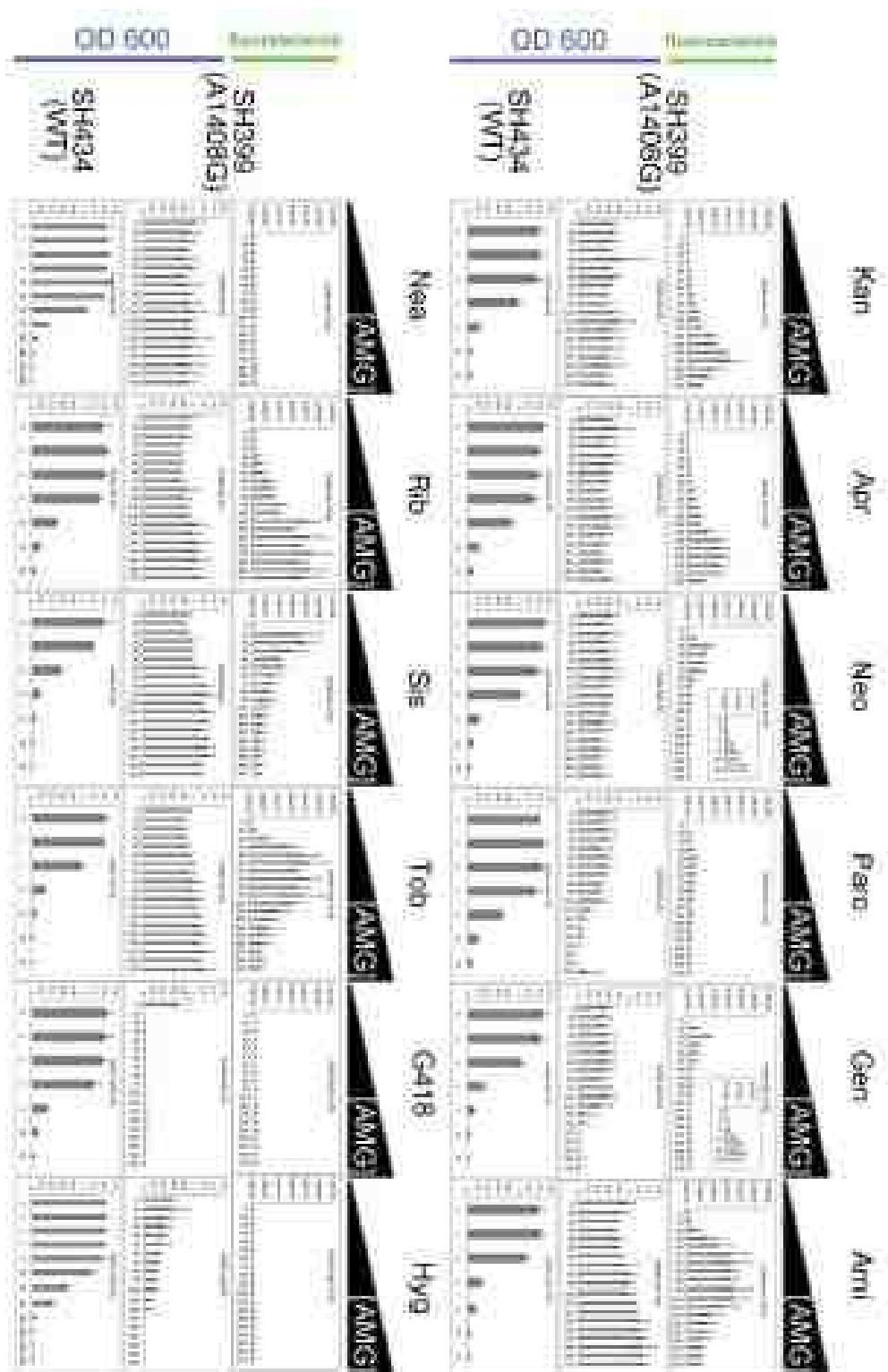
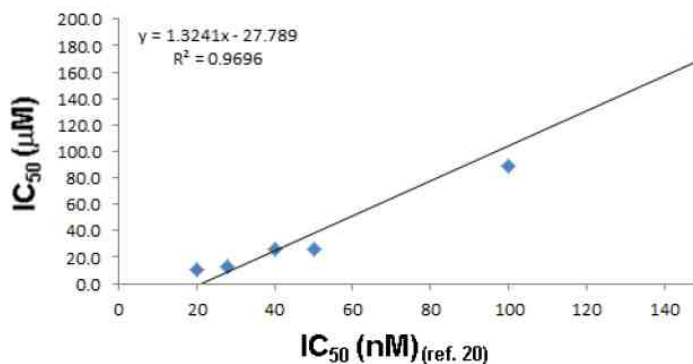
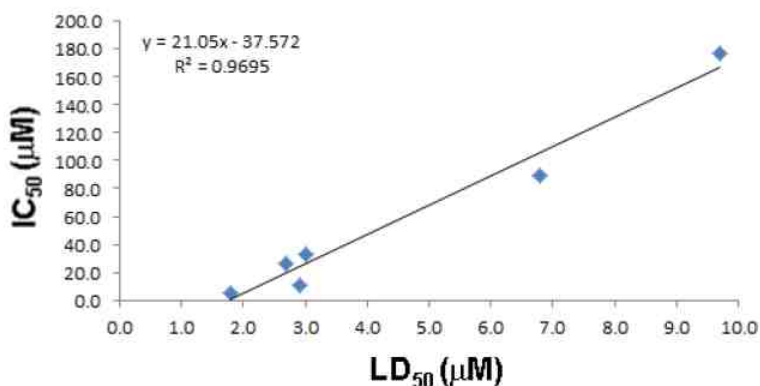


Figure 2-22 Fluorescence quantification (top row of graphs) and OD600 quantification (middle row of graphs) of *E. coli* SH399 (pSH6-KF, pRRSH2-A1408G) cells grown in a range of concentrations (0-500 μM) of each of the twelve aminoglycosides examined; and OD600 quantification (bottom row of graphs) of *E. coli* SH434 (pSH6-KF, pRRSH2) cells grown in a range of concentrations (0-32 or 0-1024 μM , 2-fold serial dilutions) of each of the twelve aminoglycosides examined. The scale of x and y axes is consistent for each row of bar charts. Further discussion of these results is presented in the main article.

| AMG | IC ₅₀ (nM) (main text, ref 28) | IC ₅₀ (μM) |
|------|---|------------------------------------|
| Gen | 20 | 10.8 |
| Neo | 28 | 12.5 |
| Paro | 40 | 25.5 |
| Tob | 50 | 26.2 |
| Rib | 100 | 89.0 |
| Kan | 150 | 183.0 |



| AMG | LD ₅₀ (μM) | IC ₅₀ (μM) |
|-----|------------------------------------|------------------------------------|
| Sis | 1.8 | 5.2 |
| Tob | 2.7 | 26.2 |
| Gen | 2.9 | 10.8 |
| Ami | 3.0 | 32.6 |
| Rib | 6.8 | 89.0 |
| Apr | 9.7 | 177.0 |



| AMG | LD ₅₀ (μM) | IC ₅₀ (μM) |
|------|------------------------------------|------------------------------------|
| Sis | 1.8 | 5.2 |
| Tob | 2.7 | 26.2 |
| Gen | 2.9 | 10.8 |
| Ami | 3.0 | 32.6 |
| Neo | 5.3 | 12.5 |
| Kan | 5.5 | 183.0 |
| Rib | 6.8 | 89.0 |
| Paro | 7.8 | 25.5 |
| Apr | 9.7 | 177.0 |
| Nea | 45.5 | ND |

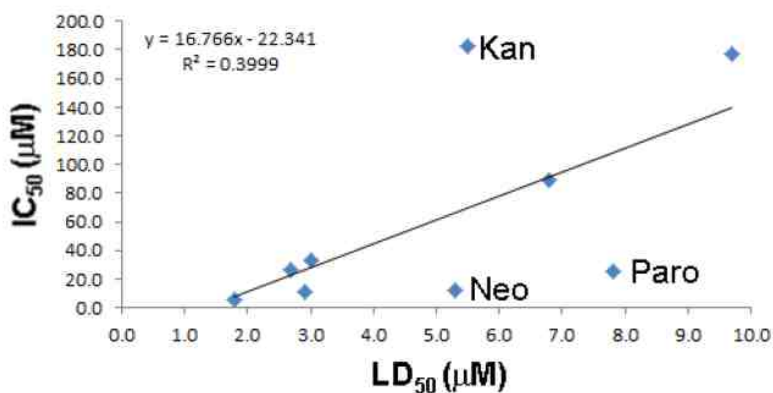


Figure 2-23 Analysis of the correlations between: (top table and graph) IC₅₀ values previously determined through *in vitro* translation assays²⁸ (column 1, x axis) and IC₅₀ values determined

from *E. coli* SH399-derived fluorescence data (column 2, y axis); (middle table and graph) LD50 values determined from growth inhibition assays of *E. coli* SH434 (column 1, x axis) and IC50 values determined from *E. coli* SH399-derived fluorescence data for the subset of 6 compounds for which there was a statistically significant correlation (column 2, y axis); and (bottom table and graph) LD50 values determined from growth inhibition assays of *E. coli* SH434 (column 1, x axis) and IC50 values determined from *E. coli* SH399-derived fluorescence data for the full set of 9 compounds (column 2, y axis). The 3 compounds that produced outlying data are labeled in the graph. Note that neamine was excluded from the analysis due to its very weak ribosome inhibition and growth inhibition activities. Further discussion of these results is presented in the main article.

Interestingly, we also observed for some aminoglycosides that at drug concentrations beyond those that give the peak response, fluorescence actually decreases and does so to varying extents with different compounds (Figure 2-21, Figure 2-22). The effect was most pronounced with neomycin B, paromomycin, and gentamicins; occurred to an intermediate extent with sisomicin, tobramycin, and amikacin; occurred to a slight extent with kanamycin A and apramycin; and was absent with ribostamycin and neamine. In the cases of paromomycin and gentamicins, these decreases in fluorescence were accompanied by growth inhibition. These results are consistent with previous structural and spectroscopic observations that neomycin B, paromomycin, and gentamicin bind to and inhibit the ribosome at a second, lower affinity site in helix 69 of the large ribosomal subunit.^{8, 10,12,15,18} In our system, binding to this site on the pRRSH2-A1408G-derived ribosome would affect translation of both GFPuv and endogenous proteins, leading to both a decrease in fluorescence and a loss of cell viability. When considered together with previous work, our observations suggests that the O-ribosome reporter system can identify, via dose-dependent fluorescence decrease at higher concentrations, aminoglycosides that inhibit the ribosome by interacting with a secondary site such as H69, and that other aminoglycosides in our panel that exhibit this phenomenon may also bind to H69 or to another secondary site. Examination of the X-ray crystal structures of neomycin B, paromomycin, and gentamicin C1a bound to H6915 reveals conserved contacts between the C-1 and C-3 amines of

the 2-DOS core, which are present in all aminoglycoside structures, and residues 1921–1923 of the 23S rRNA, leaving open the possibility that other aminoglycosides may interact with H69. Experiments to test the binding of aminoglycosides in our panel to H69 are currently underway in our laboratory.

To further explore the capabilities of the system and attempt to develop a strain that can detect O-ribosome inhibition by hygromycin B and G418, we introduced the U1406A mutation into pRRSH2. Mutations at position 1406 confer an aminoglycoside resistance spectrum distinct from that of A1408G, including resistance to G418 (U1406A)³² and hygromycin B (U1406C).³³ We tested the ability of strain SH431 carrying this mutation and reporter plasmid pSH6-KF grown to stationary phase (24 h) in the presence of a range of concentrations of each aminoglycoside to detect O-ribosome inhibition by the same set of 12 aminoglycosides. As anticipated, SH431 was able to detect O-ribosome inhibition by both G418 and hygromycin B (Figure 2-24) as well as kanamycin A and gentamicins (Figure 2-25). We observed significant growth inhibition and a lack of signal by SH431 in the presence of the remaining eight compounds, indicating that the U1406A mutation is unable to confer resistance to these compounds. Dose response patterns observed for SH431 treated with the four compounds for which fluorescence could be observed indicate that, among these, gentamicins are the most potent ribosome inhibitors, followed by G418 and hygromycin B, and with kanamycin A being the least potent (Figure 2-25, 2-26). IC₅₀ values calculated from the O-ribosome- based fluorescence assay correlated with LD₅₀ values of the parent aminoglycoside sensitive *E. coli* strain SH434 for three of the compounds (gentamicins, G418, hygromycin B; R² = 0.997, Figure 2-26), but not for kanamycin A, as was the case with SH399.

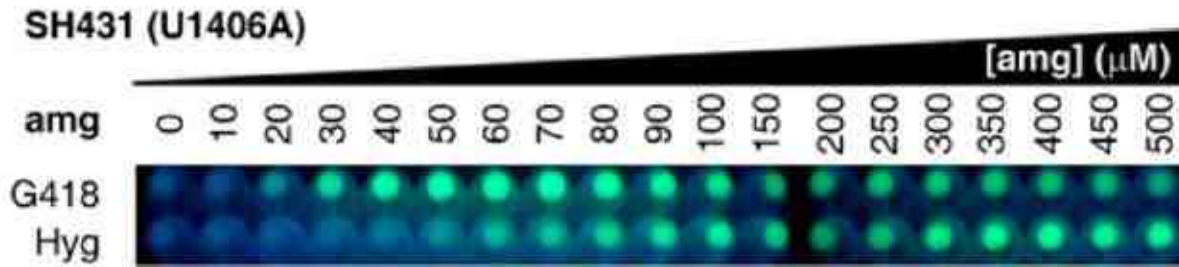


Figure 2-24 Cell pellet fluorescence of *E. coli* SH431 in response to increasing concentrations of G418, geneticin (G418); Hyg, hygromycin B.

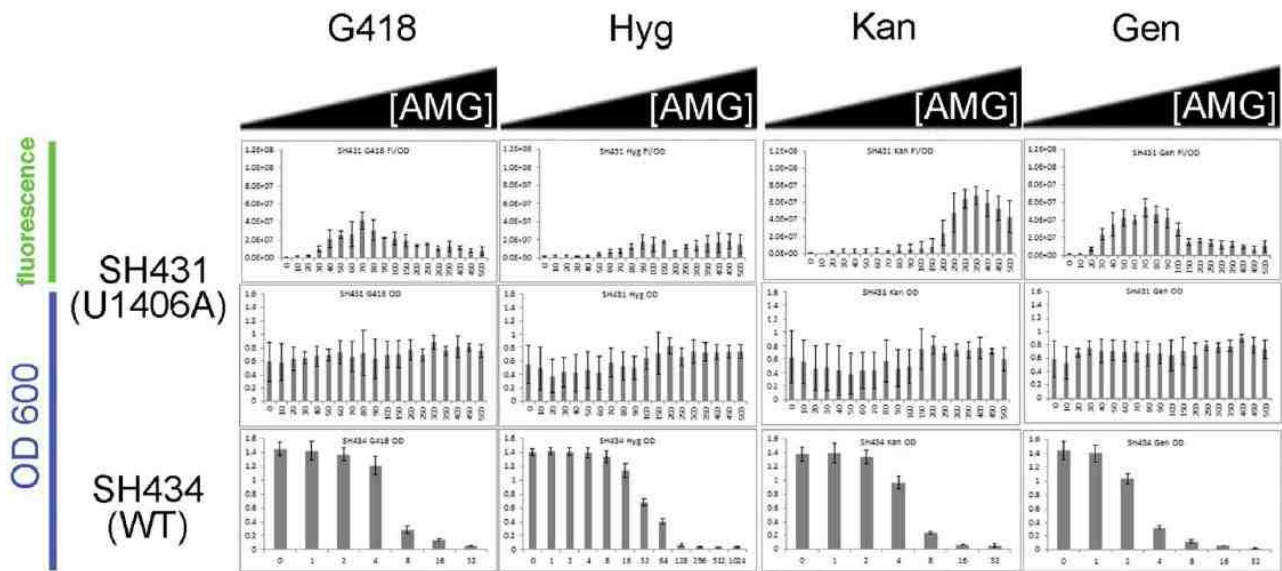
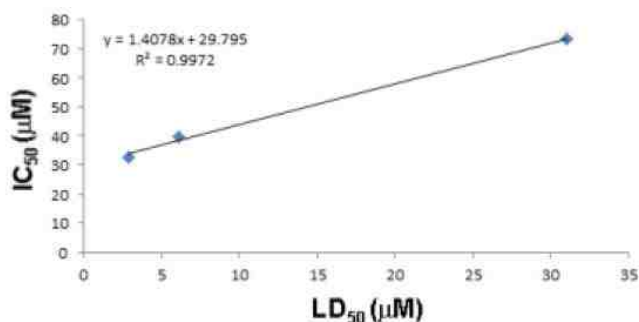


Figure 2-25 Fluorescence quantification (top row of graphs) and OD600 quantification (bottom row of graphs) of *E. coli* SH431 (pSH6-KF, pRRSH2-U1406A) cells grown in a range of concentrations (0-500 μ M) of G418, hygromycin, kanamycin, and gentamicins. The scale of x and y axes is consistent for each row of bar charts.

| AMG | LD ₅₀ (μM) | IC ₅₀ (μM) |
|------|-----------------------|-----------------------|
| Gen | 2.9 | 32.8 |
| G418 | 6.1 | 39.6 |
| Hyg | 31 | 73.3 |



| AMG | LD ₅₀ (μM) | IC ₅₀ (μM) |
|------|-----------------------|-----------------------|
| Gen | 2.9 | 32.8 |
| Kan | 5.5 | 220.5 |
| G418 | 6.1 | 39.6 |
| Hyg | 31 | 73.3 |

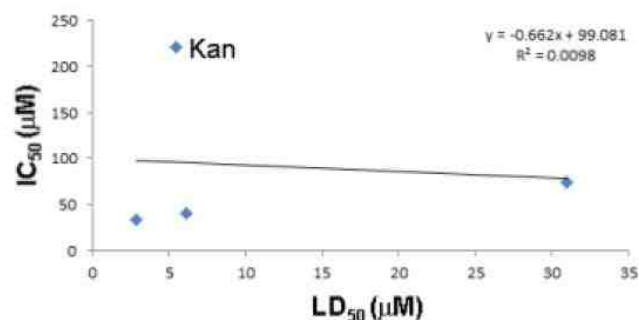


Figure 2-26 Analysis of the correlations between: (top table and graph) LD₅₀ values determined from growth inhibition assays of *E. coli* SH434 (column 1, x axis) and IC₅₀ values determined from *E. coli* SH431-derived fluorescence data for the subset of 3 compounds for which there was a statistically significant correlation (column 2, y axis); and (bottom table and graph) LD₅₀ values determined from growth inhibition assays of *E. coli* SH434 (column 1, x axis) and IC₅₀ values determined from *E. coli* SH431-derived fluorescence data for the full set of 4 compounds (column 2, y axis). The compound that produced outlying data is labeled in the graph.

4. Conclusion

In summary, we have created engineered *E. coli* strains that can directly detect and quantify ribosome inhibition at the A-site by a variety of structurally distinct aminoglycosides with high sensitivity and essentially no background. The fluorescence dose–response patterns we observed for the aminoglycosides tested correlate with their reported ribosome inhibiting potencies, demonstrating that our system can be used to determine the relative potencies of aminoglycosides as ribosome inhibitors. The observation that compounds known to act by binding to H69 show dose-dependent fluorescence decrease at high concentrations suggests that our system can also report on compound secondary binding modes. We have also demonstrated

that the selectivity of each strain for detection of specific aminoglycosides—even those with high structural similarity such as gentamicin and G418—can be controlled by employing 16S rRNA mutations that confer distinct resistance profiles. We believe that the strains developed here provide a powerful new tool for assaying and studying ribosome inhibition by aminoglycosides and other ribosome inhibitors in the context of live bacterial cells and will find broad applicability in drug discovery endeavors.

We envision that the O-ribosome reporter strategy described here can be used to assess structure–activity relationships of synthetic aminoglycoside analogs in high-throughput, to detect and quantify aminoglycosides in natural product extracts, and to detect activity of aminoglycoside biosynthetic enzymes, as was recently done with a target-based β -lactam antibiotic detection system.⁵³ We suggest that our strategy can be extended to specifically detect ribosome inhibition by compound classes acting at other 16S rRNA binding sites such as streptomycin, kasugamycin, spectinomycin, tetracyclines, tuberactinomycins, and pactamycins¹ by employing 16S rRNA resistance mutations specific to each compound class. Furthermore, with the recent development of a functional ribosome in which the 16S and 23S rRNAs are tethered,⁵⁴ our strategy may be extended to detect ribosome inhibition by compounds targeting the 23S rRNA such as macrolides, thiostrepton, avilamycin, and others.¹ Mutation of the O-ribosome A-site in the strains described here to mimic the A-site of other bacteria (e.g., Mycobacteria or other pathogens) or human mitochondria may also allow estimation of aminoglycoside potency against these bacteria, or toxicity to human cells, respectively.

5. References

1. Wilson, D.N. Ribosome-targeting antibiotics and mechanisms of bacterial resistance. *Nat Rev Microbiol.* 2014; 12(1):35-48.
2. Houghton, J. L., Green, K. D., Chen, W., and Garneau-Tsodikova, S. The future of aminoglycosides: the end or renaissance? *ChemBioChem.* 2014; 11, 880–902.
3. Becker, B., Cooper, M.A. Aminoglycoside antibiotics in the 21st century. *ACS Chem Biol.* 2013; 8(1):105-15.
4. Kotra, L.P., Haddad, J., Mobashery, S. Aminoglycosides: perspectives on mechanisms of action and resistance and strategies to counter resistance. *Antimicrob Agents Chemother.* 2000; 44(12):3249-56.
5. Flatt, P.M., Mahmud, T. Biosynthesis of aminocyclitol-aminoglycoside antibiotics and related compounds. *Nat Prod Rep.* 2007; 24(2):358-92.
6. Wehmeier, U. F. and Piepersberg, W. Enzymology of aminoglycoside antibiotics – deduction from gene clusters. In *Methods in Enzymology*, Vol. 459 (Hopwood, D. A., Ed.), pp 459–491, Academic Press, 2009; New York.
7. Park, S.R., Park, J.W., Ban, Y.H., Sohng, J.K., Yoon, Y.J. 2-Deoxystreptamine-containing aminoglycoside antibiotics: recent advances in the characterization and manipulation of their biosynthetic pathways. *Nat Prod Rep.* 2013; 30(1):11-20.
8. Wang, L., Pulk, A., Wasserman, M.R., *et al.* Allosteric control of the ribosome by small-molecule antibiotics. *Nat Struct Mol Biol.* 2012; 19(9):957-63.
9. Tsai, A., Uemura, S., Johansson, M., *et al.* The impact of aminoglycosides on the dynamics of translation elongation. *Cell Rep.* 2013; 3(2):497-508.

10. Wasserman, M.R., Pulk, A., Zhou, Z., *et al.* Chemically related 4, 5-linked aminoglycoside antibiotics drive subunit rotation in opposite directions. *Nat Commun.* 2015; 6:7896.
11. Cabañas, M.J., Vázquez, D., Modolell, J.. Inhibition of ribosomal translocation by aminoglycoside antibiotics. *Biochem Biophys Res Commun.* 1978; 83(3):991-7.
12. Feldman, M.B., Terry, D.S., Altman, R.B., Blanchard, S.C. Aminoglycoside activity observed on single pre-translocation ribosome complexes. *Nat Chem Biol.* 2010; 6(3):244.
13. Davies, J., Gorini, L., Davis, B.D. Misreading of RNA codewords induced by aminoglycoside antibiotics. *Mol Pharmacol.* 1965; 1(1):93-106.
14. Moazed, D., Noller, H.F. Interaction of antibiotics with functional sites in 16S ribosomal RNA. *Nature.* 1987; 327(6121):389-94.
15. Borovinskaya, M.A., Pai, R.D., Zhang, W., *et al.* Structural basis for aminoglycoside inhibition of bacterial ribosome recycling. *Nat Struct Mol Biol.* 2007; 14(8):727-32.
16. Borovinskaya, M.A., Shoji, S., Fredrick, K., Cate, J.H. Structural basis for hygromycin B inhibition of protein biosynthesis. *RNA.* 2008; 14(8):1590-9.
17. Matt, T., Ng, C.L., Lang, K., *et al.* Dissociation of antibacterial activity and aminoglycoside ototoxicity in the 4-monosubstituted 2-deoxystreptamine apramycin. *Proc Natl Acad Sci USA.* 2012; 109(27):10984-9.
18. Scheunemann, A.E., Graham, W.D., Vendeix, F.A., Agris, P.F. Binding of aminoglycoside antibiotics to helix 69 of 23S rRNA. *Nucleic Acids Res.* 2010; 38(9):3094-105.
19. Shalev, M., Baasov, T. When Proteins Start to Make Sense: Fine-tuning Aminoglycosides for PTC Suppression Therapy. *Medchemcomm.* 2014; 5(8):1092-1105.

20. Chang, C.W., Takemoto, J.Y. Antifungal Amphiphilic Aminoglycosides. *Medchemcomm.* 2014; 5(8):1048-1057.
21. Vicens, Q., Westhof, E. Crystal structure of geneticin bound to a bacterial 16S ribosomal RNA A site oligonucleotide. *J Mol Biol.* 2003; 326(4):1175-88.
22. François, B., Russell, R.J., Murray, J.B., *et al.* Crystal structures of complexes between aminoglycosides and decoding A site oligonucleotides: role of the number of rings and positive charges in the specific binding leading to miscoding. *Nucleic Acids Res.* 2005; 33(17):5677-90.
23. Sannes-lowery, K.A., Griffey, R.H., Hofstadler, S.A. Measuring dissociation constants of RNA and aminoglycoside antibiotics by electrospray ionization mass spectrometry. *Anal Biochem.* 2000; 280(2):264-71.
24. Hendrix, M., Priestley, E.S., Joyce, G.F., Wong, C.H. Direct observation of aminoglycoside-RNA interactions by surface plasmon resonance. *J Am Chem Soc.* 1997; 119(16):3641-8.
25. Watkins, D., Norris, F.A., Kumar, S., Arya, D.P. A fluorescence-based screen for ribosome binding antibiotics. *Anal Biochem.* 2013; 434(2):300-7.
26. Greenberg, W. A., Priestley, E. S., Sears, P. S., Alper, P. B., Rosenbohm, C., Hendrix, M., Hung, S.-C., and Wong, C.-H. Design and synthesis of new aminoglycoside antibiotics containing neamine as an optimal core structure: correlation of antibiotic activity with in vitro inhibition of translation. *J. Am. Chem. Soc.* 1999; 121, 6527–6541.
27. Benveniste, R., Davies, J. Structure-activity relationships among the aminoglycoside antibiotics: role of hydroxyl and amino groups. *Antimicrob Agents Chemother.* 1973; 4(4):402-9.

28. Sucheck, S. J., Wong, A. L., Koeller, K. M., Boehr, D. D., Draker, K.-a., Sears, P., Wright, G. D., and Wong, C.-H. Design of bifunctional antibiotics that target bacterial rRNA and inhibit resistance-causing enzymes. *J. Am. Chem. Soc.* 2000; 122, 5230–5231.
29. Salian, S., Matt, T., Akbergenov, R., *et al.* Structure-activity relationships among the kanamycin aminoglycosides: role of ring I hydroxyl and amino groups. *Antimicrob Agents Chemother.* 2012; 56(12):6104-8.
30. Kato, T., Yang, G., Teo, Y., *et al.* Synthesis and antiribosomal activities of 4' -O-, 6' -O-, 4'' -O-, 4' , 6' -O-, and 4'' , 6'' -O-derivatives in the kanamycin series indicate differing target selectivity patterns between the 4,5- and 4,6-series of disubstituted 2-deoxystreptamine aminoglycoside antibiotics. *ACS Infect. Dis.* 2015; 1, 479.
31. Recht, M.I., Douthwaite, S., Puglisi, J.D. Basis for prokaryotic specificity of action of aminoglycoside antibiotics. *EMBO J.* 1999; 18(11):3133-8.
32. Recht, M.I., Puglisi, J.D. Aminoglycoside resistance with homogeneous and heterogeneous populations of antibiotic-resistant ribosomes. *Antimicrob Agents Chemother.* 2001; 45(9):2414-9.
33. Pfister, P., Risch, M., Brodersen, D.E., Böttger, E.C. Role of 16S rRNA Helix 44 in Ribosomal Resistance to Hygromycin B. *Antimicrob Agents Chemother.* 2003; 47(5):1496-502.
34. Hui, A., De boer, H.A. Specialized ribosome system: preferential translation of a single mRNA species by a subpopulation of mutated ribosomes in *Escherichia coli*. *Proc Natl Acad Sci USA.* 1987; 84(14):4762-6.

35. Lee, K., Holland-staley, C.A., Cunningham, P.R. Genetic analysis of the Shine-Dalgarno interaction: selection of alternative functional mRNA-rRNA combinations. *RNA*. 1996; 2(12):1270-85.
36. Rackham, O., Chin, J.W. A network of orthogonal ribosome x mRNA pairs. *Nat Chem Biol*. 2005; 1(3):159-66.
37. Beck, C.F., Mutzel, R., Barbé, J., Müller, W. A multifunctional gene (tetR) controls Tn10-encoded tetracycline resistance. *J Bacteriol*. 1982; 150(2):633-42.
38. Cramer, A., Whitehorn, E.A., Tate, E., Stemmer, W.P. Improved green fluorescent protein by molecular evolution using DNA shuffling. *Nat Biotechnol*. 1996; 14(3):315-9.
39. Lutz, R., Bujard, H. Independent and tight regulation of transcriptional units in *Escherichia coli* via the LacR/O, the TetR/O and AraC/I1-I2 regulatory elements. *Nucleic Acids Res*. 1997; 25(6):1203-10.
40. J. Sambrook, D. W. Russell, *Molecular cloning: a laboratory manual 3rd edition*, Cold Spring Harbor Press, Cold Spring Harbor, NY, 2001.
41. Zaporozhets, D., French, S., Squires, C.L. Products transcribed from rearranged *rrn* genes of *Escherichia coli* can assemble to form functional ribosomes. *J Bacteriol*. 2003; 185(23):6921-7.
42. Brosius, J., Ullrich, A., Raker, M.A., *et al*. Construction and fine mapping of recombinant plasmids containing the *rrnB* ribosomal RNA operon of *E. coli*. *Plasmid*. 1981; 6(1):112-8.
43. Quan, J., Tian, J. Circular polymerase extension cloning for high-throughput cloning of complex and combinatorial DNA libraries. *Nat Protoc*. 2011; 6(2):242-51.

44. Melançon, C.E., Schultz, P.G. One plasmid selection system for the rapid evolution of aminoacyl-tRNA synthetases. *Bioorg Med Chem Lett*. 2009; 19(14):3845-7.
45. Beck, C.F., Mutzel, R., Barbé, J., Müller, W. A multifunctional gene (tetR) controls Tn10-encoded tetracycline resistance. *J Bacteriol*. 1982; 150(2):633-42.
46. Young, T.S., Ahmad, I., Yin, J.A., Schultz, P.G. An enhanced system for unnatural amino acid mutagenesis in *E. coli*. *J Mol Biol*. 2010; 395(2):361-74.
47. Mutalik, V.K., Guimaraes, J.C., Cambray, G., *et al*. Quantitative estimation of activity and quality for collections of functional genetic elements. *Nat Methods*. 2013; 10(4):347-53.
48. Mutalik, V.K., Guimaraes, J.C., Cambray, G., *et al*. Precise and reliable gene expression via standard transcription and translation initiation elements. *Nat Methods*. 2013; 10(4):354-60.
49. Lee, K., Holland-staley, C.A., Cunningham, P.R. Genetic analysis of the Shine-Dalgarno interaction: selection of alternative functional mRNA-rRNA combinations. *RNA*. 1996; 2(12):1270-85.
50. Abdi, N.M., Fredrick, K.. Contribution of 16S rRNA nucleotides forming the 30S subunit A and P sites to translation in *Escherichia coli*. *RNA*. 2005; 11(11):1624-32.
51. Inouye, S., Inouye, M. Up-promoter mutations in the lpp gene of *Escherichia coli*. *Nucleic Acids Res*. 1985; 13(9):3101-10.
52. Chen, Y.J., Liu, P., Nielsen, A.A., *et al*. Characterization of 582 natural and synthetic terminators and quantification of their design constraints. *Nat Methods*. 2013; 10(7):659-64.

53. Phelan, R. M., DiPardo, B. J., and Townsend, C. A. A high-throughput screen for the engineered production of β -lactam antibiotics. *ACS Chem. Biol.* 2012; 7, 835–840.
54. Orelle, C., Carlson, E.D., Szal, T., Florin, T., Jewett, M.C., Mankin, A.S. Protein synthesis by ribosomes with tethered subunits. *Nature.* 2015; 524(7563):119-24.

CHAPTER 3. EXTENDING THE DETECTION SYSTEM TO SENSE OTHER RIBOSOME SMALL SUBUNIT INHIBITORS AND LARGE SUBUNIT INHIBITORS.

1. Introduction

Chapter 2 has described the development of detection and quantification system for ribosome inhibition by aminoglycoside antibiotics, specifically by the 2-DOS aminoglycosides. The system is highly sensitive to detect a panel of 12 2-DOS aminoglycosides with essentially no signal background. The assay can be done by conventional over-night culturing, and the fluorescence signal can be visualized directly by eyes or can be quantified by fluorometer or microplate reader. These advantages make the system more amenable to use in any laboratory than any *in vitro* methods so far.¹ The engineered *E.coli* strains are non-pathogenic and easy to culture and distributed. These advantages make the system safer to use in any biological lab than the commonly used *in vivo* methods.¹ Thus, the system is considered to be an accurate and user-friendly method to directly detect and quantify ribosome inhibitions. It should be a powerful new tool to greatly promote the development and discover of new drugs and drug leads. Therefore, extending the detection ability of the 2-DOS aminoglycosides detection system to sense other class of ribosome inhibitors is critical to promote the application of the system. To prove our O-ribosome controlled-fluorescence reporter system can be a general platform for detecting ribosome inhibition by a variety of structurally and mechanistically distinct drug classes acting on ribosome, we tend to extend the system to sense other ribosome small subunit inhibitors which bind to different sites of 16S rRNA compared to 2-DOS aminoglycosides, and ribosome large subunit inhibitors. Eventually we hope to develop a complete O-ribosome controlled-

fluorescence reporter system that can directly detect and quantify ribosome inhibition by any small molecules targeting the ribosome.

To extend the current 2-DOS aminoglycosides detector system to sense other ribosome small subunit inhibitors, functional drug resistant rRNA mutations which can protect the ribosome from drug binding and yet support the cell survival and growth must be found and introduced into the pRRSH2 plasmid. As a proof of concept, we choose three antibiotics which have distinct structure characteristics and modes of actions as our target compounds to test. These three compounds are spectinomycin, streptomycin and kasugamycin. Spectinomycin (see structure in Figure 3-1) is aminocyclitol class antibiotics and it is widely used as a safe drug to treat gonorrhea infection all over the world. It kills bacterial pathogens by binding to the helix 45 (h45) region of 16S rRNA and consequently inhibits the translocation of tRNA during the translation.² Its mechanism of action had been well characterized by genetic experiments³ and crystallography.² The spectinomycin-bound ribosome structure shows there are many polar contacts between rRNA and spectinomycin ring A and ring B (See crystal structure in Figure 1-9). Resistance mutation on rRNA has been isolated from various bacterial pathogens.^{4, 5, 6} The mutation C1192U on 16S rRNA can confer high spectinomycin resistance and it doesn't cost fitness lost on ribosome activity.⁷ Streptomycin (see structure in Figure 3-1) is a non-2-DOS aminoglycoside antibiotic. It is one of the oldest antibiotics found in the world. It was first used as an effective treatment for tuberculosis until the drug resistance mutations emerge. It acts by binding to the helix 18 region of the 16S rRNA and consequently block the income tRNA to the decoding site (A-site) of the ribosome. Biochemical studies and crystallography show that streptomycin not only has many polar contacts with 16S rRNA, but also has some polar contacts with ribosomal protein S12⁸ (see crystal structure in Figure 3-2). Therefore, resistance mutations

had been isolated from both 16S rRNA^{9, 10} and ribosomal protein S12.¹¹ Among all these resistance mutations, C912U on 16S rRNA might be best one to be applied onto our system since it can confer high resistance to streptomycin and cost little fitness lost.⁹ Kasugamycin (see structure in Figure 3-1) is also a non-2-DOS aminoglycoside antibiotic with a unique chemical structure. It was originally isolated from Japan in 1965 to prevent growth of a fungus causing rice blast disease. Kasugamycin acts by binding to the helix 24 region of 16S rRNA and consequently disrupt the interaction of initiator tRNA and the start codon at the P-site.¹² The kasugamycin-bound ribosome crystal structure shows there are relatively fewer polar contacts between the drug and ribosome (see crystal structure in Figure3-2). Resistant mutation of kasugamycin on 16S rRNA had been isolated in the laboratory.¹³ A794G was reported to confer high resistance to kasugamycin and cost little fitness lost.¹⁴ The differences of chemical structure and mode of action among these three antibiotics make them perfect representatives for ribosome small subunit inhibitors.

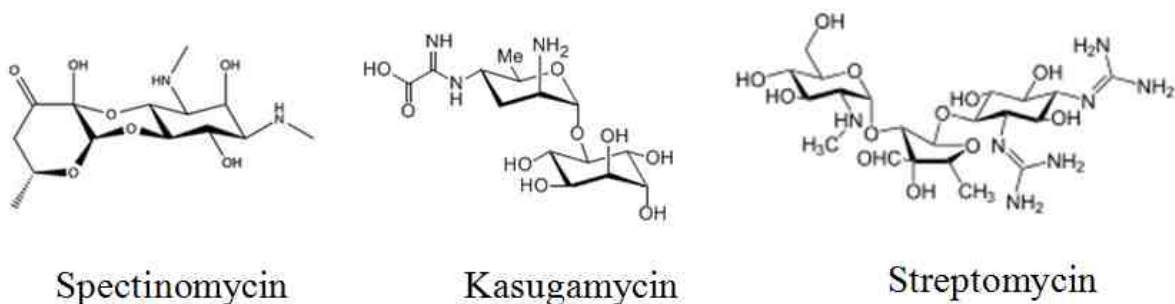


Figure 3-1 Chemical structures of spectinomycin, kasugamycin and streptomycin.

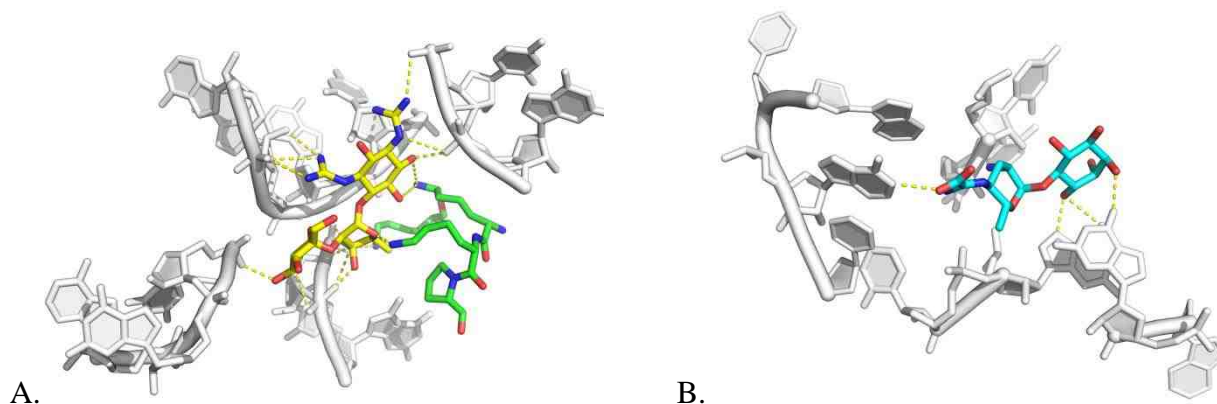


Figure 3-2 Crystal structure of drug bound ribosome. (A) Crystal structure showing interactions between streptomycin (yellow) with *Thermus thermophilus* 30S ribosomal subunit; (B) Crystal structure showing interactions between kasugamycin (cyan) with *E.coli* 30S ribosomal subunit.

To extend the ribosome inhibition detector system to sense ribosome large subunit inhibitors, the complete orthogonal ribosome system must be developed and integrated into our O-ribosome controlled-fluorescence reporter system. The current detector system harbors an O-16S rRNA which is sensitive to drug binding. The O-16S rRNA share the wild type 23S rRNA with the wild type 16S rRNA. Therefore the 23S rRNA cannot be separated to be sensitive to the drug binding, while it has to support the cell growth at the same time. Thanks to the recent development of synthetic biology, an artificial ribosome (RiboT) which has the large subunit and small subunit permanently linked together during the translation had been development by Mankin lab and Jewett Lab recently.¹⁵ By doing circularly permutation on the 23S rRNA, the original 5'end and 3' end of 23S rRNA had been closed with a short nucleotide linker and multiple new ends were opened. These newly opened ends were screened by linking to the h44 of 16S rRNA to check the ribosome activity. The one that has the best activity was chosen for further optimization. This engineered ribosome with tethered subunits can be a perfect tool for orthogonal translation since the tethered 23S-16S rRNA won't interact with wild type 23S rRNA

or 16S rRNA. What's more amazing is that the RiboT can actually support the cell survival and growth without the wild type ribosome. The RiboT, therefore, is the perfect tool to help us extend the current ribosome inhibition detection system to sense inhibitors that target the ribosome large subunit.

To develop the O-ribosome-based detector system to sense ribosome large subunit inhibitors, the RiboT was used as the drug resistant ribosome to support cell growth. By introducing specific drug resistant mutation onto the RiboT, the RiboT should be protected from drug binding (Figure 3-3). The current sensor plasmid pSH6-KF was modified by replacing the chloramphenicol acetyl transferase gene with DHFR and the O-16S rRNA fragment with orthogonal 23S-16S-5S (O-23S-16S-5S) rRNA operon. The chloramphenicol acetyl transferase can chemically modified chloramphenicol class antibiotics which target the large subunit of the ribosome, therefore it needs to be replaced. The O-23S-16S-5S rRNA operon harboring the O-ASD sequence which only translation the tetR gene will be the drug sensitive ribosome to process the signal from drug binding. As a proof of concept, we chose three antibiotics which have distinct structure characteristics and modes of actions as our target compounds to test the system development. These three compounds are erythromycin, lincomycin and linezolid (See structures in Figure 3-4).

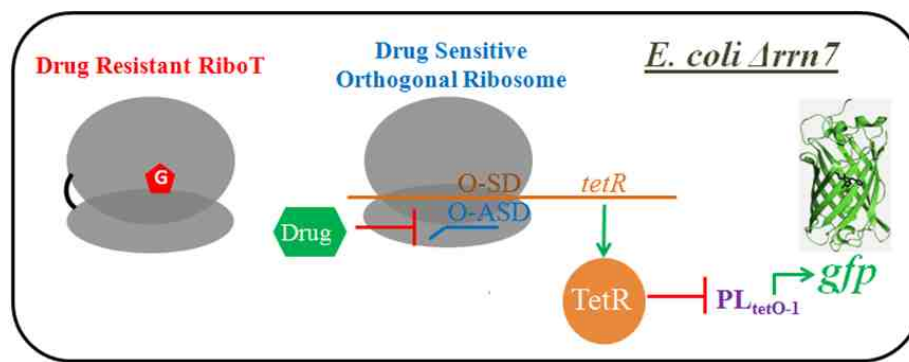


Figure 3-3. Schematic showing the ribosome large subunit inhibitor sensor



Figure 3-4. Chemical structures of erythromycin, lincomycin and linezolid.

Erythromycin is the classic macrolide antibiotic and it was discovered in 1952. It is commonly used to treat respiratory tract infections, skin infections, chlamydia infections, and syphilis. Erythromycin has a 14-member macro-lactone ring with a desosamine and a cladinose side chains attach to it. It has been used as a scaffold to generate many erythromycin-derived antibiotics, such as azithromycin, dirithromycin, telithromycin and so on.¹⁶ Erythromycin's mode of action is promoting early drop-off of nascent peptide by blocking the nascent peptide exit tunnel. Its binding site had been well characterized by biochemical studies¹⁷ and crystallography.¹⁸ (See crystal structure in Figure 3-5) The mutation A2058G on 23S rRNA can disrupt the drug binding and lead to drug resistance. Lincomycin is a classic lincosamide antibiotic that has a different chemical structure to macrolide antibiotics. It has a broader spectrum of antimicrobial activity than macrolides. Lincomycin acts by binding to the PTC of ribosome and inhibiting the peptide-bond formation.¹⁸ The same mutation A2058G can disrupt the drug binding and confer resistance to lincomycin. Linezolid is a synthetic compound first developed by Pharmacia and Upjohn Company in 1990s. It belongs to the oxazolidinone class compound and is widely used to treat gram-positive bacterial infections. Currently it is thought that the linezolid binds to the similar site as lincomycin at the PTC and consequently inhibit the peptide-bond formation (See crystal structure in Figure 3-5).¹⁹ However, the A2058G mutation

doesn't confer obvious resistance to linezolid. Therefore its mechanism of action should be different from lincomycin. Currently the investigation of linezolid mode of action is still actively going. The mutation G2576U was found in many species of bacterial to confer high linezolid resistance.²⁰ This indicates G2576U mutation should cost little fitness lost and it should be good to use in our system. These three drugs should be good representative for ribosome larger subunit inhibitors due to their chemical structure and their mechanism of actions.

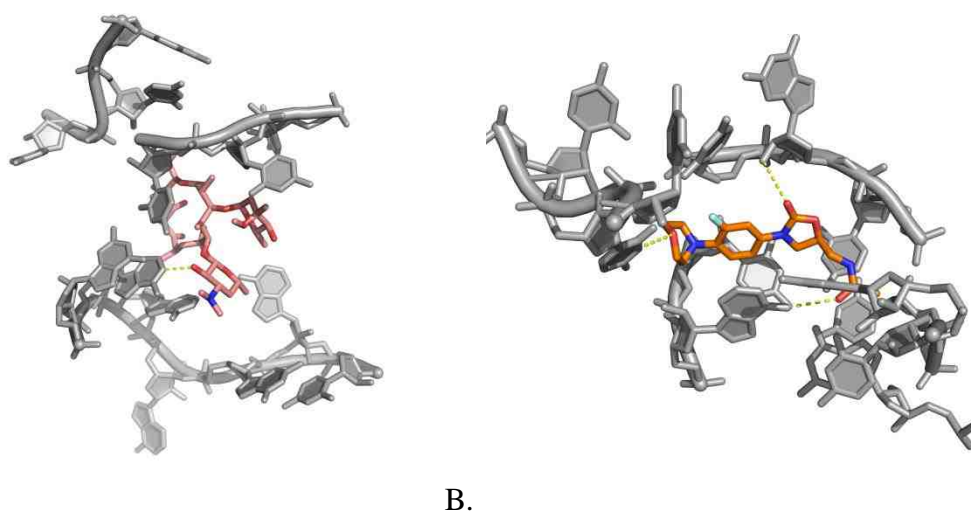


Figure 3-5 Crystal structure of erythromycin-bound (A) and linezolid-bound (B) ribosome.

With the complete ribosome inhibition detector system in hand, we set out to apply the system to examine ribosome inhibition by novel small molecules. There are several potential directions for applying our detector system. For instance, the detector can be used to detect and screen natural product extracts for ribosome inhibitors. It can also be used as the reporter system to evolve ribosome inhibitor biosynthetic enzymes *in vivo*. One of the simplest applications of the system is to screen compound libraries and study drug structure-activity relationships (SAR). As a proof of principle, we applied the system to screen a set of spectinomycin analogs and study the SAR from our sensing results. Although the fact that spectinomycin has been accepted as

general safe drug, it lacks antimicrobial activity against most of the clinically pathogens. With the increase of the drug resistance, developing new drugs from current drug arsenal is still the most promising approach. With an excellent safety index, spectinomycin could be a promising drug scaffold to modify. According to the spectinomycin-bound ribosome structure (Figure 1-9), ring A and ring B of spectinomycin have many polar contacts with rRNA and ribosomal protein S12. However, ring C presents fewer interactions with ribosome. Especially the 3' ketone group of ring C has a large space to be engineered from the structure. We therefore applied our detector system to screen the ribosome inhibition of a set of 20 spectinomycin analogs and 36 glycoside analogs. Our results show that the O-ribosome controlled reporter system can rapidly evaluate the compound potency and study the SAR. Our efforts on extending the detection system should prove that the O-ribosome controlled reporter system can be able to detect and quantify any small molecules that target the bacterial ribosome.

2. Experimental procedures

General. Most materials used for work described in this chapter have already been mentioned in the experimental procedures section of Chapter 2. Kasugamycin, erythromycin, lincomycin (U-10149A), linezolid and trimethoprim were purchased from Santa Cruz Biotechnology (Dallas, TX). Spectinomycin, streptomycin and trimethoprim were purchased from Genlantis (San Diego, CA).

Bacterial strains. Most of the bacterial strains used for work described in this chapter have been mentioned in the experimental procedures section of Chapter 2. *E. coli* SQ171fg (*E. coli* MG1655/ Δ rrnGADEHBC/prnC-sacB/ptRNA67, gift from Alexander S. Mankin)¹⁵, in which the ybeX gene which is a putative Mg21/Co21 transporter has a nonsense mutation, and the rpsA gene which encodes ribosomal protein S1 has a miscoding mutation. With these two

mutations the SQ171fg has shorter doubling time with the RiboT as the sole ribosome to support cell growth. It was used as the starting point for construction of strains capable of detecting ribosome inhibition by large subunit inhibitors.

Bacterial culture. All of the bacterial culture methods used for work described in this chapter have been mentioned in the experimental procedures section of Chapter 2. The working concentration of trimethoprim used in this work is 80µg/mL.

PCR conditions. All of the PCR conditions used for work described in this chapter have been mentioned in the experimental procedures section of Chapter 2. Gibson assembly reaction condition is the same as the reported method.²¹

Enforced replacement by sucrose counterselection. The enforced replacement method was already described in the experimental procedures section of Chapter 2.

Cell density and fluorescence assays. The methods for measuring cell density and fluorescence intensity was already described in the experimental procedures section of Chapter 2.

Construction of E.coli strain SH435. Since ptRNA67 plasmid in SQ380 has a spectinomycin resistance gene which can pump out the spectinomycin and streptomycin from the cell, it has to be replaced so that the cell can be a suitable host for building spectinomycin and streptomycin detectors. The ptRNA67 was replaced by ptRNA70 (Michael O' Connor, unpublished work) which has a tetracycline resistance gene instead of spectinomycin resistance gene. The ptRNA70 was transformed into SQ380 and the transformants were grown on tetracycline LB agar plate. After passage the cells for one generation, a few colonies were verified to lose the ptRNA67 by phenotypic screening. The resulting strain harbors two plasmids: prnC-sacB and ptRNA70, and it is named SH435 (Figure 3-6)

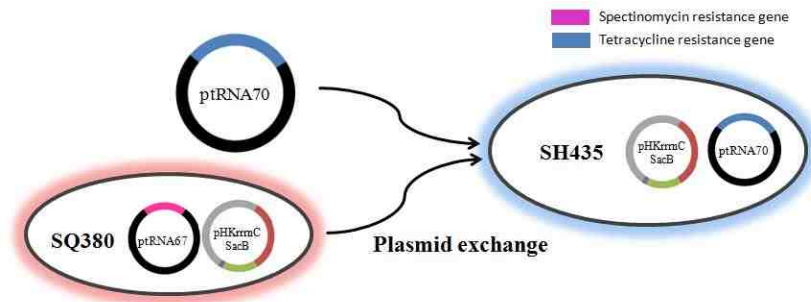


Figure 3-6 Construction of *E. coli* Δ7 strain SH435.

Construction of pRRSH2 plasmid series with various mutations. Various rRNA mutations that were reported to confer high resistance to specific antibiotics were introduced into pRRSH2 plasmid, respectively. The construction of each plasmid was described below:

1) Construction of pRRSH2-C1192U and pRRSH2-C1192U/A2058G. pRRSH2-C1192U was constructed from pRRSH2. A 2636 bp region of pRRSH2 containing the 16S rRNA C1192U site was amplified in two fragments with the mutation site at the junction of the fragments. The two fragments were joined by overlap extension PCR, the resulting PCR product digested with BsrGI and BamHI, and cloned into pRRSH2 digested with the same enzymes. Fragment 1 was amplified using primers pRRSH2-A794G-1 and pRRSH2-C1192U-2, and fragment 2 was amplified using primers pRRSH2-C1192U-3 and pRRSH2-A794G-4. pRRSH2-C1192U/A2058G was constructed from pRRSH2-C1192U by Gibson Assembly. Four fragments were amplified by PCR. The 16S rRNA fragment was amplified using primers pRRSH-rRNA1-up and pRRSH-rRNA1-dn. The 3.6 kb 23S rRNA fragment was amplified as two fragments from pRRSH2 using primer pairs pRRSH-rRNA2-up/pRiboT-A2058G-2, and pRiboT-A2058G-3/pRRSH-rRNA3-dn. The mutation site was generated at the overlap part of these two fragments. The fragment containing the p15A origin of replication and ampicillin resistance marker was

amplified from pRRSH2 using primers pRRSH-AmpR-up and pRRSH-p15A-dn. The resulting four DNA fragments were assembled by Gibson Assembly. Introduction of the mutation into each plasmid was verified by sequencing the cloned region of the plasmid containing it. The vector map of pRRSH2-C1192U/A2058G is given as an example (Figure 3-7). Primer information is given in the table 3-1 below. The C1192U and A2058G mutation sites are show in bold red in the primers that contain them.

| primer name | sequence (5' -3') | amplicon size (bp) | template |
|-----------------|---|--------------------|---------------|
| pRRSH2-A794G-1 | TCCAACGCGTAAACGCCTTGC | 440 | pRRSH2 |
| pRRSH2-C1192U-2 | GGTGGGGATGAT T GCAAGTCATCATG | | |
| pRRSH2-C1192U-3 | GACTTGAC A TCATCCCCACCTTCCTC | 2537 | pRRSH2 |
| pRRSH2-A794G-4 | CAGATCGCTGAGATAGGTGCCTCAC | | |
| pRRSH-rRNA1-up | TTTGGTTGAATGTTGCGCGGTC | 2116 | pRRSH2-C1192U |
| pRRSH-rRNA1-dn | CGGTGTCCTGGGCCTCTAGAC | | |
| pRRSH-rRNA2-up | TCTAGAGGCCAGGACACCGCCCTTTCACGGCGGTAACAG | 2322 | pRRSH2 |
| pRiboT-A2058G-2 | GTCT T CCCGTCTTGCCGCGG | | |
| pRiboT-A2058G-3 | CCGCGCAAGACGG G AAGACCCCGTGAAC | 1373 | pRRSH2 |
| pRRSH-rRNA3-dn | AGCTGCTTTCCTGATGCAAAAACG | | |
| pRRSH-AmpR-up | CGTTTTTGCATCAGGAAAGCAGCTGATATCAGACGTCAGGTGGCACTTTTC | 1970 | pRRSH2 |
| pRRSH-p15A-dn | CCGCGCAACATTCAACCAAAATTACATGTGCGTCAGACCC | | |

Table 3-1 Primers for constructing pRRSH2-C1192U and pRRSH2-C1192U/A2058G

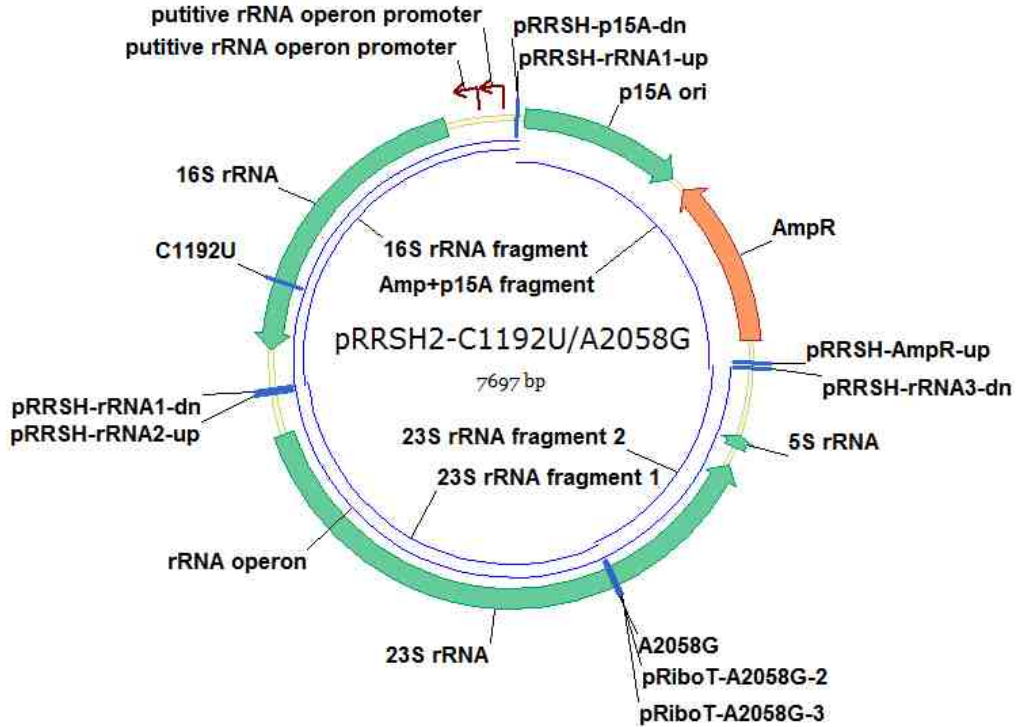


Figure 3-7 Plasmid map of pRRSH2-C1192U/A2058G

2) Construction of pRRSH2-A794G/C1192U/A2058G and pRRSH2-C912U/C1192U/A2058G. Both plasmids were constructed from pRRSH2-C1192U/A2058G. A 2636 bp region of pRRSH2-C1192U/A2058G containing the 16S rRNA A794 and C912 sites was amplified in two fragments with the mutation site at the junction of the fragments. In each case, the two fragments were joined by overlap extension PCR, the resulting PCR product digested with BsrGI and BamHI, and cloned into pRRSH2 digested with the same enzymes. For pRRSH2-A794G/C1192U/A2058G, fragment 1 was amplified using primers pRRSH2-A794G-1 and pRRSH2-A794G-2, and fragment 2 was amplified using primers pRRSH2-A794G-3 and pRRSH2-A794G-4. For pRRSH2-C912U/C1192U/A2058G, fragment 1 was amplified using primers pRRSH2-A794G-1 and pRRSH2-C912U-2, and fragment 2 was amplified using primers pRRSH2-C912U-3 and pRRSH2-A794G-4. Introduction of the mutation into each plasmid was

verified by sequencing the cloned region of the plasmid containing it. Primer information is given in the table 3-2 below. The A794G and C912U mutation sites are show in bold red in the primers that contain them.

| primer name | sequence (5' -3') | amplicon size (bp) | template |
|-----------------|--|--------------------|----------------------|
| pRRSH2-A794G-2 | GCAAACAGGATTAGATGCCCTGGTAGTC (with pRRSH2-A794G-1) | 843 | pRRSH2-C1192U/A2058G |
| pRRSH2-A794G-3 | GACTACCAGGGCATCTAATCCTGTTTGC (with pRRSH2-A794G-4) | 2142 | pRRSH2-C1192U/A2058G |
| pRRSH2-C912U-2 | GGCCGCAAGGTTAAAACCTAAATGAATTGACGGGG (with pRRSH2-A794G-1) | 850 | pRRSH2-C1192U/A2058G |
| pRRSH2- C912U-3 | CAATTCATTTAAGTTTAAACCTTGCGGCC (with pRRSH2-A794G-4) | 1295 | pRRSH2-C1192U/A2058G |

Table 3-2 Primers for constructing pRRSH2- A794G/C1192U/A2058G and pRRSH2-C912U/C1192U/A2058G

Construction of detector strains SH442, SH446 and SH456. pRRSH2-C1192U, pRRSH2-C1192U/A2058G, pRRSH2-A794G/C1192U/A2058G and pRRSH2-C912U/C1192U/A2058G were transformed into SH435 respectively. prnC-sacB plasmid was cured out by sucrose counter-selection. One of the four plasmids, pRRSH2-C1192U, was fail to support the cell survival and growth. This is proven by the failure of curing out prnC-sacB in SH435. Three *E.coli* strains SH438 (pRRSH2-C1192U/A2058G & ptRNA70), SH445 (pRRSH2-C912U/C1192U/A2058G & ptRNA70) and SH470 (pRRSH2-A794G/C1192U/A2058G & ptRNA70) were generated as the host for the detector strains. The spectinomycin detector strain was constructed by transforming the best reporter plasmid pSH6-KF (described in chapter 2) into SH438, resulting in the detector strain SH442. The streptomycin detector strain was constructed by transforming pSH6-KF into SH445, resulting in SH446. The kasugamycin detector strain was constructed by transforming pSH6-KF into SH470 and resulting in SH456.

Optimization of the streptomycin detector. To improve the sensitivity of the streptomycin detector SH446, the same approach described in chapter 2 was used to combinatorial adjust promoter strength of tetR and O-16S genes. pSH3-KF - pSH14-KF (except pSH6-KF) were transformed into SH445 and the resulting strains were subjected to ATC titration assay (Figure 3-8) and ribosome inhibition assay with a range of streptomycin concentrations (Figure 3-9). Fluorescence intensity was determined by plate reader. The strain SH475 shows the best sensitivity against streptomycin and therefore was chosen as the final streptomycin detector strain.

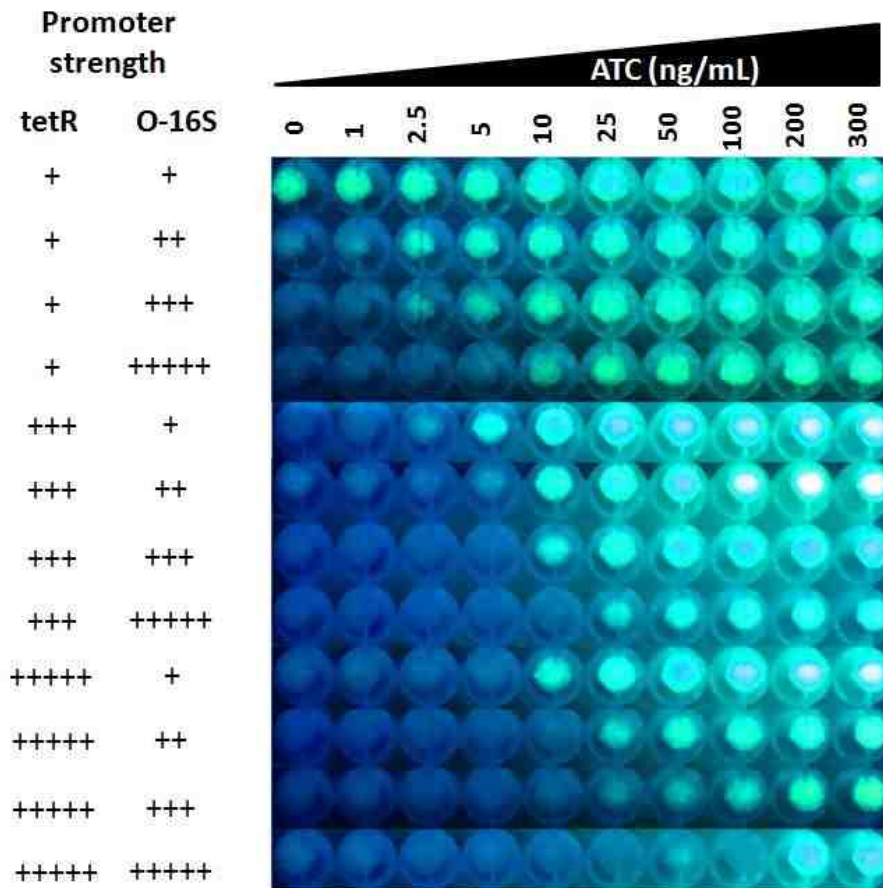


Figure 3-8 Cell pellet fluorescence showing ATC titration of 12 streptomycin detector strains. The tetR and O-16S promoter strengths have been combinatorially altered (promoter strengths are shown on the left: +, very weak; ++, weak; +++, medium; +++++, strong).

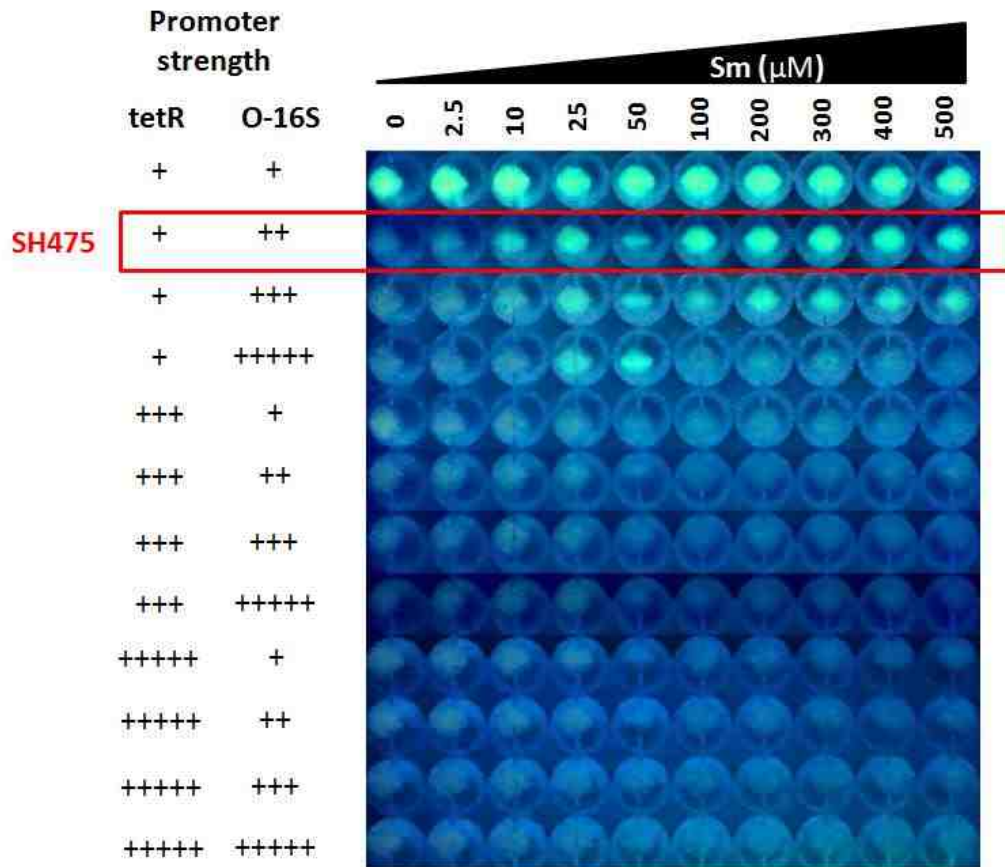


Figure 3-9 Cell pellet fluorescence showing ribosome inhibition assay by a range of streptomycin concentrations with 12 streptomycin detector strains. The tetR and O-16S promoter strengths have been combinatorially altered (promoter strengths are show on the left: +, very weak; ++, weak; +++, medium; +++++, strong). The best streptomycin detector strain SH475 was boxed in red.

Construction of pRiboT2-A2058G and pRiboT2-G2576U. pRiboT2-A2058G and pRiboT2-G2576U were constructed from poRiboT2¹⁵ (purchased from addgene). First, the orthogonal anti-Shine-Delgano sequence (O-ASD) on the RiboT of poRiboT2 was replaced with WT-ASD sequence. A 1374 bp region of poRiboT2 containing the ASD sequence was amplified in two fragments with the mutation site at the junction of the fragments. The two fragments were

joined by overlap extension PCR, the resulting PCR product digested with PvuII and XbaI, and cloned into poRiboT2 digested with the same enzymes. Fragment 1 was amplified using primers poRiboT-WTSD-1 and poRiboT-WTSD-2, and fragment 2 was amplified using primers poRiboT-WTSD-3 and pRRT-3'16S-dn. Replacement of the ASD sequence was verified by sequencing. The resulting plasmid is called pRiboT2. Then, the A2058G and G2576U mutations were introduced into pRiboT2 respectively. For introducing A2058G into pRiboT2, A 1374 bp region of pRiboT2 containing the A2058 site was amplified in two fragments with the mutation site at the junction of the fragments. Primer pairs poRiboT-WTSD-1/pRiboT-A2058G-2 and pRiboT-A2058G-3/pRRT-3'16S-dn were used to amplified fragment 1 and 2 respectively. The two fragments were joined by overlap extension PCR, the resulting PCR product digested with PvuII and XbaI, and cloned into pRiboT2 digested with the same enzymes. For introducing G2576U, the same approach used for introducing A2058G was used except the primer pairs are poRiboT-WTSD-1/pRiboT-G2576U-2 and pRiboT-G2576U-3/pRRT-3'16S-dn. Introduction of the mutation into each plasmid was verified by sequencing the cloned region of the plasmid containing it. The vector map of pRiboT2-A2058G is given as an example in figure 3-10. Primer information is given in the table 3-3 below. The ASD sequence, A2058G and G2576U mutation sites are show in bold red in the primers that contain them.

| primer name | sequence (5' -3') | amplicon size (bp) | template |
|--------------------|--|---------------------------|-----------------|
| poRiboT-WTSD-1 | CCAAGGCGCTTGAGAGAACTCGGG | 1325 | poRiboT2 |
| poRiboT-WTSD-2 | TTTAAGGTAAGGAGGTGATCCAACCGCAGG TTC | | |
| poRiboT-WTSD-3 | TTGGATCACCTCCTTACCTTAAAGAAGCGTAC | 456 | poRiboT2 |
| pRRT-3'16S-dn | TCACAACCCGAAGATGTTTCTTTCG | | |
| pRiboT-A2058G-2 | GTCTT CCCGTCTTGCCGCGG (with poRiboT-WTSD-1) | 426 | pRiboT2 |
| pRiboT-A2058G-3 | CCGCGCAAGACGG G AAGACCCCGTGAAC (with poRiboT-WTSD-4) | 1352 | |
| pRiboT-G2576U-2 | CGACGTTCTAAACCCAGCT A GCGTACCACCTTAAATGGCGAAC (with poRiboT-WTSD-1) | 958 | pRiboT2 |

| | | | |
|-----------------|--|-----|--|
| pRiboT-G2576U-3 | GTTCGCCATTTAAAGTGGTACGCTAGCTGGGTTTAGAACGTCG (with poRiboT-WTSD-4) | 843 | |
|-----------------|--|-----|--|

Table 3-3 Primers for constructing pRiboT2, pRiboT2-A2058G and pRiboT2-G2576U

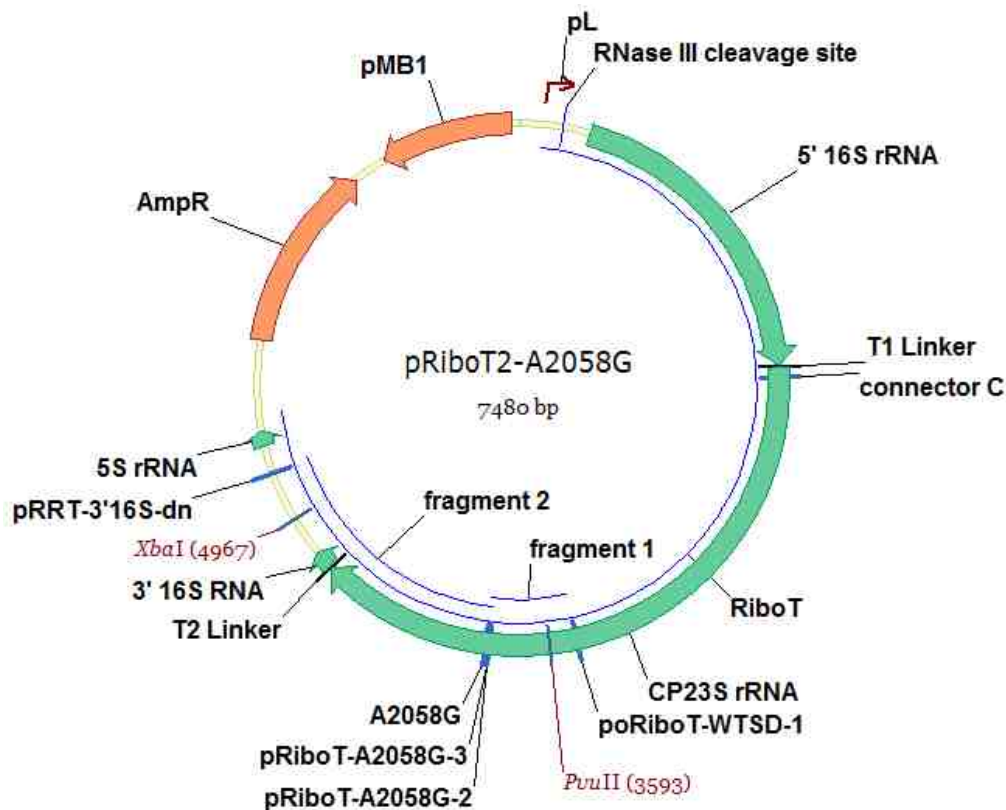


Figure 3-10 Plasmid map of pRiboT2-A2058G

Construction and function testing of pSH18. pSH18 is the modified version of pSH6-KF. The chloramphenicol resistance gene on pSH6-KF was replaced with DHFR gene (Jeff Tabor, unpublished). And the mutated pMB1 origin of replication was replaced with ColE1 origin (Chad Melancon, unpublished). The 23S rRNA and 5S rRNA were integrated into the downstream of the O-16S rRNA to make it a complete rRNA operon with the same anti-Shine-Delgano sequence as the pSH6-KF. The plasmid map of pSH18 is shown in Figure 3-13. To construct pSH18, two intermediate plasmids, pRRSH2b (Figure 3-11) and pSH18BB (Figure 3-

12), were construct by Gibson assembly. For pRRSH2b, in which two restriction enzyme cutting sites (SpeI and NotI) were introduced at both ends of the rRNA operon, a four-fragment Gibson assembly was performed to build the plasmid. The fragment 1, O-16S rRNA fragment (1802 bp), was amplified from pSH6-KF by primers pSH15-16S-up and SH16-O16S-dn. Fragment 2, part of the 23S rRNA fragment (2226bp), was amplified from pRRSH2 by primers SH16-rRNA2-up and pRRSH-rRNA2-dn. Fragment 3, another part of 23S rRNA and 5S rRNA (1809 bp), was amplified from pRRSH2 by primers pRRSH-rRNA3-up and SH16-rRNA3-dn. Fragment 4, the ampicillin resistance marker and p15A origin fragment (1974 bp), was amplified from pRRSH2 by primers pRRSH2b-AmpR-up and pRRSH2b-p15a-dn. The 4 fragments then were used for assembling pRRSH2b by Gibson assembly. For pSH18BB, a three-fragment Gibson assembly was performed to build the plasmid. The fragment 1, gfpuv and tetR fragment (2093 bp), was amplified from pSH6-KF by primers SH16Backbone-up and pSH18-tetR-dn. Fragment 2, the ColE1 origin fragment (689 bp), was amplified from pBKCM7b (Chad Melancon, unpublished) by primers pSH18-ColE1-up and pSH18-ColE1-dn. Fragment 3, the DHFR fragment (675 bp), was amplified from pSH16BB (unpublished work) by primers pSH18-DHFR-up and SH16Backbone-dn-2. The three fragments were then assembled by Gibson assembly to build pSH18BB. Both pRRSH2b and pSH18BB were digested by SpeI and NotI. The 5649 bp fragment from pRRSH2b and the 3287 bp fragment from pSH18BB were purified and ligated by T4 ligase. The resulting plasmid pSH18 was verified by restriction enzyme digestion and sequencing on the key components (tetR promoter, O-16S rRNA promoter and origin of replication). Primer information is given in the table 3-4 below. The priming region of each primer is underlined. The O-ASD sequence is shown in bold red in the primers that contain them. The NotI and SpeI sites are shown in bold blue.

| primer name | sequence (5' -3') | amplicon size (bp) | template |
|-------------------|--|--------------------|----------|
| pSH15-16S-up | <u>TACCCATTGATCCAACCGCAGG</u> | 1802 | pSH6-KF |
| SH16-O16S-dn | <u>GCAGGGTCGC</u> <u>ACTAGT</u> <u>TTGTGCATGC</u> | | |
| SH16-rRNA2-up | <u>CCTGCGTTGGATCAA</u> TGGGGT <u>ACCTTAAAGAAGCGTACTTTGTA</u> GTGC (used with pRRSH-rRNA2-dn) | 2226 | pRRSH2 |
| SH16-rRNA3-dn | GCGGCCGC <u>AGCTGCTTTCCTGATGCAAAAACG</u> (used with pRRSH-rRNA3-up) | 1809 | pRRSH2 |
| pRRSH2b-AmpR-up | <u>TTTCATCAGGAAAGCAGCT</u> GCGGCCGC <u>AGACGTCAGGTGGCACT</u> <u>TTTCGGG</u> | 1974 | pRRSH2 |
| pRRSH2b-p15a-dn | <u>GCATGCACAA</u> ACTAGT <u>GCGACCCTGCATTACATGTGCGTCAGACC</u> <u>C</u> | | |
| SH16Backbone-up | <u>CGGATCTAGCGTTACAAGTAGCTAGCACTGTACCTAGGACTGAGCT</u> <u>AGCCGTCAATCGTG</u> | 2093 | pSH6-KF |
| pSH18-tetR-dn | <u>CTCACGTTAAGGGATTTTGGTCATGATTAAGACCCACTTTCACATT</u> <u>TAAGTTG</u> | | |
| pSH18-ColE1-up | <u>TCATGACCAAAAATCCCTTAACGTGAGTTTTTCG</u> | 689 | pBKCM7b |
| pSH18-ColE1-dn | <u>CATATGGGCCGCGTTGCTGGCG</u> | | |
| pSH18-DHFR-up | <u>CCAGCAACGCGGCCCATATGTGCTTGGATTCTCACCAATAAAAAA</u> <u>C</u> | 673 | pSH16BB |
| SH16Backbone-dn-2 | <u>CTAGCTACTTGTAACGCTAGATCCGATAGTTTA</u> GCGGCCGC <u>CATTC</u> | | |

Table 3-4 Primers for constructing pRRSH2b and pSH18BB

ColE1 origin of replication fragment sequence. Primer binding sites are underlined, and the ColE1 origin region is shown in blue.

TCATGACCAAAAATCCCTTAACGTGAGTTTTCGTTCCACTGAGCGTCAGACCCGTAGAAAAGATCAAAGGATCTTCTTGAGATC
CTTTTTTCTGCGCGTAATCTGCTGCTTGCAAACAAAAAACACCGCTACCAGCGGTGGTTTGTTCGCGGATCAAGAGCTAC
CAACTTTTTCCGAAGGTAAGTGGCTTCAAGAGAGCGCAGATACCAATACTGTCTTCTAGTGTAGCCGTAGTTAGGCCACC
ACTTCAAGAACTCTGTAGCACCGCCTACATACCTCGCTCTGTAATCCTGTTACCAGTGGCTGCTGCCAGTGGCGATAAGTCGT
GTCTTACCGGGTTGGACTCAAGACGATAGTTACCGGATAAAGCGCAGCGGTCGGGCTGAACGGGGGGTTCGTGCACACAGCC
CAGCTTGGAGCGAACGACCTACACCGAACTGAGATACCTACAGCGTGAGCATTGAGAAAGCGCCACGCTTCCGAAGGGAGA
AAGGCGGACAGGTATCCGGTAAGCGGCAGGGTCGGAACAGGAGAGCGCACGAGGGAGCTTCCAGGGGGAACGCCTGGTA
TCTTTATAGTCTGTCGGGTTTCGCCACCTCTGACTTGAGCGTCGATTTTTGTGATGCTCGTCAGGGGGGCGGAGCCTATGGAA
AAAGCCAGCAACGCGGCCCATATG

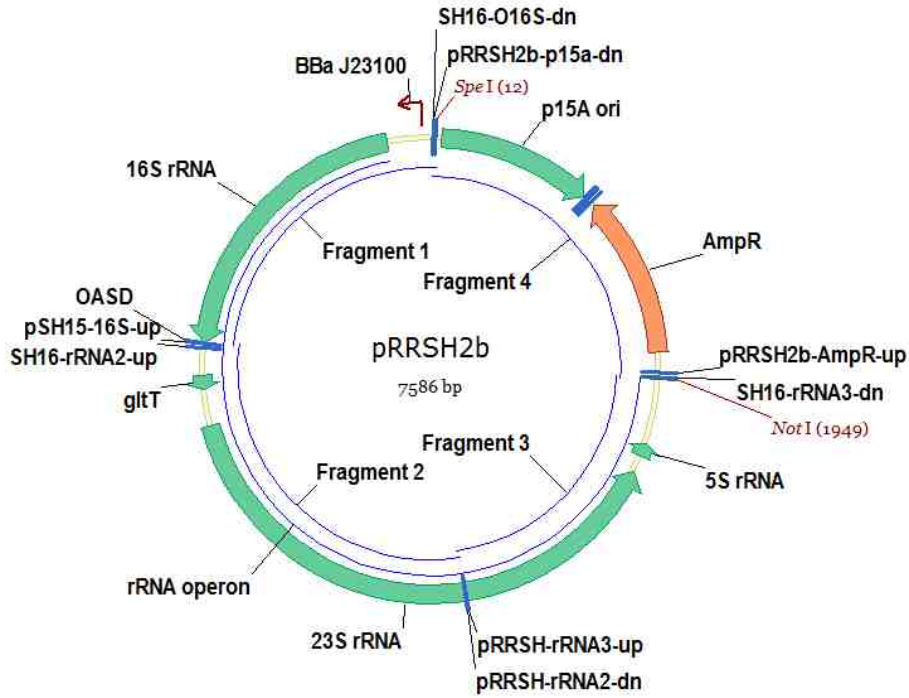


Figure 3-11 Plasmid map of pRRSH2b

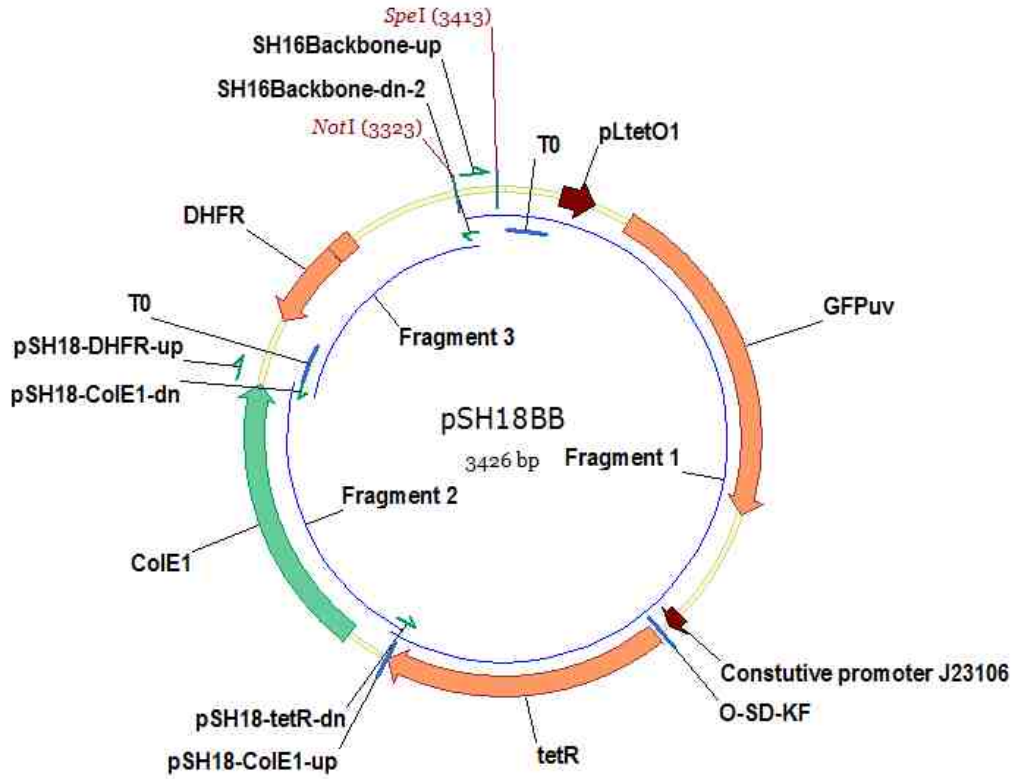


Figure 3-12 Plasmid map of pSH18BB

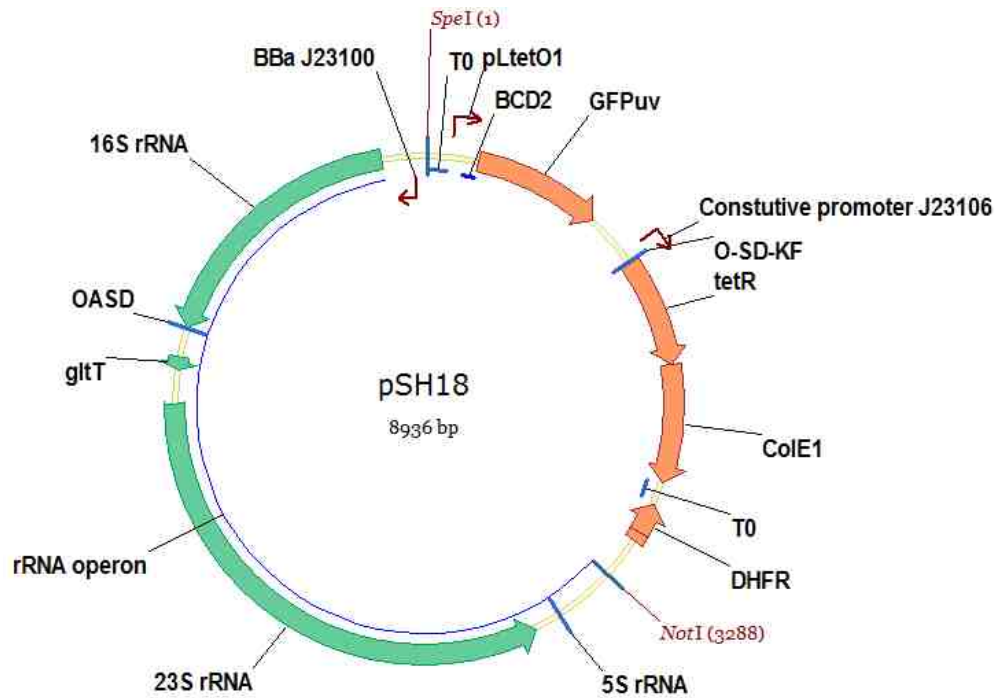


Figure 3-13 Plasmid map of pSH18

The pSH18 was then transformed into SH437fg which is constructed from SQ171fg (Mankin, RiboT paper) by replacing the prnC-sacB with pRiboT2-A2058G to construct the ribosome large subunit inhibitor detector strain. The resulting strain is called SH440 and it was tested with its ability to detect ribosome inhibition by erythromycin. The SH440 cells were grown in the presence of various concentrations of erythromycin ranging from 0-500 μ M and analyzed by fluorescence assay (method was described in chapter 2). The SH440 cells were also grown in the presence of various concentrations of ATC to test the functionality of O-ribosome controlled tetR-gfpuv genetic circuit. SH440 displayed no sensitivity to erythromycin and low sensitivity to ATC (Figure 3- 14). The results suggest that the O-ribosome controlled tetR-gfpuv genetic circuit is detuned. The copy of tetR is much more than the copy of gfpuv mRNA, leading

to an insensitive O-ribosome controlled tetR-gfpuv genetic circuit. Further optimizations need to be done to tune the sensitivity of SH440.

Optimization of ribosome large subunit inhibitor detector strain. To tune the sensitivity of the current detector strain SH440, we applied the same approach described previously (both on this chapter and chapter 2) to combinatorially adjust promoter strength of tetR gene and O-16S rRNA gene. According to ribosome inhibition assay and ATC titration assay results from SH440, the expression of tetR gene needs to be down-regulated. Therefore, we first replace the O-16S rRNA promoter from BBa_J23100 (strong strength) to BBa_J23108 (medium strength), BBa_J23114 (weak strength) and lpp promoter (original promoter for O-16S rRNA, chapter 2), respectively. Three intermediate plasmids pRRSH2b-J23018, pRRSH2b-J23114 and pRRSH2b-lpp were constructed by Gibson assembly. The construction procedure is similar to the pRRSH2b assembly except the O-16S rRNA fragments were amplified from different templates with the same primer pair (pSH15-16S-up/ SH16-O16S-dn). For pRRSH2b-J23018, the O-16S rRNA was amplified from pSH7-KF. For pRRSH2b-J23114, the O-16S rRNA was amplified from pSH8-KF. For pRRSH2b-lpp, the O-16S rRNA was amplified from pSH3-KF. The pRRSH2b-J23018, pRRSH2b-J23114 and pRRSH2b-lpp were digested by SpeI and NotI, respectively. The 5649bp fragments from the three digestion reactions were purified and ligated to the digested pSH18BB (3426 bp, described in previous paragraph), respectively. The resulting plasmids were named pSH29 (with BBa_J23108), pSH30 (with BBa_J23114) and pSH20 (with lpp). The plasmids summary can be found in table 3-5 below.

To further tune down the expression of tetR gene, we replace the tetR gene promoter from BBa_J23106 (medium strength) to BBa_J23115 (weak strength) on pSH18, pSH29, pSH30 and pSH20. The intermediate plasmid pSH22BB was constructed by using similar approach as

pSH18BB except the *gfpuv* and *tetR* fragment was amplified from pSH5-KF with the same primer pair (SH16Backbone-up/pSH18-tetR-dn). The pSH22BB was then digested with *SpeI* and *NotI*. The resulting 3287 bp fragment was purified and ligated to the 5469 bp digested fragments from pRRSH2b, pRRSH2b-J23108, pRRSH2b-J23114 and pRRSH2b-lpp, respectively. The four new plasmids were named pSH24 (BBa_J23100 on O-16S rRNA), pSH26 (BBa_J23108 on O-16S rRNA), pSH28 (BBa_J23114 on O-16S rRNA) and pSH22 (lpp on O-16S rRNA). The plasmids summary information is shown in the table 3-5.

| plasmid | tetR | | O-16S | |
|---------|------------|---------------|------------|---------------|
| | promoter | strength | promoter | strength |
| pSH18 | BBa_J23106 | medium (0.47) | BBa_J23100 | strong (1.0) |
| pSH29 | BBa_J23106 | medium (0.47) | BBa_J23108 | medium (0.51) |
| pSH30 | BBa_J23106 | medium (0.47) | BBa_J23114 | weak (0.10) |
| pSH20 | BBa_J23106 | medium (0.47) | lpp | ND |
| pSH24 | BBa_J23115 | weak (0.15) | BBa_J23100 | strong (1.0) |
| pSH26 | BBa_J23115 | weak (0.15) | BBa_J23108 | medium (0.51) |
| pSH28 | BBa_J23115 | weak (0.15) | BBa_J23114 | weak (0.10) |
| pSH22 | BBa_J23115 | weak (0.15) | lpp | ND |

Table 3-5 Plasmid summary information

The seven new plasmids, pSH29, pSH30, pSH20, pSH24, pSH26, pSH28 and pSH22, were transformed into SH437fg. The resulting strains and the SH440 were tested with their sensitivity on erythromycin and ATC. One of the strains SH460, which harbors the plasmid pSH26 (see table 3-5 for more information), exhibit best sensitivity against erythromycin (Figure 3-15). It was used as the detector strain to detect ribosome inhibition by lincomycin.

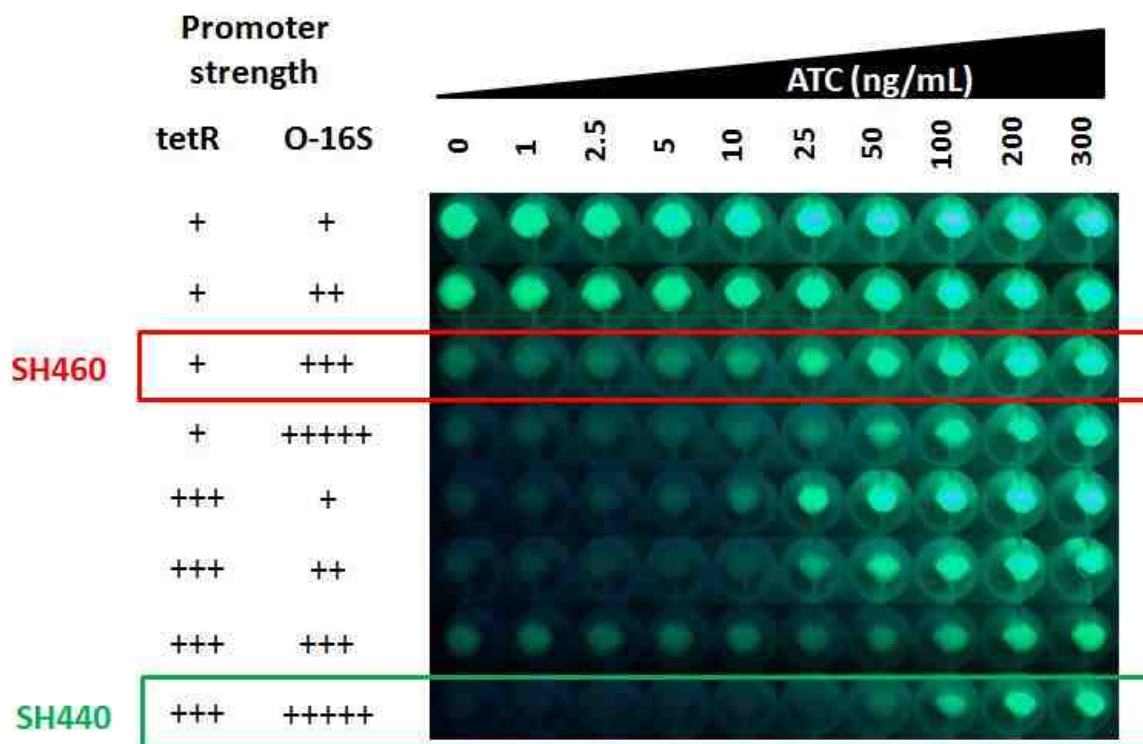


Figure 3-14 Cell pellet fluorescence showing ATC titration of 8 large subunit unit inhibitors detector strains. The tetR and O-16S promoter strengths have been combinatorially altered (described previously). The original detector strain SH440 is boxed in green and the optimized detector strain SH460 is boxed in red.

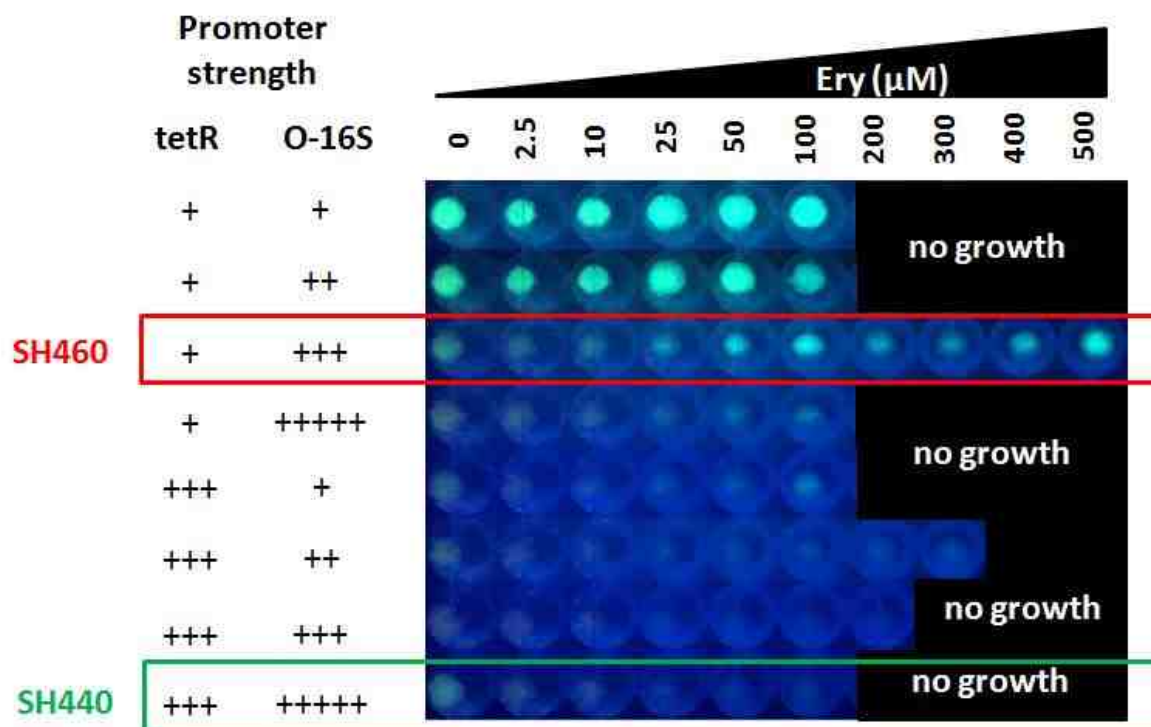


Figure 3-15 Cell pellet fluorescence showing ribosome inhibition assay by a range of erythromycin concentrations with the 8 detector strains. The tetR and O-16S promoter strengths have been combinatorially altered (described previously). The original detector strain SH440 is boxed in green and the optimized detector strain SH460 is boxed in red.

Direct measurement of ribosome inhibition by spectinomycin analogs. A set of 16 spectinomycin analogs and 20 glycoside analogs with unknown potency were subjected to ribosome inhibition assay by spectinomycin detector SH442. All the 36 compounds were synthesis by Throson Lab (Jon Throson, unpublished). For the 16 spectinomycin analogs, the 3' ketone group was replaced with different substituents. The 20 glycoside analogs are the intermediate compounds with the opening ring B. A certain amount of H₂O was added to each compound to make it 100 μM stock solution. Each compound was diluted to a range of 12 concentrations from 0 μM to 500 μM . The ribosome inhibition fluorescence assay was performed

as previously described (chapter 2). Calculation of IC50 value was done previously described method (chapter 2). The chemical structures of the 36 compounds were shown in the Figure 3-16.

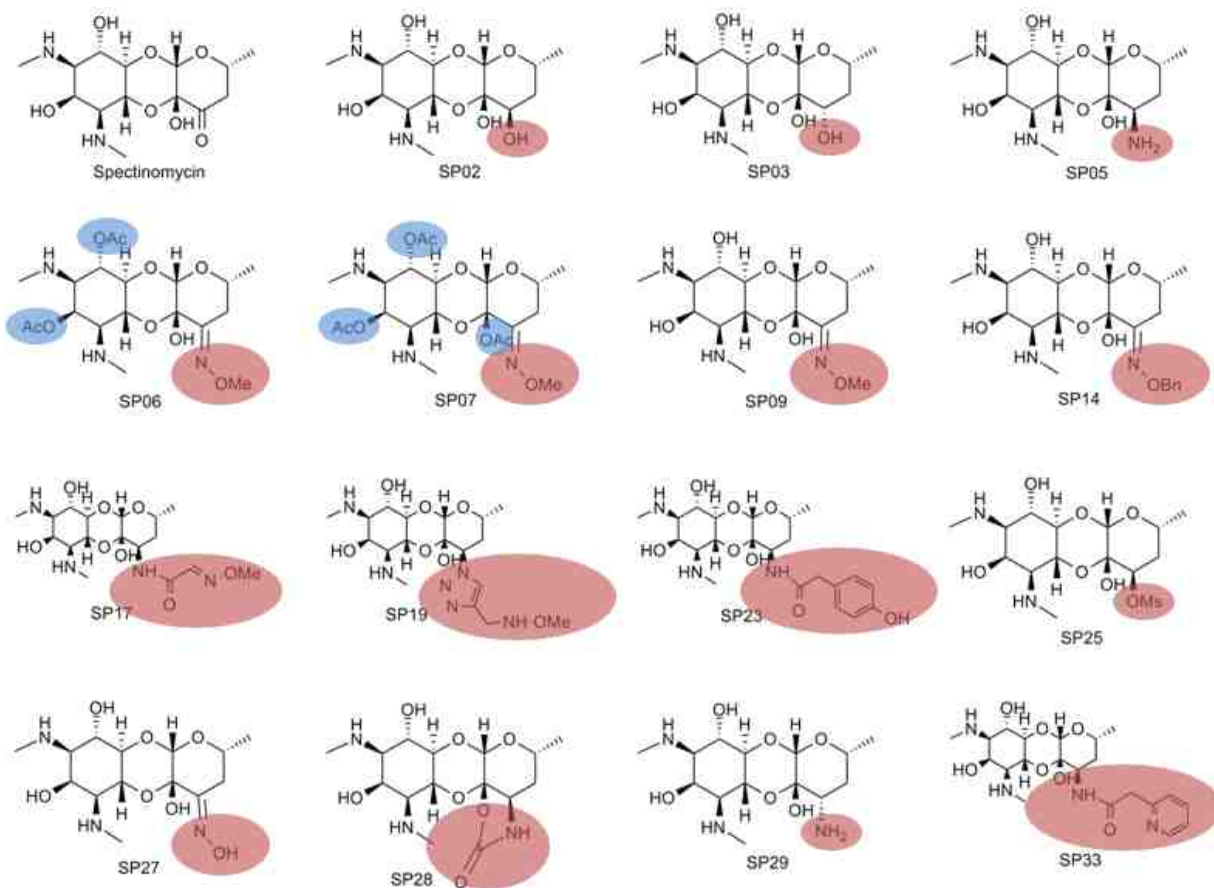


Figure 3-16 Chemical structures of spectinomycin analogs used in this work

Continue on next page

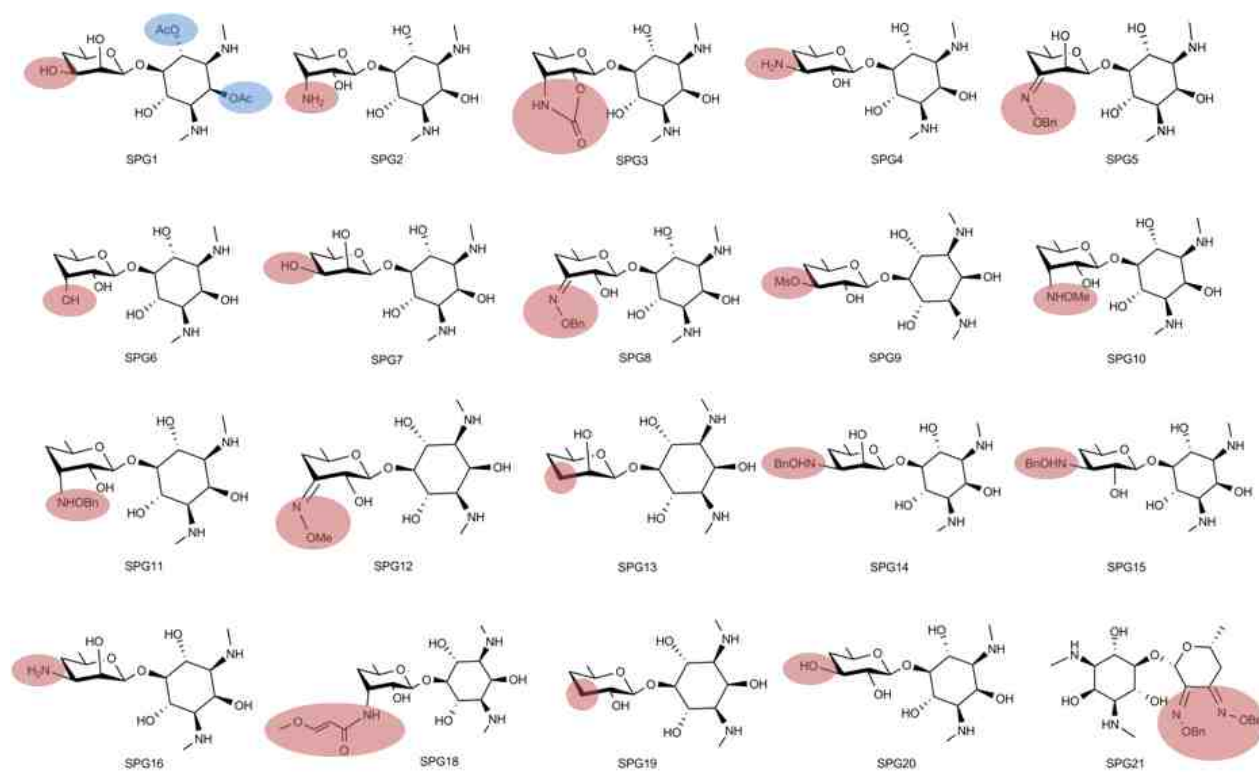


Figure 3-16 Chemical structures of spectinomycin analogs used in this work

3. Results and discussion

Extending the aminoglycosides detector to other ribosome small subunit inhibitors. By introducing different rRNA mutations which can prevent drug binding on rRNA and yet don't cause serious fitness lost onto the WT rRNA operon of the detector system, the aminoglycoside antibiotics detector system can be easily extended to detect spectinomycin and kasugamycin. The ribosome inhibition assay shows that spectinomycin has very strong anti-ribosome activity based on our results. The fluorescence signal shows up as early as 10 μ M spectinomycin and the detector strain displays robust fluorescence intensity in higher concentrations (Figure 3-17). This is consistent with previously reporter results.²² Despite spectinomycin possess high anti-

ribosome activity, it still lacks anti-bacterial activity against most of the clinical pathogens due to the efflux system in these bacterial. Because of the high safe index of spectinomycin, chemical structure modification is worthwhile to pursue in order to improve the drug potency. Compare to spectinomycin, kasugamycin displays very low ribosome inhibition activity based on our assay result. This correlates with the fact that kasugamycin has generally fewer polar contacts with rRNA than other ribosome inhibitors from crystal structures..

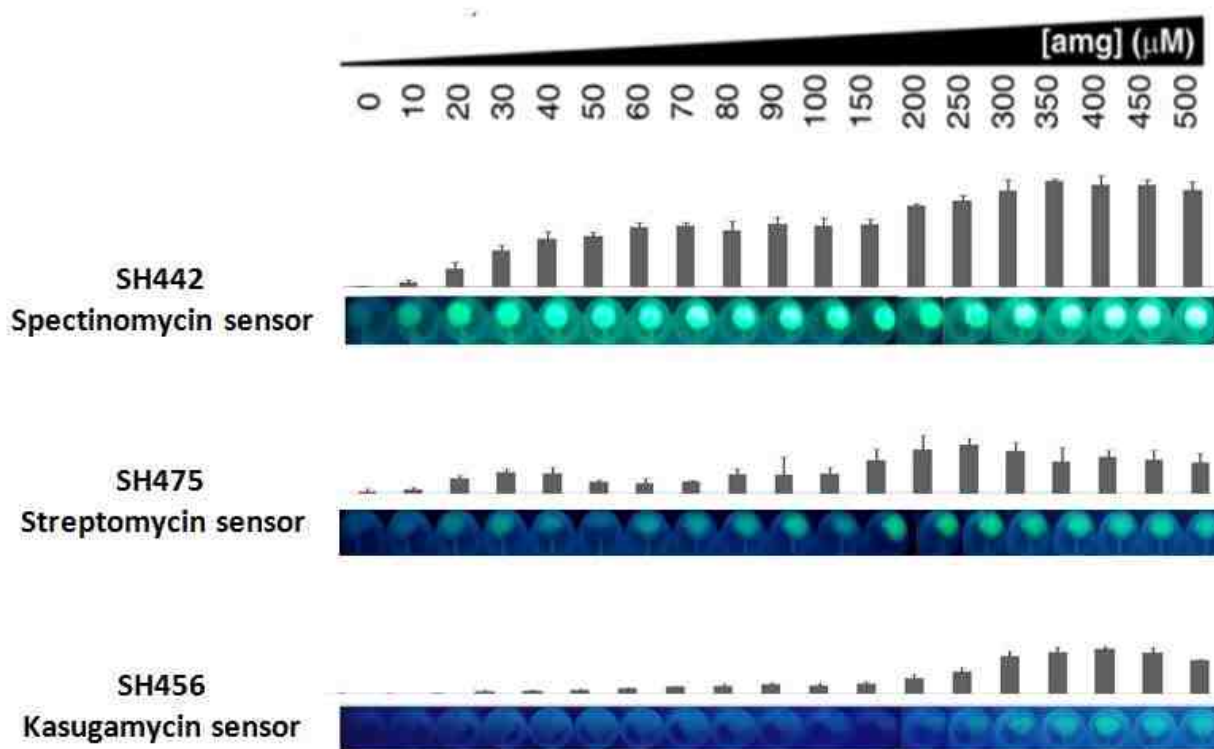


Figure 3-17 Cell pellet fluorescence of *E. coli* SH442, SH475 and SH456 in response to increasing concentrations of target molecules.

Unlike spectinomycin and kasugamycin detector strains, streptomycin detector displays very low sensitivity against streptomycin after direct transfer of sensing plasmid pSH6-KF. We hypothesises that is due to the C912U mutation can cause more fitness lost than other mutations

we used and consequently cause disequilibrium effect on the O-ribosome controlled tetR-gfpuv circuit. The ATC titration assay result proves our hypothesis (Figure 3-18). Four of the five detector strains (SH399, SH431, SH442, SH456 and SH446) begin to show fluorescence signal between 1 – 10 ng/mL ATC. However, the streptomycin detector strain displays weaker sensitivity to ATC with the fluorescence signal comes up as early as 25ng/mL. The streptomycin detector strain also displays generally lower fluorescence intensity than other 4 detectors.

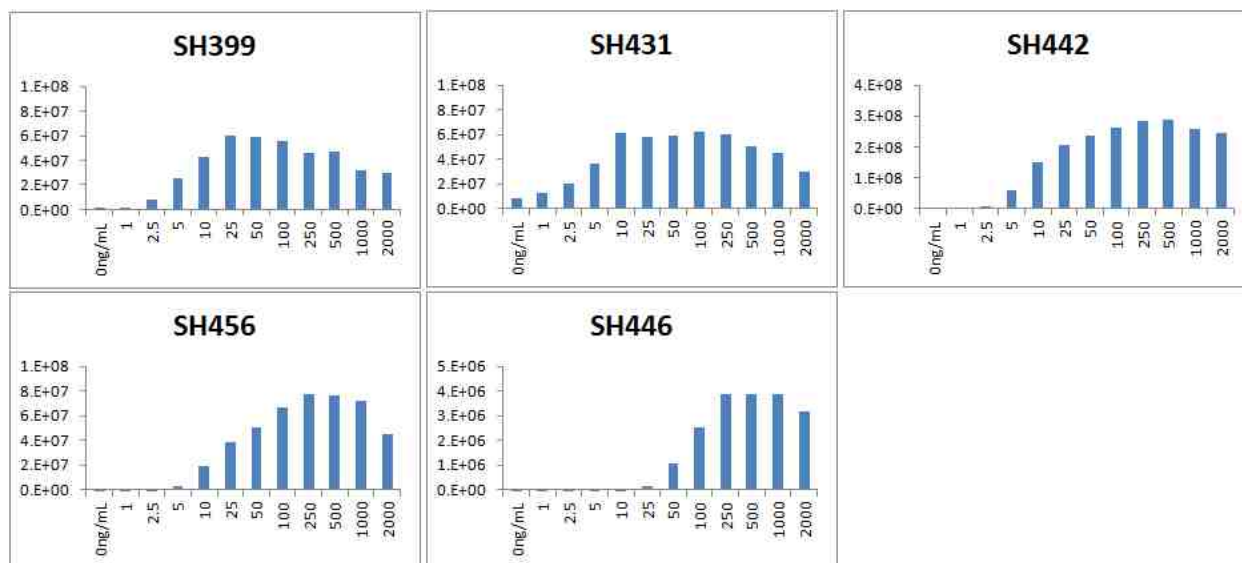


Figure 3-18 Bar graph figures showing the ATC titration of 5 detector strains. SH399 and SH431 are the 2-DOS aminoglycosides detectors (Chapter 2); SH442 is spectinomycin detector; SH456 is the kasugamycin detector; SH446 is the streptomycin detector. Note that the scales of y axis of the bar graphs are not the same due to the difference of the signal intensity between each detector.

These results promote us to down-regulate the expression of tetR for optimizing the sensitivity of streptomycin detector. The optimized streptomycin detector strain SH475 displays good sensitivity against streptomycin and it is capable to detect as low as 20 μ M streptomycin *in vivo* (Figure 3- 17). One interesting phenomenon we observed is that streptomycin only at 50 μ M concentration can always inhibit the detector strains' growth, which resulting in a strange bi-phase signal pattern. The detector strains can still grow in the presence of high concentration

streptomycin. We speculate this is due to the incomplete protection of WT rRNA by the C912U mutation. According to the streptomycin-ribosome co-crystal structure⁸, there are several polar contacts between the streptomycin and ribosomal protein S12. Genetic studies also show that mutation on S12 can lead to high resistance level to streptomycin.¹¹ Therefore, the single rRNA mutation C912U may not be able to completely block the streptomycin binding to ribosome and consequently affect the growth of the streptomycin detector strains.

Extending the ribosome inhibition detector to ribosome large subunit inhibitors. Thanks to the development of RiboT, our ribosome inhibition detector system can be extended to sense ribosome large subunit inhibitor as well. We therefore set to develop a complete ribosome inhibition detection system capable of sensing any small molecules that target ribosomal RNA. With the drug-resistant RiboT supporting cell growth, the 23S-16S-5S rRNA operon with an orthogonal ASD can be completely orthogonal to the RiboT protein synthesis machinery. We first used the same promoter combination of tetR and O-16S rRNA from pSH6-KF to build the ribosome large subunit inhibitor detector strain. We found that the resulting strain SH440 is insensitive to erythromycin and shows weak sensitivity to ATC. Therefore we applied the same strategy to tune down the production of tetR by altering the promoter strength of tetR and O-16S rRNA. The best detector strain SH460 harboring pSH26 exhibits good sensitivity against erythromycin with the signal comes up as early as 80 μ M erythromycin (Figure 3-19). The signal displays a bi-phase pattern similar to the streptomycin detector's signal against streptomycin. We speculate this is also due to the incomplete protection of the RiboT with the single rRNA mutation A2058G. The detector strain SH460 was then used to detection the ribosome inhibition by lincomycin, a different class of ribosome inhibitor compared to erythromycin. The signal of

ribosome inhibition by lincomycin shows up later than erythromycin (Figure 3-19), suggesting lincomycin has lower anti-ribosome activity than erythromycin.

To prove the ribosome large subunit inhibitor detection system is extendable, we introduced another mutation G2576U which is reported to confer high resistance to linezolid onto the RiboT and try to extend to detector to sense linezolid. The resulting strain SH493 harboring pSH26 is capable to detect linezolid with good sensitivity. The ribosome inhibition assay shows that linezolid has a very weak anti-ribosome activity compared to erythromycin and lincomycin. The fluorescence signal shown at 100 μ M – 200 μ M (Figure 3-19). This is probably due to *E.coli* strains have intrinsic efflux system to dilute the linezolid concentration.²³

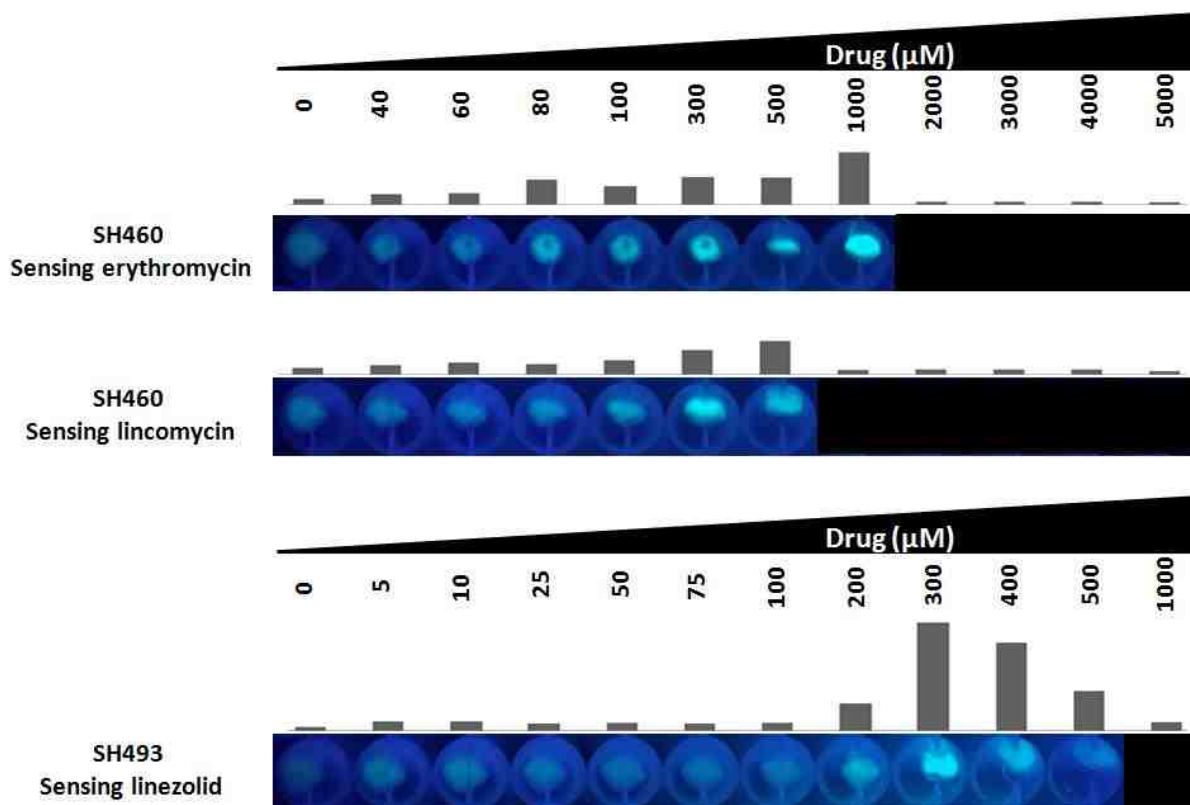


Figure 3-19 Cell pellet fluorescence of *E. coli* SH460 and SH493 in response to increasing concentrations of target molecules. (Black box means growth inhibition)

The results we show here have proven our O-ribosome controlled reporter system can be extended to detect ribosome inhibition by large subunit inhibitors. By integrating the complete orthogonal translation system RiboT into our detection system, we were able to free the 23S rRNA from supporting cell growth and assign it as the regulatory element to sense drug binding. Our results suggest that the large subunit detector should be able to detect macrolide antibiotics and lincosamide antibiotics with decent signal intensity. To prove the system can be extended to sense other large subunit inhibitors targeting different region of rRNA, we introduced another rRNA mutation G2576U into the RiboT and turned the system to sense linezolid. In principle, the detector system is able to sense any ribosome large subunit inhibitors that bind to the 23S rRNA.

Determination of ribosome inhibition by spectinomycin analogs. Technologies that can rapidly assess the relative potency or bioactivity of new compounds in high-throughput manner are critical for drug development. Here we show that the use of O-ribosome controller fluorescence reporter system can easily determine the ribosome inhibition activity of a spectinomycin compound library. The assay is done in conventional over-night culturing and the signal can be visualized by eyes or quantified by microplate reader. The detector strain is a non-pathogenic *E.coli* and is easy to distribute. We suggest the O-ribosome controller fluorescence reporter system can be a general tool for direct measurement of ribosome inhibition by small molecules.

The ribosome inhibition assays of spectinomycin analogs by detector SH442 show that 3 of the spectinomycin analogs, SP05, SP28 and SP33, have higher or comparable anti-ribosome activity compared to the parent compound spectinomycin (SP01) (Figure 3-20). By looking at the structure, these three compounds have an amine substituent at the 3' position of ring C in the

‘S’ configuration. Although this 3’ amine substituent seems to be important in the ribosome inhibition effect, the other two compounds (SP17 and SP23) which also have a 3’ amine substituent don’t exhibit obvious ribosome inhibition activity. These results suggest that the side chain attached to the 3’ amine substituent also play important roles in ribosome binding. By looking at the assay result, the stereochemistry of the 3’ substituent can affect the ribosome binding as well. SP02/SP03 and SP05/SP29 are two set of compounds with a different stereochemistry at the 3’ substituent. The ‘S’ configuration of the compound (SP02 and SP29) displays higher anti-ribosome activity than the ‘R’ configuration of the compound (SP03 and SP05).

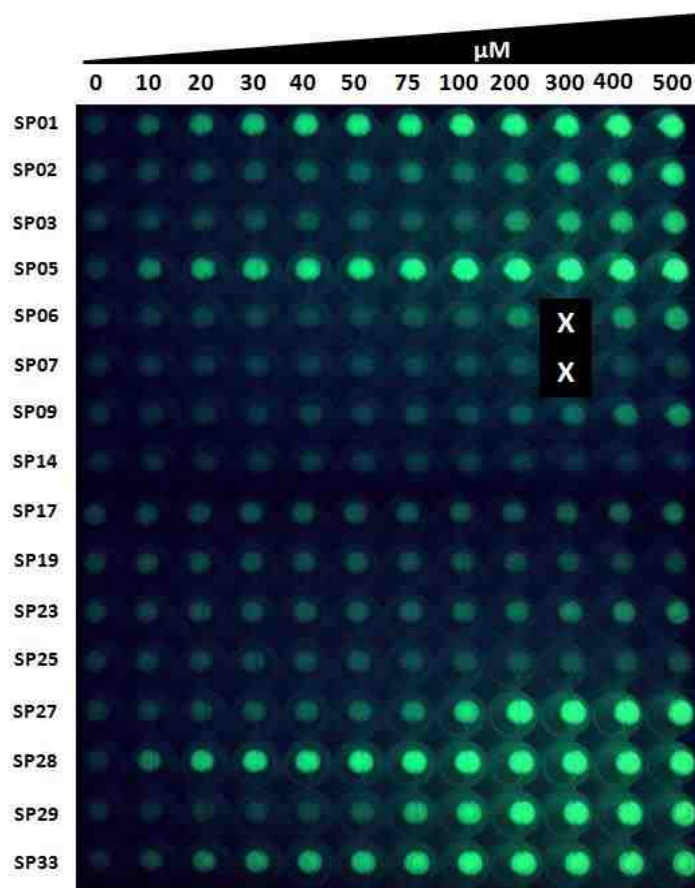


Figure 3-20 Cell pellet fluorescence of *E. coli* SH442 in response to increasing concentrations of spectinomycin analogs. (Black box with ‘X’ means outlier data)

For the ribosome inhibition assay of glycoside analogs, none of the 20 compounds display good anti-ribosome activity (Figure 3-21). By looking at the spectinomycin-ribosome crystal structure, the broken ring B of these glycoside analogs disrupts most of the polar contacts. One of the compound SPG10 shows growth inhibition to the detect strain at high concentrations. This suggests the SPG10 has other target sites other than the h34 of 16S rRNA. One interesting result we observed is the SPG8 which is the intermediate of SP14 has higher anti-ribosome activity than SP14. This result suggests that the 3' substituent group restores the ribosome binding even though the broken ring B abolished some polar contacts.

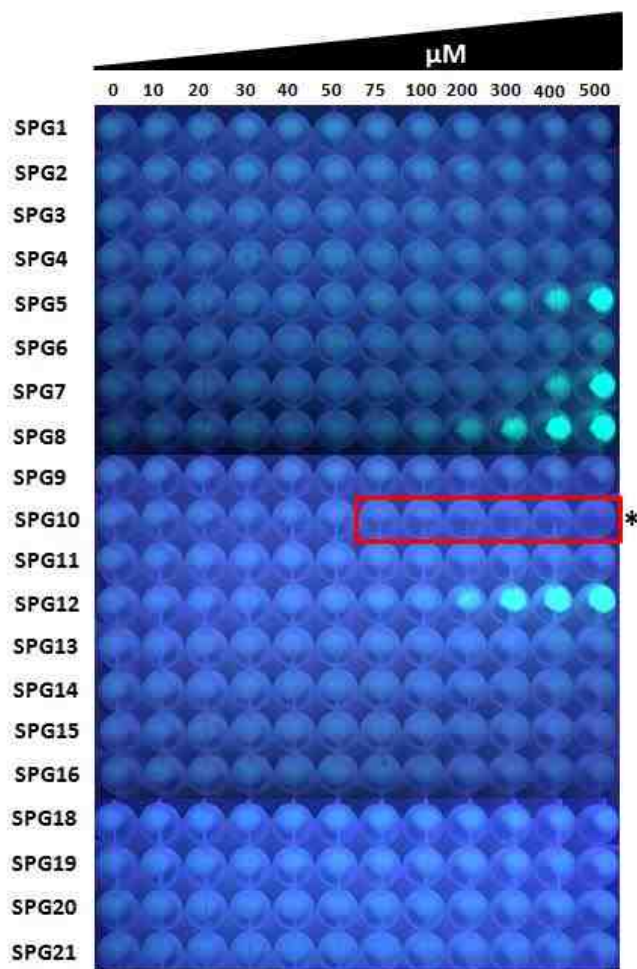


Figure 3-21 Cell pellet fluorescence of *E. coli* SH442 in response to increasing concentrations of glycoside analogs. (Red box indicated growth inhibition.)

These results demonstrate the O-ribosome controlled reporter system is capable to determine ribosome inhibition activity by small molecules with unknown activity. It is also able to be a target-based screening technique to screen inhibitors that target specific region of ribosome. We suggest the O-ribosome controlled reporter system can be a pre-screening tool to rapidly find the compound with good anti-ribosome activity at the early stage of drug development.

4. Conclusion

To conclude this chapter, we have extended our O-ribosome controlled fluorescence reporter system to detect and quantify ribosome inhibition by a variety of ribosome small subunit inhibitors and ribosome large subunit inhibitors. In principle, the current detectors systems should be able to detect and quantify ribosome inhibition by any small molecules targeting ribosome. The detector system can be also considered as target-based screening tool. Different detector strains developed in this work can be used to detect and classified a variety of antibiotics classes. The key to extend the O-ribosome controlled fluorescence reporter system to detect different ribosome inhibitors is to find suitable rRNA mutation that can block drug binding and yet cause less fitness lost on ribosome activity. Nowadays more and more drug-bound ribosome structures have been solved. It is much easier to locate the ribosome inhibitors binding site with the structure information. We envision that by using saturation mutagenesis approach on the drug binding region of rRNA, mutations that can fit into our detection system should be found for every ribosome inhibitor.

By showing the possibility of extending the detection ability of the system, we greatly promote the system towards diverse applications. We have proposed several potential

applications in chapter 2. The simplest application is to use our system as the target-based screening tool to evaluate potency of compound library. As a proof of concept, we applied the spectinomycin detector strain SH442 to evaluate the potency of a set of spectinomycin analogs. The assay can be done within 24 hours and is doable in every bio-lab. Our ribosome inhibition assay shows that 3 of the spectinomycin analogs have higher or comparable anti-ribosome activity to their parent compound. It is worthwhile to conduct future pharmacological test on these three compounds. SAR was also studied based on our ribosome inhibition assay. A 3' amine substituent at ring C of spectinomycin has the potential to increase the anti-ribosome activity. The opening ring B of spectinomycin will greatly reduce the anti-ribosome activity. Overall, we have shown the generality of our *in vivo* ribosome inhibition detection system and the possibility of applying the system to screen a compound library. We suggest that our detection system can be a general tool for early stage screening of ribosome inhibitors.

5. References

1. Osterman, I.A., Bogdanov, A.A., Dontsova, O.A., *et al.* Techniques for Screening Translation Inhibitors. *Antibiotics (Basel)*. 2016;5(3)
2. Carter, A.P., Clemons, W.M., Brodersen, D.E., *et al.* Crystal structure of an initiation factor bound to the 30S ribosomal subunit. *Science*. 2001; 291(5503):498-501.
3. Moazed. D., Noller, H.F. Interaction of antibiotics with functional sites in 16S ribosomal RNA. *Nature*. 1987; 327(6121):389-94.
4. Galimand, M., Gerbaud, G, Courvalin, P. Spectinomycin resistance in *Neisseria spp.* due to mutations in 16S rRNA. *Antimicrob Agents Chemother*. 2000; 44(5):1365-6.

5. Binet, R., Maurelli, A.T. Fitness cost due to mutations in the 16S rRNA associated with spectinomycin resistance in *Chlamydia psittaci* 6BC. *Antimicrob Agents Chemother.* 2005; 49(11):4455-64.
6. Criswell, D., Tobiason, V.L., Lodmell, J.S., Samuels, D.S. Mutations conferring aminoglycoside and spectinomycin resistance in *Borrelia burgdorferi*. *Antimicrob Agents Chemother.* 2006; 50(2):445-52.
7. Makosky, P.C., Dahlberg, A.E. Spectinomycin resistance at site 1192 in 16S ribosomal RNA of *E. coli*: an analysis of three mutants. *Biochimie.* 1987; 69(8):885-9.
8. Demirci, H., Murphy, F., Murphy, E., Gregory, S.T., Dahlberg, A.E, Jogl, G. A structural basis for streptomycin-induced misreading of the genetic code. *Nat Commun.* 2013; 4:1355.
9. Powers, T., Noller, H.F. A functional pseudoknot in 16S ribosomal RNA. *EMBO J.* 1991; 10(8):2203-14.
10. Springer, B., Kidan, Y.G., Prammananan, T., Ellrott, K., Böttger, E.C., Sander, P. Mechanisms of streptomycin resistance: selection of mutations in the 16S rRNA gene conferring resistance. *Antimicrob Agents Chemother.* 2001; 45(10):2877-84.
11. Finken, M., Kirschner, P., Meier, A., Wrede, A., Böttger, E.C. Molecular basis of streptomycin resistance in *Mycobacterium tuberculosis*: alterations of the ribosomal protein S12 gene and point mutations within a functional 16S ribosomal RNA pseudoknot. *Mol Microbiol.* 1993; 9(6):1239-46.
12. Schlunzen, F., Takemoto, C., Wilson, D.N., *et al.* The antibiotic kasugamycin mimics mRNA nucleotides to destabilize tRNA binding and inhibit canonical translation initiation. *Nat Struct Mol Biol.* 2006; 13(10):871-8.

13. Helser, T.L., Davies, J.E., Dahlberg, J.E. Change in methylation of 16S ribosomal RNA associated with mutation to kasugamycin resistance in *Escherichia coli*. *Nature New Biol.* 1971; 233(35):12-4.
14. Vila-sanjurjo, A., Squires, C.L., Dahlberg, A.E. Isolation of kasugamycin resistant mutants in the 16 S ribosomal RNA of *Escherichia coli*. *J Mol Biol.* 1999; 293(1):1-8.
15. Orelle, C., Carlson, E.D., Szal, T., Florin, T., Jewett, M.C., Mankin, A.S. Protein synthesis by ribosomes with tethered subunits. *Nature.* 2015; 524(7563):119-24.
16. Zhanel, G.G., Dueck, M., Hoban, D.J., *et al.* Review of macrolides and ketolides: focus on respiratory tract infections. *Drugs.* 2001; 61(4):443-98.
17. Vazquez-laslop, N., Thum, C., Mankin, A.S. Molecular mechanism of drug-dependent ribosome stalling. *Mol Cell.* 2008; 30(2):190-202.
18. Dunkle, J.A., Xiong, L., Mankin, A.S., *et al.* Structures of the *Escherichia coli* ribosome with antibiotics bound near the peptidyl transferase center explain spectra of drug action. *Proc Natl Acad Sci USA.* 2010; 107(40):17152-7.
19. Kloss, P., Xiong, L., Shinabarger, D.L., Mankin, A.S. Resistance mutations in 23 S rRNA identify the site of action of the protein synthesis inhibitor linezolid in the ribosomal peptidyl transferase center. *J Mol Biol.* 1999; 294(1):93-101.
20. Long, K.S., Vester, B. Resistance to linezolid caused by modifications at its binding site on the ribosome. *Antimicrob Agents Chemother.* 2012; 56(2):603-12.
21. Gibson, D.G., Young, L., Chuang, R.Y., *et al.* Enzymatic assembly of DNA molecules up to several hundred kilobases. *Nat Methods.* 2009; 6(5):343-5.

22. Bruhn, D.F., Waidyarachchi, S.L., Madhura, D.B., *et al.* Aminomethyl spectinomycins as therapeutics for drug-resistant respiratory tract and sexually transmitted bacterial infections. *Sci Transl Med.* 2015; 7(288):288ra75.
23. Piddock, L.J. Multidrug-resistance efflux pumps - not just for resistance. *Nat Rev Microbiol.* 2006; 4(8):629-36.

CHAPTER 4. DIRECTED EVOLUTION OF RIBOSOMAL RNA VARIANT TO EXAMINE THE INTERACTIONS BETWEEN AMINOGLYCOSIDE ANTIBIOTICS AND RIBOSOME.

1. Introduction

Chapter 2 and chapter 3 have described the development and extension of O-ribosome controlled fluorescence reporter system which can be used to detect and quantify ribosome inhibition by a variety of ribosome inhibitors *in vivo*. We have proven the feasibility of using the system to screen a spectinomycin compound library in a more efficient way, which is one of the potential applications we proposed. The parallel ribosome system with similar copy number represents a unique feature of our system and we have shown the success of using the O-ribosome as a detector for ribosome inhibition. We then set out to further utilize the system as a tool to study drug-ribosome interactions by fully altering the rRNA sequence at the drug binding sites. With the advantage of having two similar populations of ribosome in the cell, we envision that interesting new mutations on rRNA will be found and interactions between ribosome inhibitors and mutated ribosomes could lead us to new inside of ribosome inhibition. The new founding may lead us to develop better antibiotics in the future.

The ribosome is a highly evolved macro-molecule with many conserved functional domains across all the species in bacterial kingdom. Although ribosome is consisted of rRNAs and ribosomal proteins, only rRNAs had been proven to perform catalytic function¹. This correlates with the fact that rRNA sequence is highly resistant to alteration. As a result, nature chose the ribosome as the major target for antimicrobial agents due to its essentiality to cell survival and fragility to alterations. A large effort had been made in the past to search for

functional mutations on rRNA². Most of them aimed to characterize the role of the target rRNA sequence in protein synthesis^{3, 4}. Most of the mutations were shown to be lethal to cell and therefore their functions cannot be examined⁵, such as interactions between ribosome inhibitors and drug binding site. Previous reports had described an O-ribosome based system to study the impact of deleterious mutations on 16S rRNA to protein synthesis⁶. The system was able to systematically study the rRNA sequence of important regions for ribosome catalytic activity. However, the O-ribosome based system was used in WT *E.coli* strains and therefore the presence of genomic rRNA operons limits the system to studying ribosome inhibition by antimicrobial agents.

To develop the O-ribosome based system to study ribosome inhibition, the ratio between WT ribosome and O-ribosome is crucial. It has been suggested that the population of mutated ribosome has large impact on its drug-resistance property. For instance, the U1406A mutation can cause high resistance to geneticin when the ratio between mutant ribosome and WT ribosome is close to 1:1. However, when there are 7 copies of genomic ribosome operons present, the mutant ribosome is not functioning anymore⁷. One of the key features of our O-ribosome reporter system is that it only has one copy of WT rRNA operon and another copy of O-ribosome. This feature can help us maximize the chance to find more mutations at the drug binding site. Both WT ribosome and O-ribosome in our system can be used as the target to examine their interactions with drugs. The O-ribosome controlled fluorescence reporter was replaced with the O-ribosome controlled chloramphenicol acetyltransferase gene (CAT). CAT can transfer an acetyl group from acetyl-CoA to chloramphenicol and consequently prevent chloramphenicol binds to ribosome. The activity of CAT can be titrated by adding a concentration range of chloramphenicol. Therefore it is a perfect selection marker for selecting

O-ribosome mutants with different catalytic activity. The scheme of O-ribosome controlled CAT and its advantages is shown in figure 4-1. We anticipate different results will be observed from the two types of ribosomes. It would be interesting to compare the result in parallel.

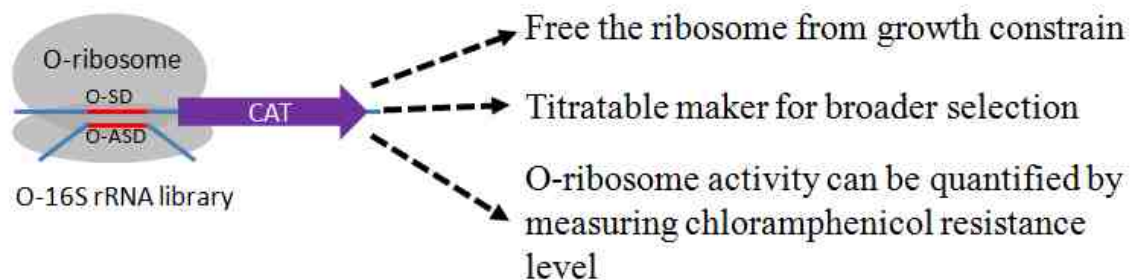


Figure 4-1 The scheme of O-ribosome controlled CAT and its advantages

One of the goals to study drug-resistant rRNA mutations is to learn how the mutations evolve in nature and anticipate possible new drug-resistant mutation in the future⁸. Current approaches to find drug-resistant mutations include structure-guided mutagenesis^{9,10} and clinical isolations of drug-resistant pathogens^{11,12}. Neither of these methods can comprehensively study the possible mutations at the drug binding sites. Single point mutation is usually studied by these methods due to the difficulty to isolate mutations on functionally important part on ribosome¹³. We propose to use directed evolution in which saturation mutagenesis was applied to drug binding site and mutants are selected towards specific drug resistance. We envision many new mutations, especially compensatory mutations, with special properties can be found.

As a proof of concept, we chose 3 aminoglycoside antibiotics, kanamycin, neomycin and gentamicin, as the testing drug to find new mutations at the drug binding site. Kanamycin is a classic 4, 6-disubstituted deoxystreptamine and neomycin is a classic 4, 5-disubstituted deoxystreptamine. They are the representative antibiotics of 2-DOS class antibiotic. Kanamycin

and neomycin also display distinguish signal pattern based on our ribosome inhibition assay by O-ribosome fluorescence reporter¹⁴. Gentamicin shows a unique signal pattern from our ribosome inhibition assay¹⁴, therefore it is also chosen as the testing antibiotic. All of the three antibiotics bind to the h44 region of 16S rRNA and a variety of drug-resistant mutations had been found from previous studies. Thus, finding new resistant mutation to the three compounds should be good examples to prove the advantage of our approach. To comprehensively explore new mutation at the binding site, we chose 9 sites (1405-1409, 1491, 1494-1496) that are at the center of the drug binding pocket as the nucleotides to alter. The A1492 and A1493 are left unchanged due to their essentiality in decoding the mRNA-tRNA recognition during translation¹⁵. Saturation mutagenesis was applied on the 9 sites to maximize the chance of getting new mutation. The rRNA library was built on both WT ribosome and O-ribosome and the results were compared to find new insides on aminoglycoside drug binding.

2. Experimental procedures

General. Most of the materials used for work described in this chapter have already been mentioned in the experimental procedures section of Chapter 2. The concentrated T4 DNA ligase (2,000,000 units/ml) was purchased from New England Biolabs (Ipswich, MA). The 96-well pin tool was purchased from V&P Scientific, Inc. (San Diego, CA).

Bacterial strains. All the bacterial strains used for work described in this chapter have been mentioned in the experimental procedures section of Chapter 2.

Bacterial culture. All of the bacterial culture methods used for work described in this chapter have been mentioned in the experimental procedures section of Chapter 2.

PCR conditions. All of the PCR conditions used for work described in this chapter have been mentioned in the experimental procedures section of Chapter 2. Gibson assembly reaction condition is the same as the reported method¹⁶.

Enforced replacement by sucrose counterselection. The enforced replacement method was already described in the experimental procedures section of Chapter 2.

Cell density and fluorescence assays. The methods for measuring cell density and fluorescence intensity was already described in the experimental procedures section of Chapter 2.

Construction of h44 9-site library on pRRSH2. pRRSH2 was used as the template to construct the h44 9-site library. The 9-site library plasmid was built by COE-PCR (see description in chapter 2 experimental procedures). 5 fragments were generated to perform the COE-PCR. Fragment 1 containing portion of 16S rRNA was amplified using primers pRRSH-rRNA1-up and pRRSH2-lib-rRNA1-dn. Fragment 2 containing the p15A origin of replication and ampicillin resistance marker was amplified using primers pRRSH-AmpR-up and pRRSH-p15A-dn. Fragment 3 containing half of 23S rRNA was amplified using primers pRRSH-rRNA3-up and pRRSH-rRNA3-dn. Fragment 4 containing another half of 23S rRNA was amplified using primers pRRSH2-lib-rRNA2-up and pRRSH-rRNA2-dn. Fragment 5 (shown in figure 4-2) containing the 9-site library was built in 3 steps. First a 132bp fragment containing the 2 randomized DNA regions at both ends was amplified using degenerate primers 16S9er-lib-2-up and 16S9er-lib-2-dn. The primers were designed to exclude the wild type sequence at the randomized regions. Secondly, 2 fragments containing overlapping ends to the 132bp fragment were amplified using primer pairs 16S9er-lib-1-up/16S9er-lib-1-dn and 16S9er-lib-3-up/16S9er-lib-3-dn. Thirdly, the 132bp fragment was assembled with the 2 fragments by primerless PCR to

generate fragment 5. These 5 fragments were used to build pRRSH2 with the h44 9-site library by COE-PCR and the reaction mixture was concentrated using the Zymo Clean and Concentrator Kit, and introduced into competent *E.coli* DH10B cells by electroporation. The transformants were serial diluted to count the colony forming unit (cfu). About 2.55×10^6 cfu was obtained from 3 transformations (around 10-fold coverage of 2.6×10^5 theoretical diversity). Library quality was assessed by sequencing of 10 naive clones. Primer information is given in the table 4-1 below. The randomized regions on degenerate primers were colored in bold red.

| primer name | sequence (5' -3') | amplicon size (bp) | template |
|-----------------------|---|--------------------|----------|
| pRRSH2-lib-rRNA1-dn | GTCTCCTTTGAGTTCCCGGC (used with pRRSH-rRNA1-up) | 1531 | pRRSH2 |
| pRRSH2-lib-rRNA2-up | CATCTTCGGGTGATGTTTGAGATTTTGCTTTTAAAAATCTGG (used with pRRSH-rRNA2-dn) | 1909 | pRRSH2 |
| 16S9er-lib-1-up | GCAAAAATCTCAAACATCACCCGAAGATGAG | 366 | pRRSH2 |
| 16S9er-lib-1-dn | ACAAGGTAACCGTAGGGGAACCTG | | |
| 16S9er-lib-2-up-1491D | CCCTACGGTTACCTTGTTAC NNNTD ACCCAGTCATGAATCAC | 132 | pRRSH2 |
| 16S9er-lib-2-up-1494D | CCCTACGGTTACCTTGTTAC NNDTTN ACCCAGTCATGAATCAC | | |
| 16S9er-lib-2-up-1495B | CCCTACGGTTACCTTGTTAC NBN TTNACCCAGTCATGAATCAC | | |
| 16S9er-lib-2-up-1496H | CCCTACGGTTACCTTGTTAC HNN TTNACCCAGTCATGAATCAC | | |
| 16S9er-lib-2-dn-1405H | GGGCCTGTACACACCGCCC HNNNN ACCATGGGAGTGGGTTG | | |
| 16S9er-lib-2-dn-1406V | GGGCCTGTACACACCGCCC NVNNN ACCATGGGAGTGGGTTG | | |
| 16S9er-lib-2-dn-1407D | GGGCCTGTACACACCGCCC NNDNN ACCATGGGAGTGGGTTG | | |
| 16S9er-lib-2-dn-1408B | GGGCCTGTACACACCGCCC NNNBN ACCATGGGAGTGGGTTG | | |
| 16S9er-lib-2-dn-1409D | GGGCCTGTACACACCGCCC NNNND ACCATGGGAGTGGGTTG | | |
| 16S9er-lib-3-up | GGTGTGTACAAGGCCCGGGAAC | | |
| 16S9er-lib-3-dn | GCCGGAACTCAAAGGAGACTGCCAG | | |

Table 4-1. Primers for constructing h44 9-site library

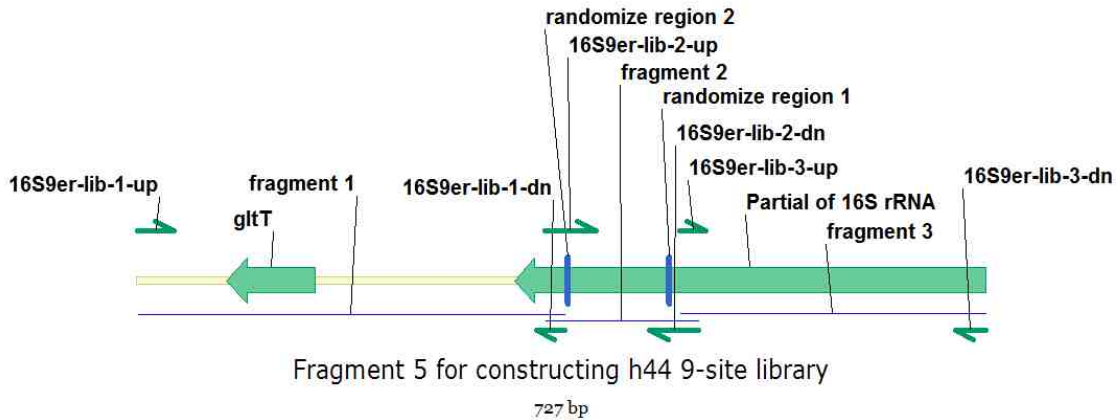


Figure 4-2. The fragment 5 for construction h44 9-site library

Transferring the h44 library into SQ380+pSH6KF. The h44 9-site library *E.coli* DH10B transformants were scraped from LB agar plates and the OD₆₀₀ was quantified by cell density meter. The library transformants were inoculated into LB medium to grow to OD₆₀₀=4. Cells were collected by centrifuge and the plasmids were isolated and purified using the QIAGEN Plasmid Mini Kit. 1 μg of the library plasmid DNA and 1 μg of the pRRSH2 was transformed into competent *E.coli* SQ380+pSH6KF cells by electroporation. The transformants were serially diluted to count the cfu. About 1.57 × 10⁶ cfu was obtained from pRRSH2 transformation (around 6-fold coverage of 2.6 × 10⁵ theoretical diversity), indicating 1 μg of library plasmid DNA should be enough for transformation to cover the diversity. About 2.1 × 10⁵ cfu was obtained from 1 μg of library plasmid transformation. This result indicates around 13% of the mutants (calculated by dividing 2.1 × 10⁵ cfu with 1.57 × 10⁶ cfu) can co-exist with WT rRNA operon (prnC-sacB). All the h44 9-site library transformants were scraped from LB agar plates and the OD₆₀₀ was quantified. 2.6 × 10⁸ cells (1000-fold coverage of 2.6 × 10⁵ theoretical diversity) were used to select on 5% sucrose LB agar plate for curing out WT rRNA operon (prnC-sacB). Around 8,500

colonies were obtained from sucrose counter-selection. They were collected for further selection and screening by aminoglycoside antibiotics.

Aminoglycoside antibiotics selections on h44 9-site library. The 8,500 colonies were scraped from LB agar plate and quantified the OD₆₀₀. Around 1,000 cells were used to select on 12 aminoglycoside antibiotics (the same set of antibiotics used in chapter 2) with killing concentrations, respectively. The killing concentrations of each aminoglycoside antibiotics used in this work were shown in table 4-2. Numbers of survivors on each aminoglycoside antibiotic selection plate were counted and shown in figure 4-2. To further characterize the phenotypes of these survivors, they were subjected to the second round of cross selection against the 12 aminoglycoside antibiotics. Various numbers of colonies were picked from each aminoglycoside antibiotic selection plate. Totally 228 survivors were grown up in 3 96-deep-well plates without the addition of aminoglycoside antibiotics. The survivors were then transferred and selected on 12 aminoglycoside antibiotics agar plates using the 96-well pin tool, respectively. The growth and fluorescence of each survivor on each of the 12 aminoglycosides was recorded and they were grouped by their phenotypes. Various mutants from each group were picked and sequence the mutated part of the 16S rRNA.

| | Kan | Apr | Neo | Gm | Paro | G418 | Hyg | Ami | Sis | Rib | Nea | Tob |
|----------------------------|-----|-----|-----|----|------|------|-----|-----|-----|-----|-----|-----|
| Concentration (μM) | 150 | 150 | 20 | 20 | 50 | 40 | 90 | 30 | 10 | 60 | 500 | 20 |
| Number of survivors | 22 | 16 | 22 | 22 | 36 | 52 | 27 | 2 | 19 | 0 | 0 | 0 |

Table 4-2. Concentration of each antibiotic used in this work. They were chosen from the result in chapter 2. The ribosome activity should be completely shut down at these concentrations.

Construction and testing of pSH-OCAT. This plasmid, which contains the chloramphenicol acetyltransferase gene under control of the constitutive promoter BBa_J23016

and O-SD-KF sequence (see chapter 2 for detail), pMB1 origin of replication, O-16S rRNA fragment from pSH6-KF and DHFR selection marker was constructed from four fragments by Gibson assembly. The chloramphenicol acetyltransferase gene fragment was built by sequential PCR. The chloramphenicol acetyltransferase gene was amplified from pSH6-KF using primers CG-cat-up-1 and GC-cat-dn. The PCR product was purified and used as the template for the sequential PCR using primers CG-cat-up-2 and GC-cat-dn. The resulting 929bp PCR product was used for the Gibson assembly to build pSH-OCAT. The pMB1 origin of replication was amplified from pUC19 using primers F3-up-tetRassem and pCL-F3-pMB1-dn. The DHFR gene was amplified from pSH18 using primers CG-DHFR-up and CG-DHFR-dn. The O-16S rRNA fragment was amplified from pSH6-KF using primers pB15-dn and CG-O16S-dn. The resulting four fragments were assembled by Gibson assembly. The reaction mixture was concentrated using the Zymo Clean and Concentrator Kit, and introduced into competent *E.coli* DH5a cells. The final construct was verified by restriction mapping and sequencing. Primer information is given in the table 4-3 below. The plasmid map of pSH-OCAT is shown in figure 4-3.

| primer name | sequence (5' -3') | amplicon size (bp) | template |
|--------------------|--|---------------------------|-----------------|
| CG-cat-up-1 | CAGCCAGAGAAAACAATCGATACATCCCCCGCAAATGGAGAAAAAATCACTGGATATACC | 705 | pSH6-KF |
| GC-cat-dn | AGAACCACCACCACCCGCCCGCCCTGCCACTCATC | | |
| CG-cat-up-2 | TTTACGGCTAGCTCAGTCCTAGGTATAGTGCTAGCCCAGCCAGAGAAAACAATCGATAC | 741 | pSH6-KF |
| F3-up-tetRassem | GCGGTAATAAGCTTACGGTTATCCAC | 738 | pUC19 |
| pCL-F3-pMB1-dn | AGACCCCGTCTAGATAGAAAAGATCAAAGGATCTTCTTGAG | | |
| CG-DHFR-up | GATCTTTTCTATCTAGACGGGGTCTCGAGCTCGATATCAAATTAGGCC | 538 | pSH18 |
| CG-DHFR-dn | GGTACCCGTGGATCCTCTAGAGGATCCAACCTGCATTGAGAATAAATAAATCC | | |
| pB15-dn | TCTAGAGGATCCACGGGTACC | 2150 | pSH6-KF |
| CG-O16S-dn | CCTAGGACTGAGCTAGCCGTAACCTGGACTCCTGTTGATAGATCC | | |

Table 4-3. Primers for constructing pSH-OCAT

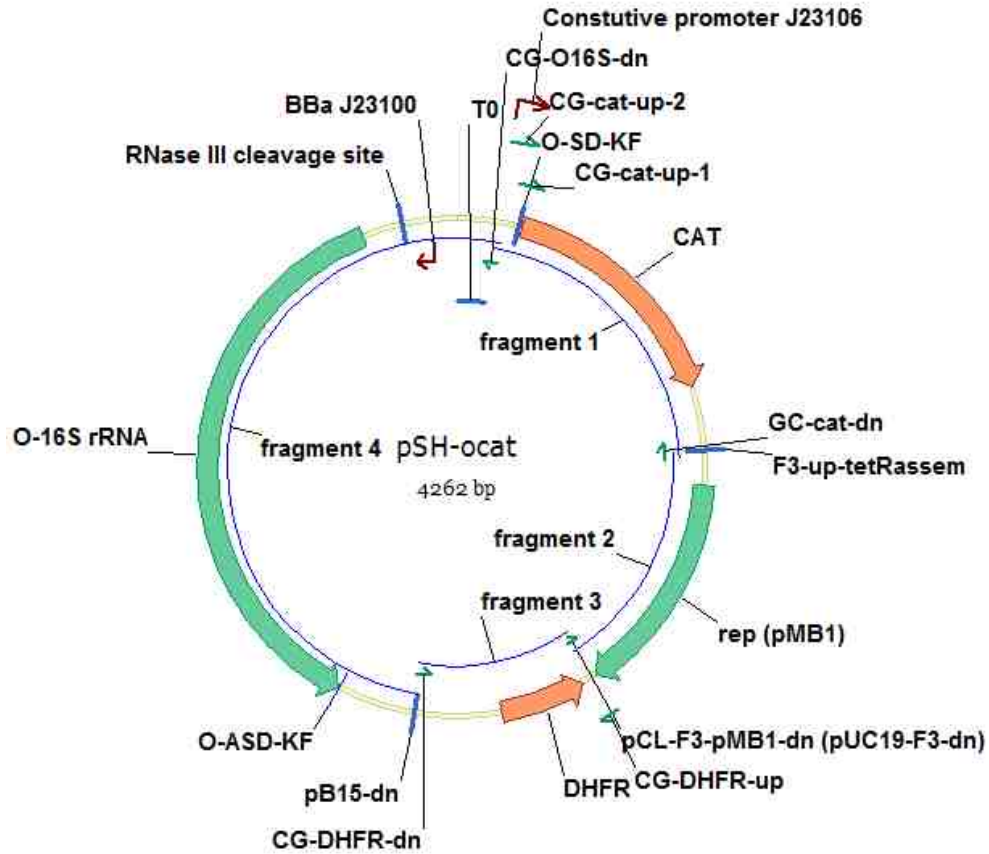


Figure 4-3. Plasmid map of pSH-OCAT

To test whether the O-ribosome activity can represent the WT ribosome activity or not, 4 rRNA single mutations with different fitness cost were chosen to introduce to the WT rRNA operon (pRRSH2) and O-ribosome (pSH-OCAT), respectively. These four rRNA mutations are A1408G, U1406A, G1491C and C1496U. The strategy to introduce these mutations onto 16S rRNA is similar to the strategy described in chapter 3 (see experimental procedure). The pRRSH2 with each of the four mutations was introduced into SQ380 and replaced the resident plasmid prnC-SacB. The resulting *E. coli* strains and SQ380 (WT rRNA operon) were grown in LB broth and the growth curve of each strain is measured using micro-plate reader (figure 4-4). The OD₆₀₀ was taken every 10 minutes and the strains were set to grow for 24 hours. The pSH-

OCA7 with each of the four mutations and without any mutation was introduced into SQ380. The resulting *E.coli* strains were grown in LB broth with the addition of a concentration range of chloramphenicol. OD₆₀₀ of each strain in each concentration of chloramphenicol was measured by micro-plate reader (figure 4-5).

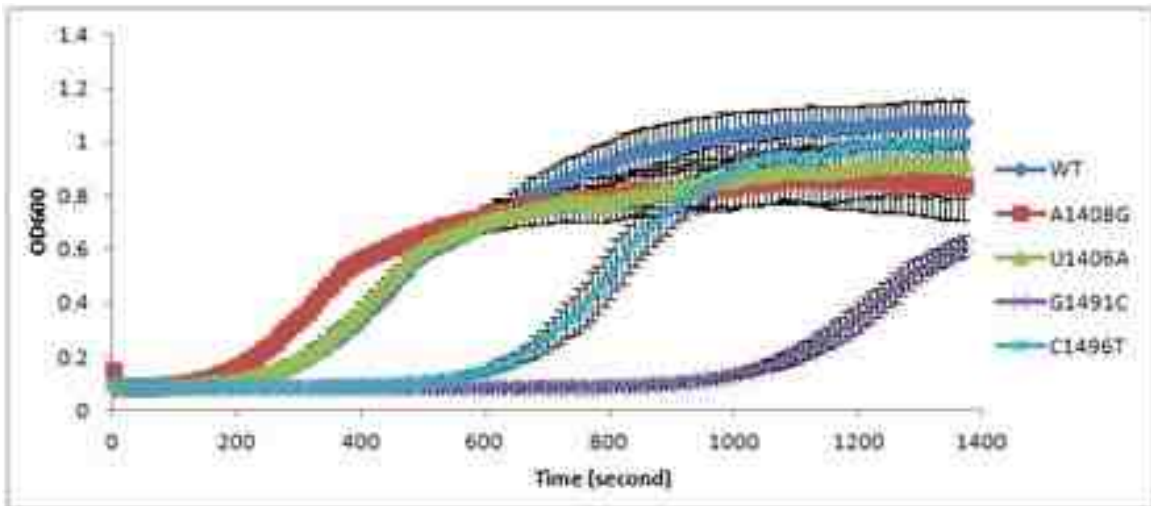


Figure 4-4. Growth curve of *E.coli* $\Delta 7$ strain with different rRNA mutations.

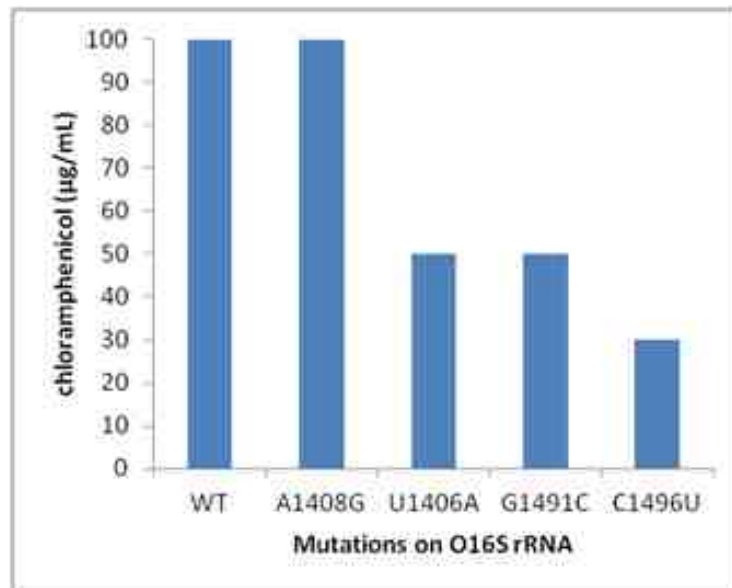


Figure 4-5. Chloramphenicol resistant level of different rRNA mutations on O-16S rRNA .

Construction of O-h44 9-site library on pSH-OCAT. pSH-OCAT was used as the template to build the O-h44 9-site library. The library was built by traditional digestion-ligation. The 1139bp insert fragment containing the randomized regions, FspI and BsrGI site, was built in 3 steps similar to the construction of h44 9-site library. The 132bp fragment containing the 2 randomized DNA regions at both ends was amplified using degenerate primers 16S9er-lib-2-up and 16S9er-lib-2-dn. Then the 2 fragments containing overlapping ends to the 132bp fragment were amplified using primer pairs CG-DHFR-up/16S9er-lib-1-dn and 16S9er-lib-3-up/16S9er-lib-3-dn. These three fragments were assembled by primerless PCR to generate the 1139bp insert fragment. The pSH-OCAT and insert fragment were digested with FspI and BsrGI, gel purified, ligated and introduced into competent *E.coli* DH10B cells by electroporation. The transformants were serially diluted to count the cfu. About 1.678×10^6 cfu was obtained from 3 transformations (around 6.4-fold coverage of 2.6×10^5 theoretical diversity). Library quality was assessed by sequencing of 10 naive clones.

Transferring the O-h44 library into SH471. SH471 was constructed by replacing the ptRNA67 with ptRNA70 in SQ380. Due to the plasmid origin of replication compatibility, SH471 displays better transformation efficiency than SQ380. Therefore we chose SH471 as the host to introduce the O-h44 library plasmid. The O-h44 9-site library *E.coli* DH10B transformants were scraped from LB agar plates and the OD₆₀₀ was quantified. The library transformants were inoculated into LB medium to grow to OD₆₀₀=4. Cells were collected by centrifuge and the plasmids were isolated and purified using the QIAGEN Plasmid Mini Kit. 1μg of the O-h44 library plasmid DNA was transformed into competent *E.coli* SH471 cells by electroporation. About 2.46×10^6 cfu was obtained from 2 transformations (around 9.4-fold

coverage of 2.6×10^5 theoretical diversity). All the transformants were scraped from the LB agar plates for further selections and the OD₆₀₀ was quantified.

Ribosome activity selection and aminoglycoside antibiotics selection on O-h44 library.

To select for rRNA mutants that possess different translation activity, the O-h44 library transformants were grown on 15 concentrations of chloramphenicol LB agar plates. Survival on each concentration of chloramphenicol represents O-ribosome translation activity. 10^8 cells of the O-h44 library transformants were used to select on each concentrations of chloramphenicol LB agar plate. Numbers of survivors on each chloramphenicol concentration plate were counted and summarized in table 4-4. 6 colonies from each chloramphenicol concentration plate were picked to sequence the randomized regions on O-16S rRNA.

| Chloramphenicol (µg/mL) | 0 | 10 | 20 | 30 | 40 | 50 | 60 | 70 | 80 | 90 | 100 | 110 | 120 | 130 | 140 | 150 |
|-------------------------|-----------------|-------------------|-------------------|------|-----|-----|-----|-----|-----|-----|-----|-----|-----|-----|-----|-----|
| Number of survivor | 6×10^7 | 8.3×10^5 | 1.3×10^4 | 1800 | 571 | 231 | 178 | 187 | 256 | 289 | 164 | 138 | 111 | 114 | 88 | 80 |

Table 4-4. Numbers of survivors on each chloramphenicol concentration plate.

Kanamycin, neomycin and gentamicin were chosen as the testing compounds for aminoglycoside antibiotics selections due to their representative structure feature. Killing concentrations of the three compounds were chosen for selecting mutants that are resistant to drug binding. 10^8 cells of naive library were used to select on killing concentrations of the three antibiotics respectively with 20µg/mL chloramphenicol. The addition of 20µg/mL chloramphenicol is to select the mutants with partial catalytic activity. 96 survivors from each of the three antibiotics selection were picked and their randomized regions on O-16S rRNA were sequenced.

Totally 155 unique mutants were identified from ribosome activity selection and aminoglycoside antibiotics selection. The ribosome activities of these mutants were determined by measuring their resistance level to chloramphenicol with and without aminoglycoside antibiotics. The 155 mutants and the control *E.coli* strain (with WT O-16S rRNA) were grown on 10 concentrations of chloramphenicol LB agar plates with or without killing concentrations of the 3 antibiotics. The phenotypes of each mutant on each condition were recorded and summarized.

3. Results and discussion

Aminoglycoside antibiotics resistant mutants from h44 9-site library. The h44 9-site library was first selected for the mutants that can support the cell growth without WT ribosome present. The diversity after the selection was estimated to be 76 based on calculation of diversity lost. This means 99.97% of the library members were not suitable for supporting cell growth. The survivors were used to do a two-round aminoglycoside antibiotics selection. The first round is selected on 12 aminoglycoside antibiotics respectively. Each antibiotic was used with a certain concentration that can inhibit ribosome function. Survivors from the first round selection were used to select on each of the 12 antibiotics with the same concentration used in the first round selection. The survivors were then grouped by their phenotypes on the 12 antibiotics. Two groups were summarized and the phenotypes of the mutants in each group were shown in figure 4-6. Mutants in the same group display variance in fluorescence intensity. Mutants with different fluorescence patterns were chosen to sequence the randomized regions. The sequencing results show mutants from the same group have the same mutation on the randomized regions despite they display different fluorescence signal pattern. Mutants in group I have the same mutation G1491U. Mutants in group I have the same mutation A1408G. Both mutations had been reported

previously. This result suggests the two mutations, G1491U and A1408G, can not only confer broad spectrum of antibiotic resistance, but also retain the ribosome activity to translation the whole proteome and support the cell growth.

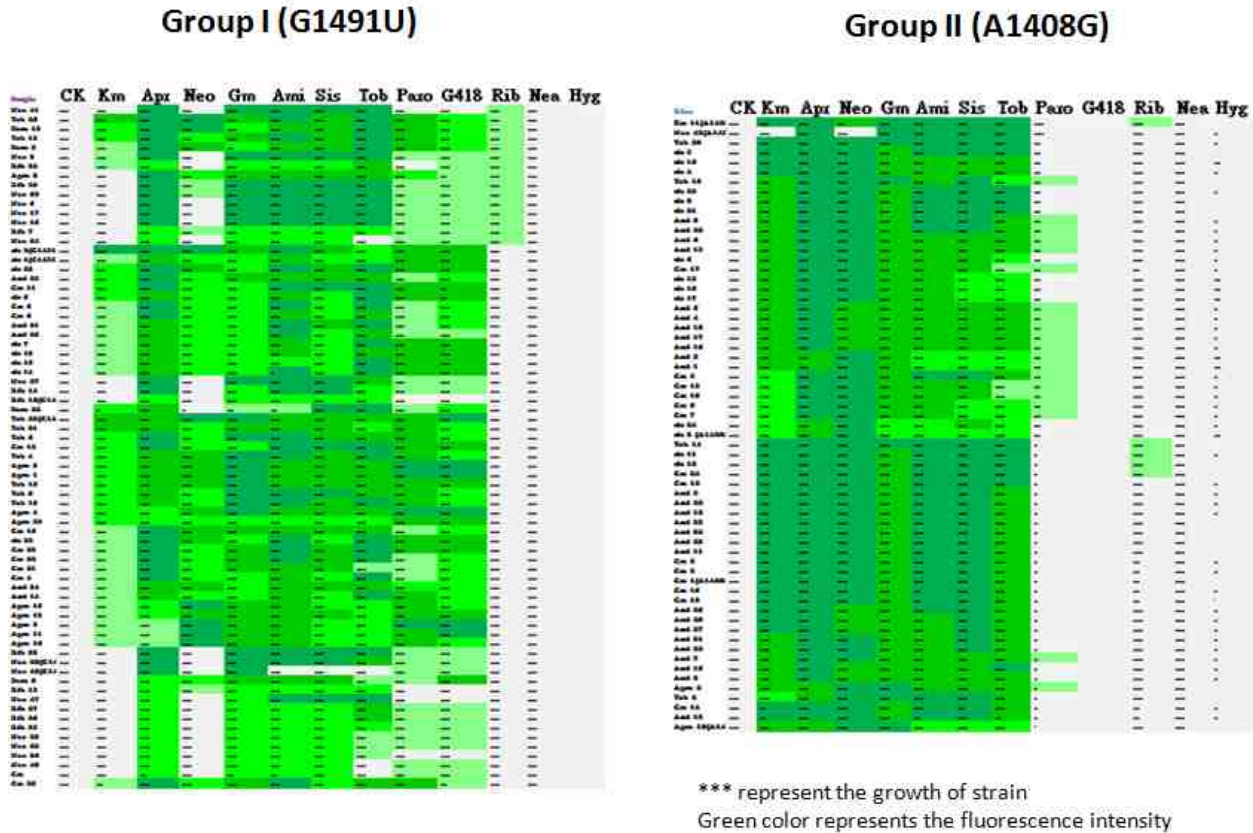


Figure 4-6. The phenotypes of mutants from h44 9-site library group I and group II

Unlike our prediction that new mutations should be found after randomized the whole drug bind site, only two known mutations were found after extensive selections on aminoglycoside antibiotics. It suggests there is a balance between drug resistance evolution and bacterial fitness. Even though the h44 9-site library may contain many drug resistance sequences at the randomized regions, they cannot go through the selections due to the bacterial fitness lost. We found that our result correlates with a report from Erik Böttger’s lab. They reconstructed the

aminoglycoside antibiotics drug resistance evolution in *Mycobacterium tuberculosis* by introducing compensatory mutations on drug binding site. They found that A1408G and G1491U are the only two mutations that can confer decent drug resistance and have less fitness cost⁹. The results from h44 9-site library selection indicate that altering the highly conserved h44 decoding A-site on WT 16S rRNA has very limited space to find new mutation due to the bacterial fitness cost.

Ribosome activity selection on O-h44 9-site library. One of the major advantages of building the h44 9-site library on O-ribosome is the activity of O-ribosome with mutations can be quantified by measuring the chloramphenicol resistance level. The O-h44 9-site library was selected for mutants with different ribosome activities by growing the naive library on a set of 15 chloramphenicol concentrations. Large amounts of the library members retain less than 10% activity (table 4-4). This result again shows the importance of h44 region to ribosome activity. The sequencing results of mutants from each chloramphenicol concentration selection show there are 64 unique mutants from 84 sequenced samples. The sequences of these mutants at the randomized regions display large variance compared to WT sequence. Interestingly, all the 5 nucleotides at randomized region 1 displays strong bias to guanine, and all the 4 nucleotides at randomized region 2 displays strong bias to cytosine (Figure 4-7). A number of hyperactive ribosomes which can confer higher chloramphenicol resistance level than the WT ribosome (survive up to 100µg/mL chloramphenicol) have been sequenced the randomized regions. Strong bias were observed at 1408 (A to G), 1494 (G to U) and 1495 (T to C or A). It has been suggested the hyperactive ribosome may lead to increasing rate of miscoding¹⁷. Considering the randomized regions are at the center of the decoding A-site, it would not be surprise many hyperactive ribosomes can be select out from ribosome activity selection. These results prove our

assumption that O-ribosome controlling translation of a single gene has much larger space to be altered than the WT ribosome controlling translation of the whole proteome.

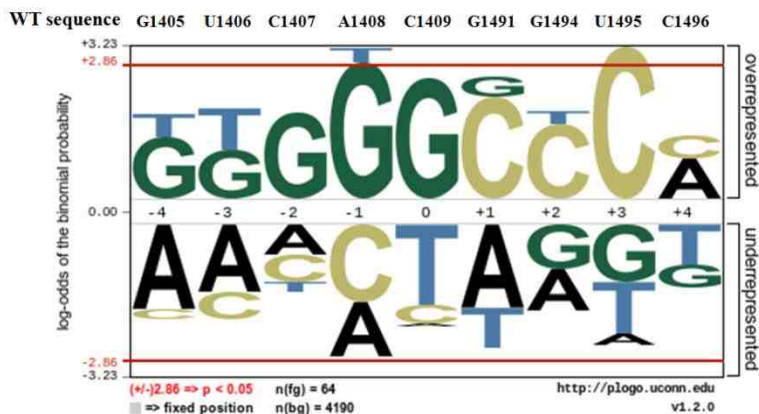
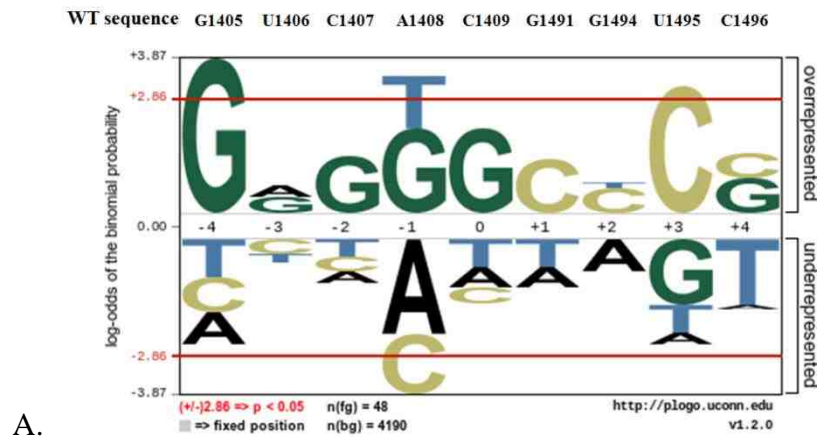


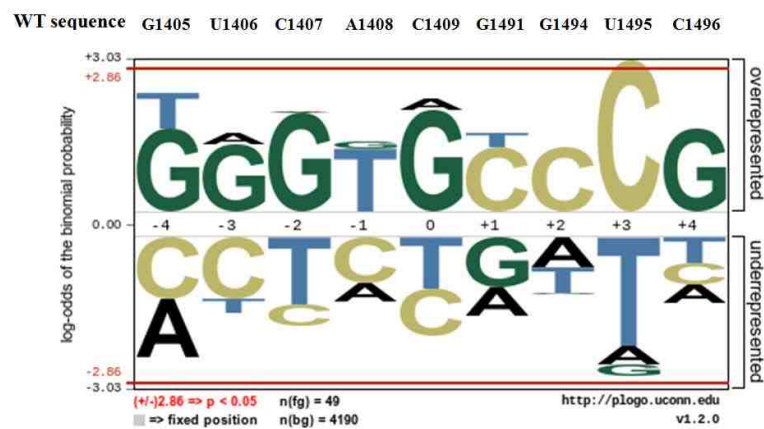
Figure 4-7 Sequence preference of mutants at randomized regions from ribosome activity selection.

Aminoglycoside antibiotics selection on O-h44 9-site library. To perform aminoglycoside antibiotics selections, a certain concentration of chloramphenicol needs to be added to retain partial of ribosome activity while selecting for mutations that disrupt drug binding. 20µg/mL chloramphenicol was chosen based on the survivor numbers during ribosome activity selection. The O-h44 9-site library was selected on 20µg/mL with 150µM kanamycin, 20µM neomycin and 20µM gentamicin respectively. 96 survivors from each selection condition were sequenced the randomized regions. The sequencing results show large sequence variance on the survivors from all three selection conditions. The mutants from kanamycin selection show strong bias to guanine at position 1405, 1407, 1408 and 1409, and strong bias to cytosine at position 1491 and 1495 on the O-16S rRNA (figure 4-8). The mutants from neomycin selection show strong bias to guanine at position 1405, 1406, 1407, 1409 and 1496, strong bias to uracil on position 1408 and strong bias to cytosine at position 1491, 1494 and 1495 on the O-16S rRNA (Figure 4-8). The mutants from gentamicin selection show strong bias to guanine at position 1405, 1406, 1407 and 1495,

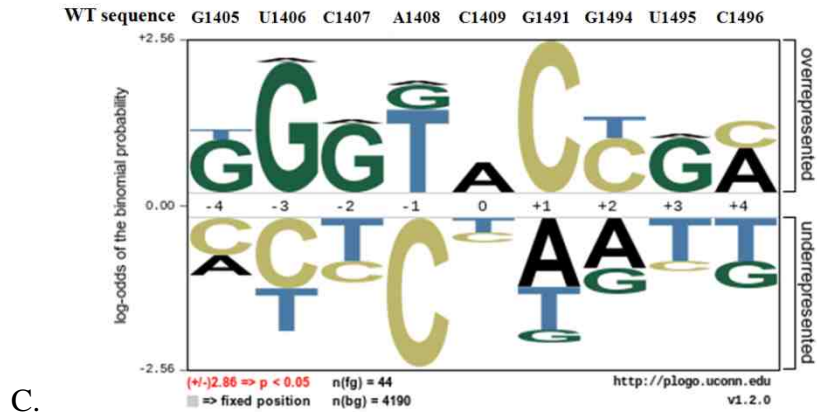
strong bias to uracil on position 1408 and strong bias to cytosine at position 1491 on the O-16S rRNA (Figure 4-8). In general, guanine is highly favorable at position 1405 and 1407; cytosine is highly favorable at position 1491. For position 1405, guanine is the WT nucleotide. Therefore the G1405 might be important for ribosome to retain catalytic activity. For position 1407 and 1491, changing to guanine and cytosine may contribute to conformational change on h44 region and consequently disrupt the drug binding. Compensatory mutations were observed on most of the mutants, suggesting the impact on ribosome activity from single rRNA mutation can be relieved by the corresponding compensatory mutations.



A.



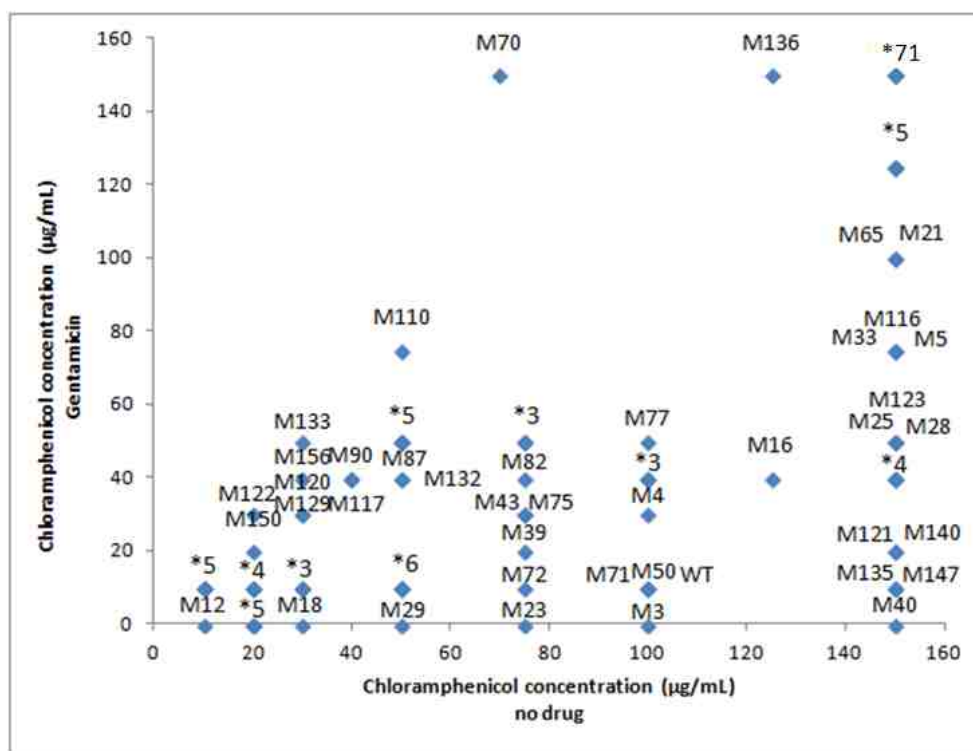
B.



C.

Figure 4-8. Sequence preference of mutants at randomized regions from kanamycin (A), neomycin (B) and gentamicin (C) selection.

To further characterize the phenotypes of O-h44 library mutants, all the unique mutants isolated from ribosome activity selection and aminoglycoside antibiotics selections were grown on a set of 10 chloramphenicol concentrations with or without aminoglycoside antibiotics to determine their O-ribosome activity in different conditions. Totally 155 mutants plus the WT O-ribosome control strain were used to measure their chloramphenicol resistance level with or without drugs. The results show all the mutants can be divided into 3 groups. Group I is drug-resistant mutants. These mutants display same chloramphenicol resistance level with or without drugs. Group II is drug-sensitive mutants. These mutants show lower chloramphenicol resistance level in the presence of drugs. Group III is drug-dependent mutants. These mutants show higher chloramphenicol resistance level in the presence of drugs (figure 4-9). Interestingly, some of the hyperactive ribosome also display strong drug resistance. However we were not able to find these mutants from the h44 9-site library. It suggests that despite the hyperactive ribosomes can confer high drug resistance and produce higher translation activity on a certain gene, they are less likely to be able to support cell growth alone. This is probably due to the high miscoding rate of these hyperactive ribosomes cannot satisfy the requirement to translate the whole



C.

Figure 4-9. Ribosome activity of 155 unique mutants with and without kanamyc (A) neomycin (B) and gentamicin (C). The X axis represents the chloramphenicol concentrations in the absence of drugs. The Y axis represents the chloramphenicol concentrations in the presence of drugs. ‘*number’ represents the number of mutants site at the same data point.

4. Conclusion

We have developed an O-ribosome controlled reporter system to study the aminoglycoside antibiotics binding sites on 16S rRNA by directed evolution approach. Saturation mutagenesis was applied to randomize the h44 region of 16S rRNA on both WT ribosome (h44 9-site library) and O-ribosome (O-h44 9-site library). The statistic results from both libraries after activity selection show that O-ribosome has much larger genetic space to be engineered. Hyperactive ribosomes were found from the O-h44 9-site library but not from the h44 9-site library. It suggests the hyperactive ribosomes are not able to support cell growth by itself but may still exist as small population of mutated ribosomes in nature.

The O-ribosome mutants with partial catalytic activity were used to examine their interactions to three representative aminoglycoside antibiotics. Mutants isolated from each drug selection display diverse sequence preference on drug binding site. G1405 position is the most conserved site among all the mutated sites. Strong guanine bias was observed on position 1405-1409 and cytosine bias was observed on position 1491, 1494-1496. This observation suggests a GC rich h44 drug binding site can strongly affect the drug binding in either positive or negative way. To further characterize the effect of the mutated rRNA sequence to drug binding, we determine the catalytic activity of all the unique mutants from both ribosome activity selection and aminoglycoside drug selections with or without addition of drugs. Three types of mutants were found based on their catalytic activity with and without drugs. Surprisingly, the drug-resistant mutants show up as the dominant phenotypes on both kanamycin and neomycin tests. It suggests the diversity of drug-resistant mutated ribosome is underestimated. However, due to the bacterial fitness cost or catalytic defect of these mutated ribosomes, they are less likely to show up in nature as the major ribosome population. Nevertheless, some of them, especially the hyperactive drug-resistant ribosome, may still exist as minor population and cause concern on the terrible drug-resistance issue.

5. References

1. Steitz, T.A., Moore, P.B. RNA, the first macromolecular catalyst: the ribosome is a ribozyme. *Trends Biochem Sci.* 2003; 28(8):411-8.
2. De stasio, E.A., Moazed, D., Noller, H.F., Dahlberg, A.E. Mutations in 16S ribosomal RNA disrupt antibiotic--RNA interactions. *EMBO J.* 1989; 8(4):1213-6.

3. Leviev, I.G., Rodriguez-fonseca, C., Phan, H., *et al.* A conserved secondary structural motif in 23S rRNA defines the site of interaction of ampicillin, a universal inhibitor of peptide bond formation. *EMBO J.* 1994; 13(7):1682-6.
4. Mankin, A.S., Leviev, I., Garrett, R.A. Cross-hypersensitivity effects of mutations in 23S rRNA yield insight into aminoacyl-tRNA binding. *J Mol Biol.* 1994; 244(2):151-7.
5. Hirabayashi, N., Sato, N.S., Suzuki, T. Conserved loop sequence of helix 69 in *Escherichia coli* 23S rRNA is involved in A-site tRNA binding and translational fidelity. *J Biol Chem.* 2006; 281(25):17203-11.
6. Laios, E., Waddington, M., Saraiya, A.A., *et al.* Combinatorial genetic technology for the development of new anti-infectives. *Arch Pathol Lab Med.* 2004; 128(12):1351-9.
7. Recht, M.I., Puglisi, J.D. Aminoglycoside resistance with homogeneous and heterogeneous populations of antibiotic-resistant ribosomes. *Antimicrob Agents Chemother.* 2001; 45(9):2414-9.
8. Shcherbakov, D., Akbergenov, R., Matt, T., *et al.* Directed mutagenesis of *Mycobacterium smegmatis* 16S rRNA to reconstruct the *in vivo* evolution of aminoglycoside resistance in *Mycobacterium tuberculosis*. *Mol Microbiol.* 2010; 77(4):830-40.
9. Matt, T., Ng, C.L., Lang, K., *et al.* Dissociation of antibacterial activity and aminoglycoside ototoxicity in the 4-monosubstituted 2-deoxystreptamine apramycin. *Proc Natl Acad Sci USA.* 2012; 109(27):10984-9.
10. Pfister, P., Risch, M., Brodersen, D.E., Böttger, E.C. Role of 16S rRNA Helix 44 in Ribosomal Resistance to Hygromycin B. *Antimicrob Agents Chemother.* 2003; 47(5):1496-502.

11. Criswell, D., Tobiason, V.L., Lodmell, J.S., Samuels, D.S. Mutations conferring aminoglycoside and spectinomycin resistance in *Borrelia burgdorferi*. *Antimicrob Agents Chemother.* 2006; 50(2):445-52.
12. Kim, J.M., Kim, J.S., Kim, N., *et al.* Gene mutations of 23S rRNA associated with clarithromycin resistance in *Helicobacter pylori* strains isolated from Korean patients. *J Microbiol Biotechnol.* 2008; 18(9):1584-9.
13. Finken, M., Kirschner, P., Meier, A., *et al.* Molecular basis of streptomycin resistance in *Mycobacterium tuberculosis*: alterations of the ribosomal protein S12 gene and point mutations within a functional 16S ribosomal RNA pseudoknot. *Mol Microbiol.* 1993; 9(6):1239-46.
14. Huang, S., Zhu, X., Melançon, C.E. Detection and Quantification of Ribosome Inhibition by Aminoglycoside Antibiotics in Living Bacteria Using an Orthogonal Ribosome-Controlled Fluorescent Reporter. *ACS Chem Biol.* 2016; 11(1):31-7.
15. Carter, A.P., Clemons, W.M., Brodersen, D.E., *et al.* Functional insights from the structure of the 30S ribosomal subunit and its interactions with antibiotics. *Nature.* 2000; 407(6802):340-8.
16. Gibson, D.G., Young, L., Chuang, R.Y., *et al.* Enzymatic assembly of DNA molecules up to several hundred kilobases. *Nat Methods.* 2009; 6(5):343-5.
17. Saraiya, A.A., Lamichhane, T.N., Chow, C.S., *et al.* Identification and role of functionally important motifs in the 970 loop of *Escherichia coli* 16S ribosomal RNA. *J Mol Biol.* 2008; 376(3):645-57.